Transilvania University of Brașov

HABILITATION THESIS

LASER CLADDING: FROM EXPERIMENTAL RESEARCH TO INDUSTRIAL APPLICATIONS

Domain: Industrial engineering

Author: Assoc. Prof. Dr. Alexandru PASCU

University: Transilvania University of Brașov

BRAȘOV, 2019

CONTENT

Acknowledgements

The habilitation thesis entitled: **Laser cladding: from experimental research to industrial applications** is based on research activity conducted by the author and co-authored with:

Croitoru Cătălin	Stanciu Elena Manuela
Geantă Victor	Țierean Mircea Horia
Hulka Iosiv	Uțu Dragoș
Mirza Roșca Julia	Voiculescu Ionelia
Roată Ionuț Claudiu	Balteș Liana

List of notations and terms

Nomenclature

Ac	Clad area [mm^2]
AFM	Atomic force microscope
Am	Molten area [mm^2]
ASC	As cladded
CNT	Carbon nanotubes
CW	Continuous wave
DL	Dilution [%]
DOE	Design of experiments
Ds	Laser spot diameter [mm]
EDAX	Energy dispersive X-ray
E$_p$	Laser energy density [J/cm^2]
HA	Hydroxyapatite
HAZ	Heat affected zone
Hd	Clad height above the unclad substrate [mm]
L	Clad width [mm]
LC	Lase cladding
LHT	Laser heat treatment
LSP	Laser shock processing
MMC	Metal matrix composite
Pd	Clad depth of penetration
PLC	Pulsed laser cladding
Pp	Laser power density [kW/cm^2]
PTA	Plasma transferred arc
SEM	Scanning electron microscopy
STT	Solar thermal treatment
WC	Tungsten carbide
XRD	X-ray diffraction
α	Wetting angle, angle between the substrate surface and the tangent to the single-track surface at the contact edge

REZUMAT

Teza de doctorat *Îmbunătățirea proprietăților mecanice prin depuneri laser ale pieselor utilizate în industria auto*, susținută în anul 2011 a abordat un domeniu care este de actualitate și în prezent, respectiv tehnologia de recondiționare cu fascicul laser și pulberi metalice. Pe parcursul studiilor doctorale am fost fascinat de rapida și continua evoluție a tehnologiei laser, remarcând avantajele utilizării acestei tehnologii la prelucrarea materialelor metalice. Pasiunea și interesul pentru acest domeniu a continuat și după terminarea stagiului doctoral, materializându-se prin continuarea activităților de cercetare - inovare în această direcție.

Depunerile cu fascicul laser și pulberi metalice au reprezentat pilonul principal al cercetărilor efectuate în ultimii opt ani, concretizate prin optimizarea procesului de depunere dar și prin obținerea de noi straturi aliate, amorfe, compozite sau nano-compozite. Întreaga activitate științifică a reprezentat un tandem continuu între cercetarea fundamentală și aplicațiile industriale ale procesului de depunere cu laser și pulberi.

Teza de abilitare cu titlul *Depunerea cu Laser: de la Experimental la Aplicații Industriale* este o sinteză a articolelor personale publicate în domeniul tehnologiei laser după susținerea tezei de doctorat. Teza este alcătuită din trei părți: *stadiul actual*, *cercetări fundamentale* și *aplicații industriale* care reflectă realizările personale în plan științific și profesional.

Teza de abilitare debutează cu o scurtă descriere a realizărilor profesionale obținute sub egida Universității Transilvania din Brașov. Rezultatele științifice sunt prezentate în patru capitole, după cum urmează:

Capitolul I abordează, din punct de vedere teoretic, tehnologia de depunere (placare) cu fascicul laser. În acest capitol cititorul se familiarizează cu tehnologia laser, parametrii generali și diferite tehnici de depunere cu laser și pulberi metalice. Capitolul se încheie cu o trecere în revistă a literaturii de specialitate despre optimizarea procesului și aliaje utilizate la fabricarea de straturi amorfe sau nano-compozite.

În capitolul doi sunt prezentate contribuțiile personale din domeniul depunerilor cu laser și pulberi pe bază de nichel, în special a aliajelor de tipul Inconel. Prima contribuție este optimizarea parametrilor de depunere și obținerea unor straturi pe bază de nichel cu

proprietăți mecanice superioare. Ulterior procesului de depunere, creșterea suplimentară a calității straturilor obținute s-a efectuat prin aplicarea unui tratament termic cu energie solară concentrată.

Capitolul al treilea prezintă diferite tehnici avansate de depunere cu laser și pulberi metalice. O primă contribuție descrie o nouă metodă de depunere cu laser realizată prin utilizarea unui strat tampon între depunerea dură și materialul de bază, având rolul de a reduce tensiunile interne și de a diminua susceptibilitatea de fisurare a depunerilor dure. Obținerea de straturi amorfe prin folosirea de materiale ceramice sau fabricarea de straturi nano-compozite prin armarea cu nanotuburi de carbon a aliajelor de nichel sunt, de asemenea, contribuții originale prezentate în acest capitol.

Capitolul 4 este dedicat aplicațiilor industriale ale tehnologiei de depunere cu laser și pulberi metalice. Sunt prezentate două studii de caz prin care se dovedește aplicativitatea tehnologiei de depunere cu laser pentru recondiționarea componentelor uzate. Primul caz, diseminează tehnologia de recondiționare cu laser și pulbere a unor matrițe utilizate în industria auto pentru fabricarea componentelor din cauciuc. Reperele au fost recondiționate prin depunerea unui aliaj de tipul NiCrBSiFe pe muchia activă a matrițelor.

Al doilea studiu de caz, descrie procesul de recondiționare a unei pale de compresor de la motoarele cu reacție utilizate în industria aeronautică. Pala de compresor este de proveniență rusească și este fabricată din aliajul VT3-1, iar procesul de recondiționare a fost realizat prin depunerea cu laser a unui cordon din titan pur pe conturul exterior al palei. Rezultatele studiului validează capacitatea acestei tehnologii pentru recondiționarea, și prelungirea duratei de exploatare a palelor de turbină de la motoarele cu reacție.

Ultima parte a tezei de abilitare este rezervată prezentării planurilor de evoluție și dezvoltare a carierei academice. Luând în considerare contribuțiile personale din cadrului prezentei teze de abilitare, direcțiile viitoare de cercetare pot fi sintetizate după cum urmează:

- Proiectarea și realizarea unui sistem inovativ de depunere cu laser prin pulverizare coaxială care să permită mixarea insitu a pulberilor metalice cu densități diferite;
- Continuarea cercetărilor experimentale în domeniul tehnologiei laser cu scopul dezvoltării de noi tehnici de tratament termic, termo-mecanic și de sudare;

- Sinteză de nanomateriale utilizând energia solară concentrată;
- Pe termen scurt, o activitate prioritară este brevetarea rezultatelor deja obținute.

Contribuțiile personale diseminate în cadrul acestei teze de abilitare au la bază 12 articole publicate în jurnale de specialitate indexate în baze de date internaționale.

Întreaga activitate de cercetare este valorificată prin publicarea a peste 50 de articole științifice, din care 36 sunt indexate în Web of Science Core Collection, iar 22 sunt cotate cu factor de impact. De asemenea, am fost director a 4 proiecte de cercetare internaționale și membru în 9 proiecte internaționale și 4 naționale. Totodată, fac parte din colectivul de cercetare a 2 proiecte internaționale finanțate de mediul economic.

Activitatea de cercetare este recunoscută de mediul academic prin citarea rezultatelor în jurnale de prestigiu precum *Optics and Laser Technology*, *Materials and Manufacturing Processes*, *Surface and Coatings Technology* etc. Indicele Hirsch în Scopus și Web of Science este 5.

B Scientific and professional achievements and the evolution and development plans for career development

B1. Professional achievements

This habilitation thesis summarizes a part of my research results obtained after defending my PhD thesis, in September 2011. My professional background and my career evolution can be summarized as follows:

I have been a welding engineer since 2005, when I graduated from the Faculty of Materials Science and Engineering with specialization in Welding Equipment and Technology from Transilvania University of Brasov. In 2008, I graduated from the master's programme in Welding Engineering at the same institution. I was a production engineer at an automotive company for three years, from 2005 until 2008.

I began the doctoral programme in the Industrial Engineering domain in 2008 at department of Materials Engineering and Welding, Transilvania University of Brasov and, in 2011, I defended the PhD thesis entitled Improvement of mechanical properties of automotive parts through laser cladding. The thesis was an experimental-based research in the field of laser cladding technology, and all experimental activity was conducted at the Centro Laser department at the Universidad Politécnica de Madrid, where I developed my research ability and improved my technical skills and expertise in laser technology.

In the same period, i.e., 2009 – 2011, I graduated with a Master of Laser Technology from the Applied Physics Department ETS Ingenieros Industriales from Universidad Politécnica de Madrid, with the master thesis entitled Laser cladding: The key to the improvement and repair metallic surfaces.

In 2011, after completing my PhD, I decided to continue to research different topics related to laser technology as member in different research grants with national or international founding. Laser processing, especially welding, cladding, and heat treatment, as well as nanomaterials synthesis by concentrated solar radiation, are some of the research areas that I have followed in the last eight years.

During the 2014-2016 period, I participated in an 18-month postdoctoral programme at the Transilvania University of Brasov, a programme that allowed me, financially, to continue to further develop research activities in the field of laser cladding technology. Fine tuning of the

laser cladding process parameters and designing of a novel multilayer coating with improved wear resistance characteristics resulted from the postdoctoral stage.

In the same period, I was proactively involved in development of the Advanced Welding Eco-Technologies research centre, which is a part of the R&D Infrastructure of the Transilvania University of Brasov. Since 2016, I have been the coordinator of the above mentioned centre, which aims to research and develop new products and technologies in the field of welding engineering following the new worldwide ecotechnological trends by implementing modern and novel laser processing technologies. Today, the R&D centre plays a strategic role in the Materials Science and Engineering Faculty in terms of the research infrastructure and through the continuous development of new collaborative partnerships with other research organizations and countries.

The activity at the Transilvania University of Brasov is based on two main directions, i.e., teaching and research. Both directions have numerous interdisciplinary activities that complete the academic career (e.g., managing, promoting, tutoring, research dissemination, conferences, founds attraction and so on.)

The starting point of my academic career was in 2013, when I begin to teach as collaborator at the Transilvania University of Brasov. In October 2015, I joined to the University staff as an assistant professor. Since 2013, my academic activities have involved teaching courses, seminars and practical laboratories covering materials science, welding design, welding automatization and robotics, project management at the bachelor and master's degree levels. In addition to the teaching activities, the continuous tutoring of undergraduate and master students for their final projects is an activity that further enhanced my teaching experience. I have coordinated 9 undergraduate students and 6 master students in finishing their bachelor's final project and master's dissertation, respectively.

My teaching skills have been continuous improved by continuously following a roadmap based on the student's feedback. Updating the courses content, using real engineering case studies and presenting the latest technology developments are only a few examples of my daily teaching methods. Furthermore, as Faculty Erasmus+ coordinator, I proactively promote the students exchanges from and to highly ranked universities and research institutes. Simultaneously, a close relation with the industry is maintained by encouraging visits and practical placements of students in private Romanian companies during the summer.

The research activity conducted during my career has been based on fundamental and applied research. Topics such as laser cladding of various alloys, optimizing the laser cladding process,

enhancing the wear/corrosion resistance of cladded layers and reconditioning by laser cladding of shafts, moulds/dies or compressor engine blades are examples of the research investigations carried out in the field of industrial engineering.

Those topics have been the foundation of the research projects performed at the Transilvania University of Brasov over the last 8 years. As project director, I have conducted 4 international research grants, SFERA II (Solar Facilities for the European Research Area):

- **Project title**: Residual stress relieve of Ni based coatings fabricated by laser cladding, European Solar Research Infrastructure for Concentrated Solar Power - SFERA II, 2015, location: France.

- **Project title**: Synthesis of carbon nanotubes using solar radiation and Al_2O_3-Mn/Cu_2O catalyst, European Solar Research Infrastructure for Concentrated Solar Power - SFERA II, 2015, location: France.

- **Project title**: Al_2O_3/TiO_2 cladding in pre-placed powder geometry using concentrated solar radiation, European Solar Research Infrastructure for Concentrated Solar Power - SFERA II, 2017, location: France.

- **Project title**: Corrosion improvement of FeCrAl alloys designed for molten salt reactors, European Solar Research Infrastructure for Concentrated Solar Power - SFERA II, 2017, location: Italy.

As member in the project team, my research activity was carried out in different national and international research grants, such as the following:

- Project title: Improvement of electric contact corrosion resistance, European Solar Research Infrastructure for Concentrated Solar Power - SFERA II, 2014, location: Italy.

- Project title: Mechanical proprieties improvement of Cu10Al laser cladded on aluminium, European Solar Research Infrastructure for Concentrated Solar Power - SFERA II, 2014, location: Spain.

- Project title: Improvement of corrosion and thermal resistance by thermal cladding of Ni-based coating on copper, European Solar Research Infrastructure for Concentrated Solar Power - SFERA I, 2013, location: Spain.

- Project title: Corrosion and wear behavior of NiCrBSi coatings fabricated by laser cladding, European Solar Research Infrastructure for Concentrated Solar Power - SFERA II, 2015, location: Italy.

- Project title: Increasing of SC ELDON SRL competitivity by optimising the manufacturing technology of floor standing enclosures | BRIDGE type grant no. PN-III-P2-2.1-BG-2016-0349, during: 2016-2018.

- Project title: Performant materials and technology for obtaining of asphalt milling tool | MATFREZ, PNII type grant no. 188/02.07.2012, during: 2012-2016.

The research activity also involved private sector projects from the European Community, e.g., Project titles: Studies concerning the real time monitoring of the laser welding/cutting process (8407/21.07.2015 | Netherlands) and New methods for cutting metallic waste (4452/17.04.2015 | Netherlands).

The academic community recognized the research results by bestowing the work with 5 CNCSIS (Romanian National University Research Council) awards for ISI papers and a gold medal distinction, which was awarded at the European Exhibition of Creativity and Innovation EUROINVENT 2016. The scientific activity has been disseminated by publishing the results in Web of Science Core Collection indexed journals, journals indexed in other International Databases (BDI) and by presentations at international conferences, as follows:

- 22 papers with impact factors indexed in the Web of Science Core Collection;
- 14 papers published in conference proceedings indexed in the Web of Science Core Collection;
- 14 papers published in journals indexed in other international databases (BDI);
- participation at 10 international conferences;
- 1 patent proposal.

In addition, related to the research activity, my involvement in the organizing committee of the International Conference on Materials Science and Engineering – BraMat 2017 and 2019 – should be mentioned. Additionally, I am reviewer for the following ISI journals: Applied Surface Science, Journal of Spectroscopy, Solar Energy Journal, and Coatings.

The scientific content of this habilitation thesis is based on the information presented in the following scientific papers presented at international conferences or published in scientific journals after the PhD thesis was defended:

1. Pascu A., Stanciu E.M., Croitoru C., Roată I. C., Tierean M.H., Mirza Rosca J., Cimpoesu N., Bogatu C., Pulsed laser cladding of NiCrBSiFeC hardcoatings using single-walled carbon nanotubes additives, Journal of Nanomaterials 2019, 1-12, (2019), IF 2.23.

2. Pascu A., Stanciu E.M., Roată I. C., Hulka I., Uțu D., Maior I., Influence of the laser cladding parameters and solar heat treatment on the properties of biocompatible Inconel 718 coatings, Romanian Journal of Materials 47 (2), p. 157 – 165, (2017), IF 0.66.

3. Pascu A., Rosca J. M., Stanciu E. M, Laser cladding: from experimental research to industrial applications, Materials Today: Proceedings 19, (3), p. 1059-1065, (2019).

4. Stanciu E.M, Pascu A, Tierean M.H., Voiculescu I, Roata I.C., Croitoru C., Hulka I., Dual coating laser cladding of NiCrBSi and Inconel 718, Materials and Manufacturing Processes 31, Issue 12, p. 1556-1564, (2016), IF 2.27.

5. Pascu A., Stanciu E.M., Savastru D., Geanta V., Croitoru C., Optical and microstructure characterisation of ceramic – hydroxyapatite coating fabricated by laser cladding, Journal of Optoelectronics and Advanced Materials 19, Issue 1-2, (2017), IF 0.383.

6. Stanciu E.M., Pascu A., Roată I.C., Croitoru C., Tierean M., Rosca J. Mirza, Hulka I., Solar radiation synthesis of functional carbonaceous materials using Al_2O_3/TiO_2-Cu-HA doped catalyst, Applied Surface Science 438, p. 33–40, (2018), IF 4.43.

7. Hulka I., Serban V.A., Utu D., Duteanu N.M, Pascu A., Roată I.C., Maior I., Wear resistance of laser cladding NiCrSi composite coatings, Romanian Journal of Materials, 46 (1), p. 49 – 54, (2016), IF 0.563.

8. Pascu, E. M. Stanciu, C. Croitoru, I. C. Roata, M. H. Tierean, Pulsed laser cladding of Ni based powder, IOP Conf. Ser.: Mater. Sci. Eng. 209, 012058, (2018).

9. Pascu A., Hulka I., Tierean M. H., Croitoru C., Stanciu E. M., Roată I. C., A comparison of flame coating and laser cladding using Ni based powders, Solid State Phenomena. 254, p. 77-82, (2016).

10. Pascu A., Stanciu E. M., Roata I., Croitoru C., Baltes L., Tierean M.H., Parameters and behaviour of NiCrFeSiB Laser cladding in overlapped geometry, Bulletin of the Transilvania University of Brașov 9 (58) Issue 2, p. 9-16, (2016).

11. Pascu A., Stanciu E.M., Roată I. C., Laser cladding of Metco 68F-NS-1 cobalt based powder, Journal RECENT 16, No. 2 (45), p. 115-118, (2015).

12. Pascu A., Stanciu E. M., Roată I., Croitoru C., Tierean M., Hulka I., Mirza Rosca J., Reconditioning of compression moulds by laser cladding, Annals of Faculty of Engineering Hunedoara – International Journal of Engineering XVII (4), p. 41-44, (2019).

Several unpublished results are also included for better presentation of the scientific content of this habilitation thesis.

The Minimum criteria of Romanian National Council for Titles, Diplomas and Certificates (Industrial Engineering and Management domain, according OMENCS Nr. 6129 / 20.12.2016 [MO, I, 123 / 15.02.2017) requested for defending the present habilitation thesis are accomplished or exceeded.

MINIMUM CRITERIA			Minimum requested	Accomplished
A1. Teaching & training			130	**133.20**
A2. Research			300	**469.17**
A3. Recognition & impact of research activity			100	**193.28**
MANDATORY MINIMUM TERMS SUBCATEGORIES			Minimum requested	Accomplished
A.1.1.1. Books / chapters in engineering as author (first author)			2	**2**
A.1.2.1. Didactic textbook, laboratory guidance / applications (first author)			4 (2)	**4 (2)**
A.2.1. Articles in ISI Thomson Reuters journals & proceedings				
of which	Minimum 8 articles in ISI Thomson Reuters journals and proceedings - *in the last 5 years*		8	**36**
	of which	in ISI Thomson Reuters journals	3	**22**
		as first author in ISI Thomson Reuters journals	3	**3**
		in a Q1 or Q2 rated journal	1	**7**
A.2.2. Articles in journals and volumes of scientific events indexed in international databases - *in the last 5 years*			8	**8**
A.2.5 Research grants (obtained by competition)				
A.2.5.1 As director/responsible	International grant		2	**4**
	National grant			**-**
A.2.5.2 As member/participant	International grant		-	**5**
	National grant			**5**

B2. Scientific achievements

Laser cladding: from experimental research to industrial applications

Chapter 1. BACKGROUND AND BASIC OVERVIEW

1.1 LASER and laser cladding technology

The LASER, an acronym for Light Amplification by Stimulated Emission of Radiation, evolved in less than 60 years, including all the stages from concept to experimental research and to industrial applications. Currently, the laser is synonymous with precision, quality, speed and is an integrated part of all the modern manufacturing processes.

Laser technology is used for industrial processing, such as cutting, welding, heat treatment, and cladding, and for surgical interventions, engraving, restoring artefacts, scanning barcodes in supermarkets, among other uses.

The laser concept was born in the 1900 when Max Plank postulated the relation between energy and radiation frequency and was the basis of the Einstein concept of stimulated light emission; however, the first ruby-based resonator was built in 1961.

Immediately after the first laser beam was emitted, new types of lasers were developed and reported (1963 - Carbon Dioxide (CO_2) laser; 1964 – Nd:YAG laser; 1967 - tuneable dye laser; 1970 - excimer laser and semiconductor laser; and 1975 - continuous-wave semiconductor laser).

Figure 1.1 underlines the rapid evolution from 1 mW to 1000000 mW, which occurred in only 3 years from the invention of CO_2 lasers, proving the impact of the technology in the 20th century. In the same line, Figure 1.2 presents the most important milestones in the evolution of laser technology from the realizing of the first ruby laser in 1961 by Mainman, until the last decade, when the laser evolved and gained importance in various industrial sectors, such as automotive, aerospace, petrochemical and so on.
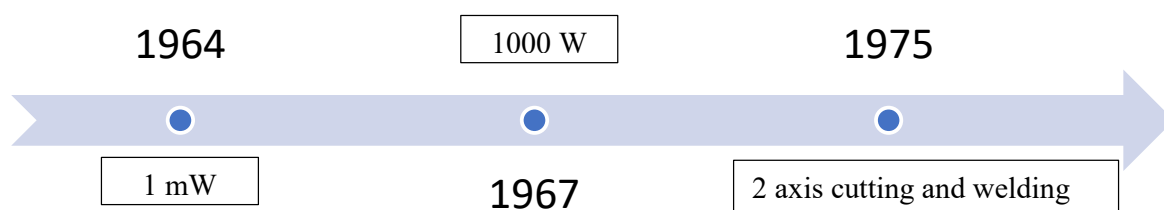
Fig. 1.1. Discovery and evolution of CO_2 lasers.
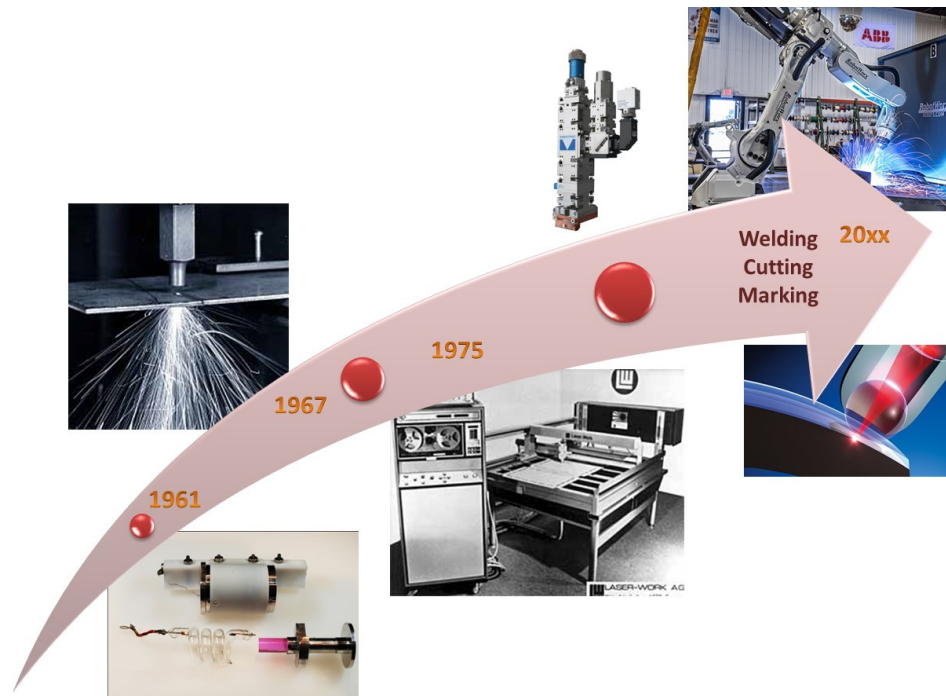
Fig. 1.2. Evolution timeline of the laser technology.

The laser was rapidly evolving, as solid-state lasers, semiconductor lasers, gas lasers with continuous or pulsed emission were developed and had a broad range of applications in science (e.g., laser spectroscopy). Even so, the industrial application of the technology was limited due to difficulties in the automatization of the processes. This gap between the laser technology and processing limitation was filled in 1981 with the introduction of the first personal computer and the fast evolution of robots and computer numerical control systems. Currently, the LASER is a mature technology that can provide the best results in terms of quality and processing speed.

The laser processing for industrial applications represents a special category of procedures defined by a high energy density applied to the surface of a unit, which puts this technology in first place in terms of precision, efficiency and productivity. As a defining characteristic, laser radiation is transformed into heat energy upon contact with the processed surface, thus achieving a change in the physical-chemical or mechanical behavior of the material.

In addition to the well-known processes of laser cutting, marking and welding, in the 1980s the laser deposition/cladding process was developed and, since then, there have been many benefits from the technological boom of the laser technology. Laser deposition can be fabricated by the following two methods:

- PLD (Pulsed Laser Deposition) is a physical vapor deposition where a laser vaporizes a target material that will be deposited as a thin film on a substrate. The process implies a vacuum chamber and a complex mechanism of ablation, plasma plume formation, vaporization, nucleation and growth of the thin film. The technique of pulsed laser deposition is currently used to fabricate high-quality thin films of ceramic oxides and nitrides with well-defined stoichiometry.
- LC (Laser Cladding) is a method for fabricating fully dense coatings as complete layers or even in high-volume build-ups.

The laser cladding technique is similar to the welding overlay process by CO_2 welding, Metal Inert Gas welding (MIG), Tungsten Inert Gas welding (TIG) or by Plasma Transferred Arc (PTA), having the purpose to create a hardfacing layer on a substrate. The laser beam is used as the heat source to melt and fuse the filler material to fabricate a defect free coating (cladding) with high corrosion and wear resistance on the surface of the base material. The process is meant to enhance the mechanical proprieties of the base material and/or to restore the original dimensions of the component. The process is characterized by several key characteristics that require higher investments and running costs for the technology, as follows:

- Full metallurgical bonding of the coating / substrate;
- Easy automatization trough CNC productions systems of robotic cells;
- Precise control of the geometrical feature of the cladded layers;
- Low heat input compared with the conventional welding methods;
- Controlled dilution with the substrate;
- Wide choice of filler materials in the form of powder;
- Precise control of the coating thickness in one layer or in multipass layers, i.e., 0.1 mm up to several centimeters;

High compatibility with the 3D rapid prototyping techniques.

Different names, same technology

Laser Cladding (LC) or Laser Deposition (LC) is a process that applies a metallurgical-bonded layer (coating) by using a laser beam as the heat source. This technique (LC) or the fabrication of three-dimensional parts by using this technique can be found in the literature as the following terms: Laser Powder Deposition (LPD), Direct Metal Deposition (DMD), Laser Rapid Manufacturing (LRM), Laser Additive Manufacturing (LAM), Laser Engineering Net Shaping (LENS), and Freeform Laser Consolidation (FLC).

1.2 Methods of laser cladding

There are various laser cladding techniques, which differ regarding the shape of the filler material (wire or powder) used and by the process procedure, i.e., two-step or one-step laser cladding processes, respectively. As further described below, the one-step laser cladding process is performed by continuous adding of the filler material in the melted bath, and the two-step process involves the preplacing of the filler material as a paste on the surface that will be cladded.

The easiest method to obtain a cladded layer is by mixing the powder with a binding to form a paste and preplacing the mixture onto the substrate. The binding (alcohol, polyvinyl) must have no influence during the melting and solidification of the mixture. In the second step of the process, the laser beam melts the powder mixture, thus creating the cladded layer by overlapping the laser path (Figure 1.3(a). The melting process is shielded by a protective gas, usually Ar.

The preplaced cladding technique is easy and does not require a specialized laser cladding cell (powder feeder, cladding head) being successfully realized by a common optical focus head. Even so, the process is time consuming and is limited to components with plain surfaces where easy placing of the powder bead is compulsory. The main challenge is the uniform distribution of the paste and the prevention of the pore formation due to the binder evaporation during the laser processing. Because of its simplicity, numerous studies use this method to rapidly analyse the behaviour of new alloy powder recipes.

The preplaced laser cladding method is also used by the author to obtain composite claddings, Al_2O_3/TiO_2 glass/ceramic coatings and coatings with carbon nanotubes (CNTs) additives, as described in chapter 3 of this habilitation thesis.

The limitations of the two-step cladding technique are overcome by delivering the filler material directly into the melt pool. In this case, the filler material, i.e., wire or powder, is supplied off-axis and intersected with the laser beam, which simultaneously melts the wire and the substrate surface, creating a cladded track. Partially overlapping tracks can form a uniform cladded layer, as schematically described in Figure 1.3(b). Laser cladding with wire is an economical and clean process and is particularly used for reconditioning of high precision surfaces (e.g., dies, moulds). The alloyed wire is cheaper than powders, but the off-axis feeding of the materials have some drawbacks in terms of the limitation of the travel direction and alignment of the wire with the laser beam. Recently, the process has evolved, and coaxial

feeding of the wire has become possible, thus enabling the laser processing of components with complex shapes. The Fraunhofer Institute for Material and Beam Technology IWS [IWS19] has been constructing a coaxial laser wire cladding head – COAXwire – especially for applications where a 3D contour must be reconstructed.
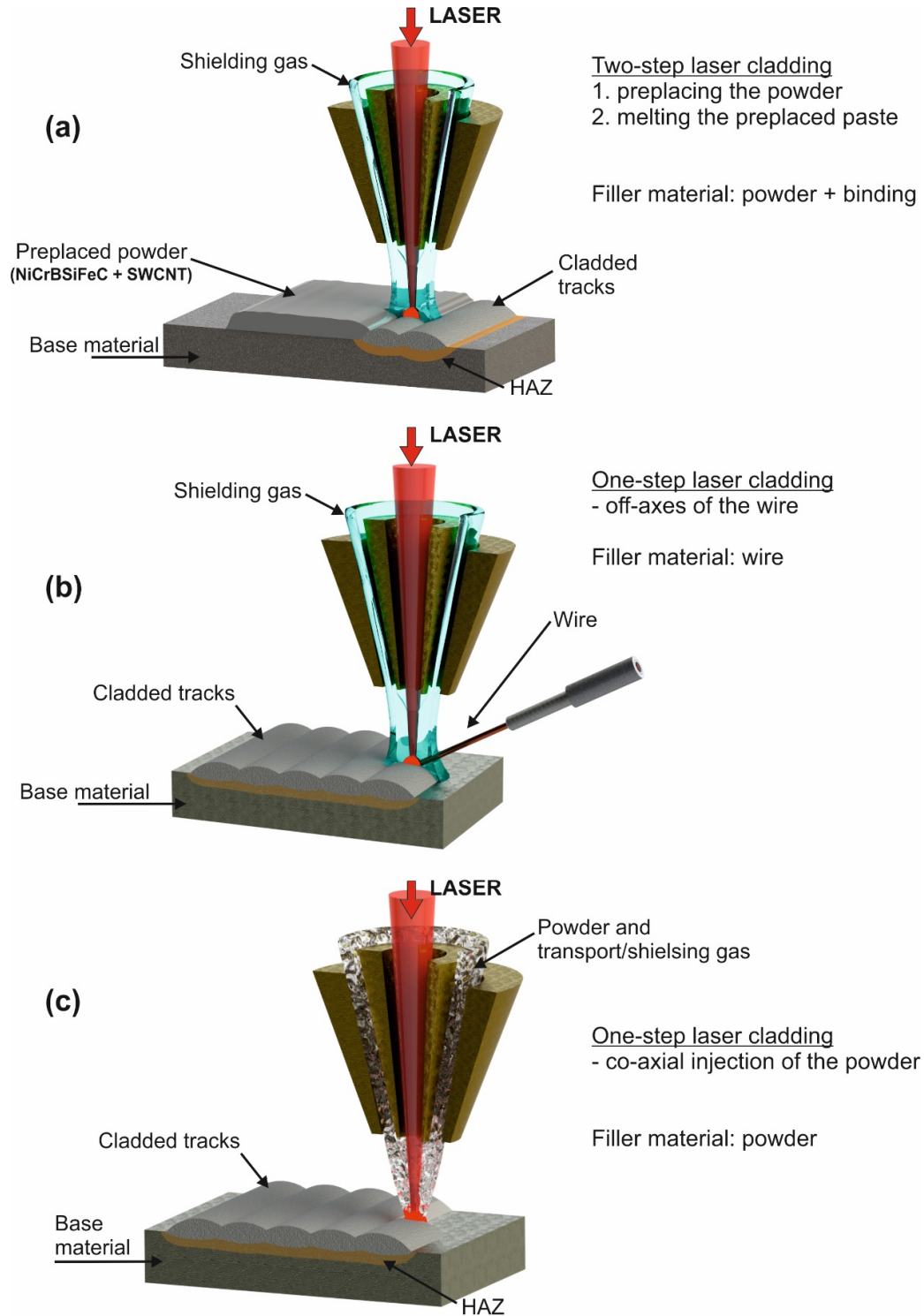
Fig. 1.3. CAD rendering of laser cladding methods, a) preplaced laser cladding, b) laser cladding with wire, c) laser cladding by coaxial powder injection.

The laser cladding with powder can be realized by side feeding of the powder, similar to the wire feeding, or by coaxial injection. In this case, the powder is pulverised in the shape of a cloud / cone, coaxial with the laser beam; the tip of the cone is intersected with the laser at the surface of the workpiece. As the laser beam travels inside the powder cone, the particle will absorb and reflect a part of the laser energy, reducing the intensity of the laser at the contact with the work peace, providing a more uniform distribution of the laser energy [MAZ17], [SCH98] and [REA97]. During laser processing, the melted powder particles are blown into the melt pool created by the laser beam on the substrate, thus providing a perfect bond between the two materials. A defect free compact layer with minimal dilution and HAZ results. One track per laser travelling is obtained, and full cladded layers can be fabricated by partially overlapping the tracks at a ratio of 30–60%.

The schematic representation of the process is presented in Figure 1.3(c). An inert gas, usually Ar, is used to transport the powder and to protect the melted bath during the process. The gas also has the role of shaping the cloud of powder.

Whether for reconditioning, creating new 3D surfaces or for improving the corrosion/wear resistance of the workpiece, the coaxial laser cladding is the best cladding technique available due to the freedom to control the process parameters related to the laser, powders and process automatization. The quality of the layer is directly dependent on the process parameters.

LASERS

For laser cladding, a continuous wave laser is usually used that can provide high and constant power for the process [LLL15], [JAN15] and [HOD13]. The CO_2, Nd:YAG and diode types are common continuous lasers involved in laser cladding processes.

Intuitively, the laser power is the most important parameter in the case of CW laser cladding or in any laser related process and must be corelated with the focal distance and the processing speed. The laser power must always be calculated as the power density (laser powder / spot diameter) or as energy density if we add the processing speed into the equation (laser power / spot diameter and processing speed):

$$P_\rho = \frac{P}{S} \quad ; \quad E_\rho = \frac{P}{S \cdot D_s} \tag{1}$$

where E_p – energy density, P_p – powder density, S – cladding speed, and D_s – spot diameter.

The laser power is directly responsible for the amount of the melt depth of the substrate and, therefore, for the dilution ratio between the coating and the work piece. It is obvious that a dilution with the base material that is as small as possible is desirable to preserve the chemistry of the high alloyed powder, which will mitigate the proprieties of the cladded layer. At the same time, superficial melting of the substrate is necessary to obtain good bonding with the coating. A maximum 5% dilution is desirable in case of laser cladding but values up to 30% can be accepted in certain application.

A recent study [PSR16] highlights the laser power's influence on the dilution and geometry of the cladded layers. For a better understanding the relation between laser parameters and coating proprieties, I have been using a DOF (**D**esign **O**f **E**xperiments) matrix to determine the influence of the laser power, feed rate and cladding speed on the geometrical profile of the cladded layers. A pore- and crack-free coating with almost zero dilution with the substrate have been obtained by using a defocused 2.5 mm laser beam and an increased processing speed.
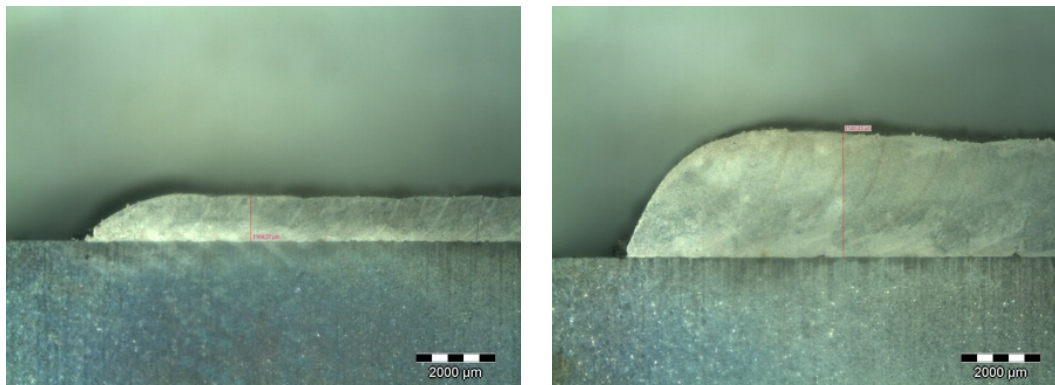
Fig 1.4. Example of Ni-based coating with zero dilution [PSR16]
Laser CW Rofin DY3300, Coating: Metco 15E, Substrate: AISI 5140, Overlapping 40%.

The direct influence of the process parameters can be observed by comparing the height of the cladded layers presented in Figure 1.4. An almost triple coating height can be obtained by varying the laser power and cladding speed.

In contrast, a pulsed laser is able to provide the laser energy in plusses, which means that the power density can be tuned by setting the pulse duration and the number of pulses per time unit.

Compared with the continuous wave (CW), the pulsed laser deposition bears more specific parameters regarding the pulse frequency, duration, and energy which have a pronounced influence on the quality of the coatings. The general aim of the laser cladding process is to use

low amounts of energy to avoid overheating the substrate. At the same time, it is necessary to have enough power density to melt the powder and to create a strong bond with the substrate. This fine tuning of the laser energy could be obtained by using a pulsed laser that allows controlling of the pulse length and the number of pulses employed per unit area.

Conversely, in another study [PSC18], I determined the pulsed laser's influence on the cladding profile and quality (microhardness) by using the DOE approach. In the case of the pulsed laser, the results show that the power and frequency combination have no significant influence on the cladded layer. In contrast, the interaction is severe in the case of the pulse in combination with the power or laser frequency settings (Figure 1.5).

The data, which express the interrelationship between the laser cladding parameters and the characteristics of the clad produced, can be used to find the optimum laser parameters and predict the responses, thus contributing to a better understanding of the laser cladding process.
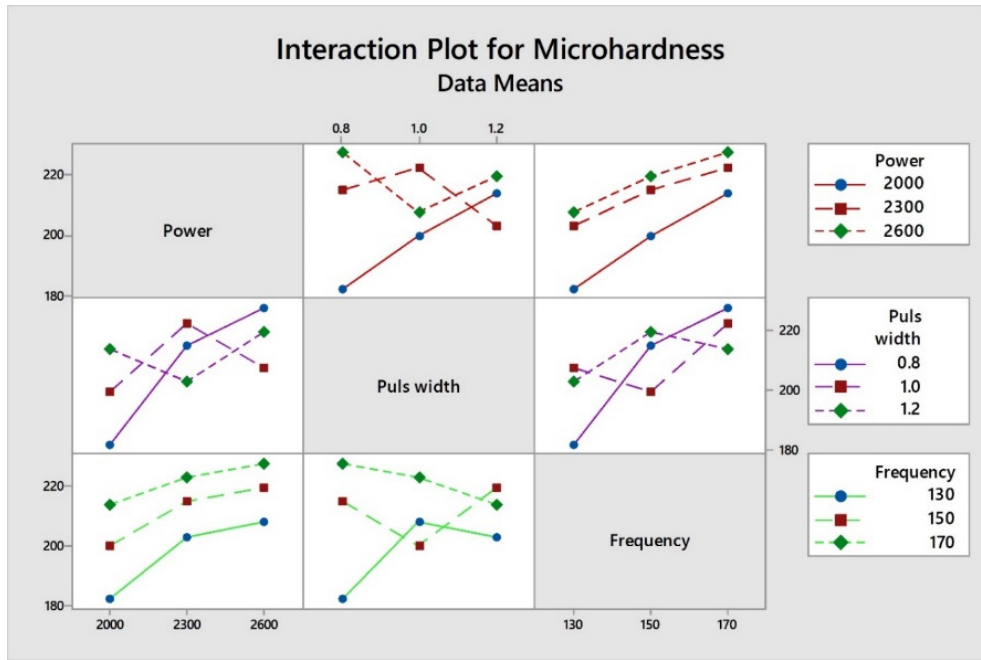
Fig. 1.5 Interaction plot between microhardness and power, pulse width and laser frequency
LASER TRUMPH TruPulse 556, 2 mm spot diameter, powder feed rate of 4g/min [PSC18].

During last 8 years and using different types of lasers (CW or pulsed), I have performed numerous experimental tests by coaxial laser cladding with powders with the aim to further develop the cladding technique, to optimize the process parameters and to enhance the quality of the cladded layers, as an answer to the demands of the industrial sectors. I advanced the industrial applications of laser cladding by reconditioning various components, such as the

following: injection / compression dies or moulds and various tooling or jet engine turbine blades. One of the main advantages of using the coaxial laser cladding technique with blown powder as the filler material is the ability to vary the composition of the powder by mixing different alloyed powders, either directly or by using different powder feeders [KUM14]. This feature allows the metallurgical behaviour of endless recipes variations of alloyed powders and coatings – substrate combinations to be studied.

From the same considerations, I have predominately used this laser cladding technique to fabricate single tracks or partially overlapped layers with pure and ceramic / composite powders to better understand the interdependence between the laser process parameters and the materials used.

1.3 Powders for laser cladding

One aim of this habilitation thesis is to analyse the main features and characteristics of the laser cladding process with powders, considering that special attention must be paid to the filler materials, which are in the form of powders. The cladding process is characterized by the diffusion phenomena, which creates good metallurgical compatibility between the substrate and the cladding.
To choose the right filler material, the following criteria must be considered:

- The type of filler materials (wire or powder);
- The physical, chemical and mechanical proprieties of the cladded layer (density, porosity, chemical composition, corrosion resistance, hardness, etc.);
- The metallurgical compatibility of the filler material and the substrate;
- The physical compatibility between the materials (similar or close melting points, thermal expansion coefficients).

Additionally, the powders for laser cladding must have a high coefficient of absorption for laser radiation and a highest vaporization temperature [JOH05].
The powders recommended for laser cladding are fabricated worldwide by prestigious companies that usually respect the ISO 9001 and AS 9000 quality standards. There are two main categories of powders, i.e., pure (e.g., Ni 100%) and alloyed powders (e.g., NiCrBSi).

The high-alloyed powders (superalloys) are fabricated by gas/ water atomizing in which each particle will have the same chemical composition or the alloyed power will be a mix of two or more pure/alloyed materials by mechanical blending. Depending of the chemical composition and manufacturing process, the shape of the powder particle may be acicular, lamellar or spherical.

Currently, the most used powders for laser cladding have the base element of a minimum of 50% Ni, Co or Fe alloyed with Cr, Al, Mn, B, Si, Ti and W. The powders are spherical (10 - 150 µm) and are obtained by atomization in water because the particle surface is more rugged (compared with gas atomization), with benefits on absorption of the laser energy.

There are a large number of studies reporting on the elaboration of new alloys recipes and optimization of the laser cladding parameters depending on the alloy used. Table 1.2 presents the main alloyed powders used in the various experimental studies that are discussed in this habilitation thesis.

Alloyed powders used for experimental tests and international references   Table 1.2

Filler material	Base material	Laser type	References	
			Author	International
Metco 15 E (NiCrBSiFeC)	AISI 5140	Rofin YC3300	[PSR16]	[DFK18], [DMA18]
Metco 439NS (Alloy Ni + WC)	C45	Coherent F1000	[SII13]	[DPG15], [LLL15]
Inconel 718 (Inconel 718)	AISI 304	TRUMPH TruPulse 556	[PSC18]	[NHL17]
Inconel 718 (Inconel 718)	AISI 5140	Coherent F1000	[PSR17]	[SLX19]
Metco 68F-NS-1 CoCrSiMo	AISI 5140	Coherent F1000	[PSR15]	[TAA08]
Metco 16C NS+ Inconel 718	AISI 5140	Coherent F1000	[SPT15]	[GGF08]
Metco 131 VF (Al_2O_3+TiO_2)	Cupru electrolitic	Coherent F1000	[PSS17]	[GTL12]
Metco 4010 A (Ti 99%)	VT3-1	TRUMPH TruPulse 556	[PMS19]	[LDZ17], [UKK15]

1.3.1 Nickel based powders

The Ni-based powders exhibit good resistance at high temperatures, high toughness and high corrosion and oxidation resistance. The NiCrBSi alloys are used for applications in the aeronautic industry, petrochemical industry and nuclear plants. The main alloying elements are boron and silicon, which have the role of enhancing the adherence with the substrate, and chromium, which enhances the oxidation resistance; through using different ratios of Cr-B-Si, the hardness and the wear resistance of the coating can be tuned. Coatings fabricated with Ni-based alloys are dense, compact and suitable for embeaming hard particles.
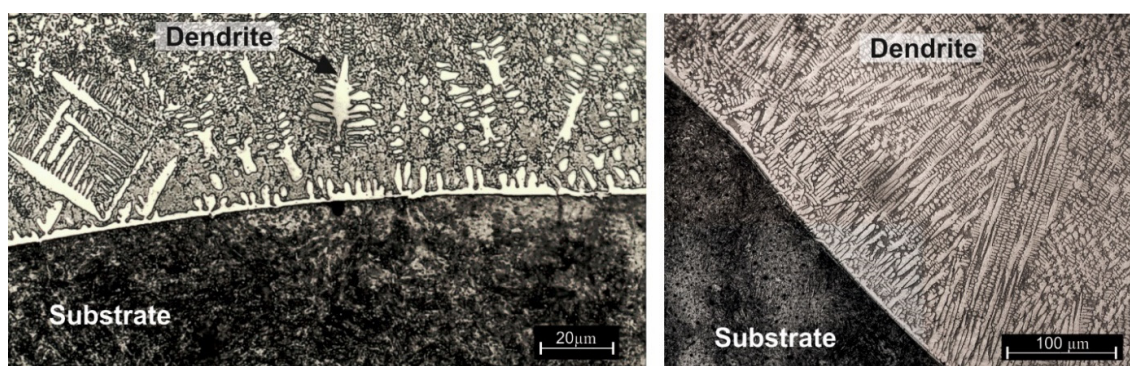
Fig. 1.6. Columnar dendrite structures at the interface with the substrate.

The microstructure of the cladded layers fabricated with a superalloy of 50% nickel is presented in Figure 1.6. Dendritic structures with the growth direction towards the solidification front are at the interface with the substrate.

As mentioned above, the Ni-based powders can be used as a binder for chromium-boron carbides or WC-based cemented carbide, which can strengthen the metal matrix. To exemplify, Figure 1.8 shows the laser-cladded layer of a Metco 439 NS alloy on a C45 steel substrate. The chemical composition of the powder is presented in Table 1.3. It can be observed that the Metco 439 NS is obtained by mechanical blending of a self-fluxing Ni-based alloy and a WC-Co hard particle.

Chemical composition of Metco 439NS [Oerlikon Metco® datasheet]   Table 1.3

Chemical composition	WC12Co [%] from total	Ni [%]	Al [%]	Cr [%]	B [%]	Fe [%]	Si [%]	C [%]
Metco 439NS	50	82	2.8	5.8	1.3	1.4	1.4	0.3
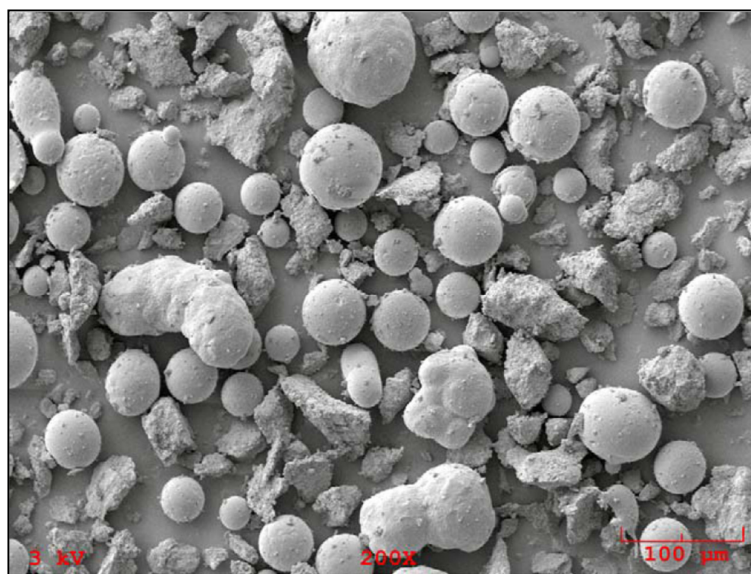
Fig. 1.7 Mechanically blended alloy Metco 439NS [***OER19].

According to the manufacturer specification [OER19], Metco 439NS (figure 1.7) can produce hard, dense coatings with a hardness between 50 to 56 HRC (depending the temperature of the melted bath, dilution and solidification rate). The cladded layers with Metco 439 NS are abrasion, cavitation and erosion resistant up to 820 °C. A preheating temperature and controlled cooling are key factors to reduce the cracking susceptibility of the cladded layer fabricated with this alloy.

Figure 1.8 reveals the tungsten carbide embedded in a nickel matrix. The tungsten carbides are not uniformly distributed, as they are agglomerated in islands. The absence of dissolution of the WC in the nickel matrix and the fast cooling of the metal bath produced isolated porosities in the proximity of the carbide islands. Additionally, during the microstructural examinations, a higher degree of porosity was observed at the substrate-clad interface where the high-density WC particles are trapped in a Ni- iron matrix.

Fig. 1.8. a) Cladded track b) and c) agglomeration of tungsten carbides, Etching: *Aqua regia* [SII13].

Nickel powders could produce coatings with low, medium or high hardness that are specially designed for applications where thermal expansion is a key attribute. A special category of the Ni-based powders is represented by the Inconel alloys. There are various types of Inconel alloys, but all are Ni based, and the main alloy element is chromium, in addition to Nb, Ta, Ti and Mo. The Inconel coatings are dense, pore free and exhibit excellent creep and stress rupture coupled with a good co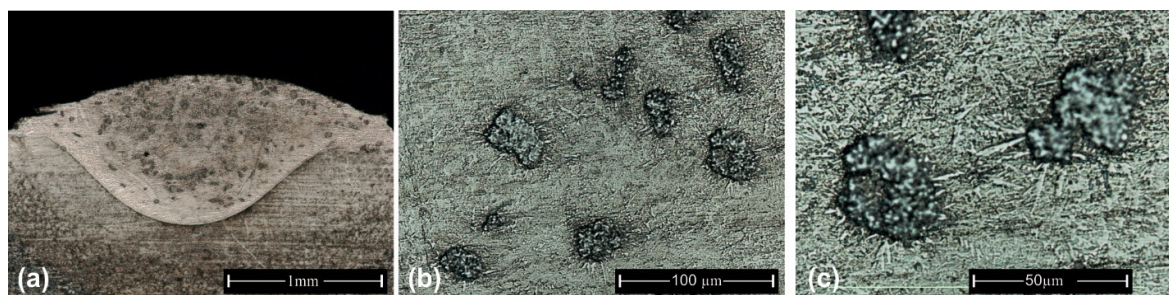rrosion resistance at high temperatures (up to 700°C). Once heated, the alloy forms a supplementary layer with high corrosion resistance.

The Inconel alloys can be used to repair worn parts, for enhancing new parts of metallic surfaces or for fabricating new parts by 3D laser cladding rapid prototyping.
In case of laser cladding with Inconel alloys (Inconel 718, Inconel 600, Inconel 625, Inconel 690), special attention must be given to the cooling time (solidification rate) to prevent the formation of phases and unwanted comp, which can reduce the harness or increase the cracking susceptibility.

To overcome this limitation, a post-heat treatment can be applied, according to the study presented in caption 3 of the habilitation thesis.

1.3.2. Cobalt based powders

Cobalt-based powders exhibit outstanding resistance to high temperature wear and are suitable for use in rough working environments where lubrication is a problem.
The cladded layers with Cobalt-based powders have a different aspect compared with nickel ones; they are darker, brittle and have a non-uniform geometry. Even so, the layers cladded with cobalt alloys (Stellite and Tribaloy) have high hardness, high wear resistance and a low friction coefficient.

As presented in [PSR15], Figure 1.9 shows the laser cladding of a Metco 68F-NS-1 alloy in a single-track experiment on an AISI 5140 substrate. The cladded tracks have been fabricated using a CW laser Coherent F1000 and a Precitec YC 50 cladding head.

Chemical composition of the powder and base material   Table 1.4

Material	C %	Co %	Si %	Mn %	Cr %	Ni %	Mo %
AISI 5140	0.36	-	0.22	0.65	0.98	0.09	0.01
Metco 68F-NS-1	-	49.4	3.4	-	17.5	-	28.5
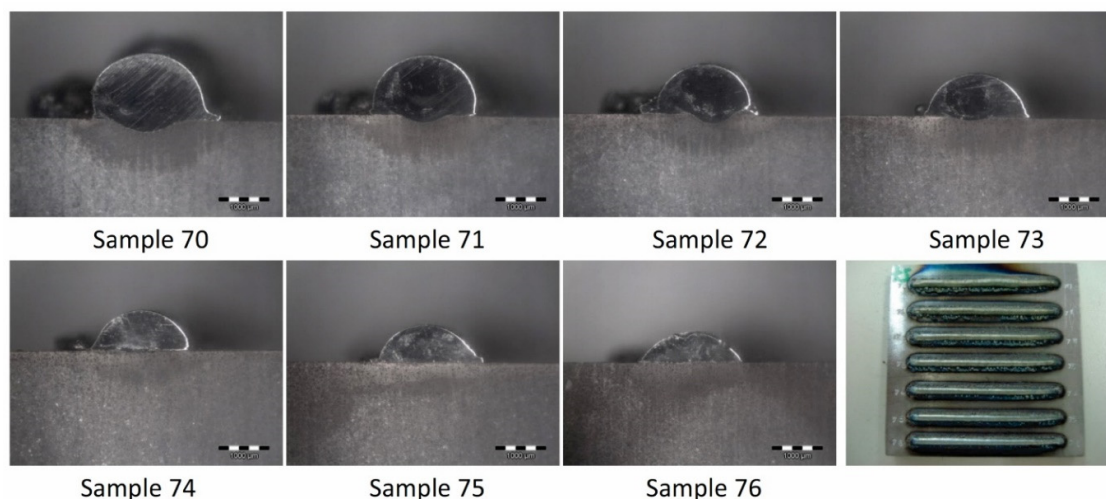
Fig. 1.9. Cross section of the laser cladding with the Metco 68F–NS-1 (mag. 10×) [PSR15].
(Laser power 1000W, powder feed rate 7g/min, cladding speed 3 – 9 mm/s).

The microstructural analyses of the Metco 68F–NS-1 tracks show the presence of superficial cracks, low dilution with the substrate and a very high wetting angle (between 45 – 90 degrees). All obtained cladded tracks have a dendritic microstructure. In fact, during the microstructural examinations, it was observed that dendrite formations are oriented towards to the middle of the cladded track to the area where the thermal gradient is more pronounced. Hard precipitations, molybdenum-silicon-based intermetallic Laves phases, are evenly dispersed in the solid solution cobalt matrix and confer high hardness to the coating.
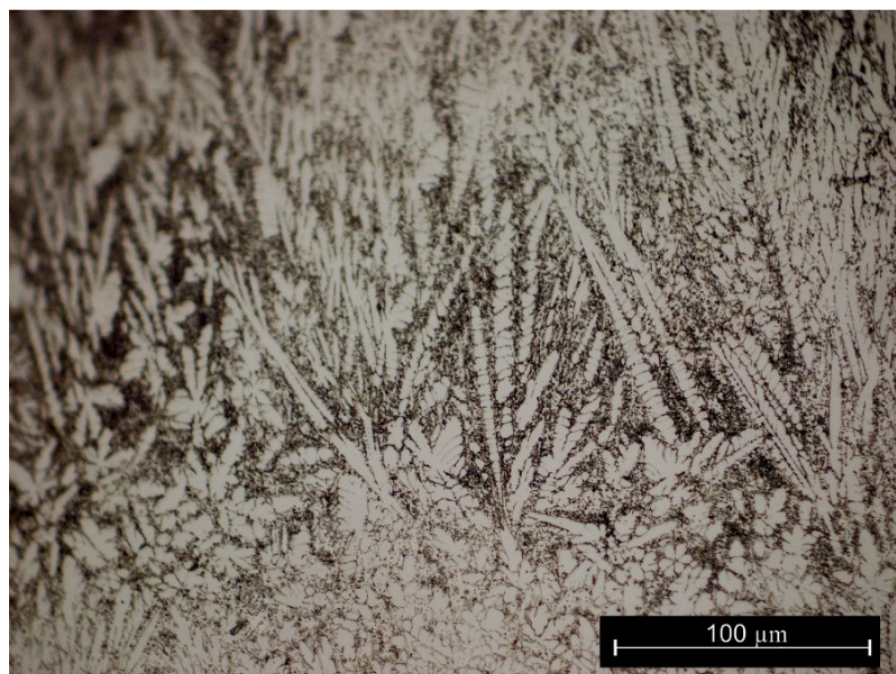
Fig. 1.10. Microstructure of the cobalt base cladded layer [PSR15].

27

Cobalt-based powders can exhibit the best corrosion resistance, especially with the addition of W, Cr or B carbides. The Cr and B form complex carbides and borides that enhance the resistance of the metal matrix, and the WC remains unmelted and partially distributed in the cobalt matrix. Those powders are the best choice if the best wear resistance is required. Nonetheless, the cladding of carbide alloyed cobalt powders is a very difficult process because of the specific problems, such as cracks, porosity, poor adhesion and the optimization of process parameters is mandatory for obtaining high-quality coatings. Special attention must also be accorded to the powder humidity, as cobalt is highly hygroscopic.

After numerous experimental tests with nickel- and cobalt-based powders, the author compares the challenges, advantages and disadvantages of each material and discovers the high potential of using the nickel superalloys for a variety of research directions and industrial applications [PSS17], PSR17], [PSC18]. Therefore, Ni-based alloys will be preferentially used for the further experimental research presented in this habilitation thesis.

1.4 Laser cladding in scientific research

The advantages of the laser cladding process are recognized by the industry and by the international researchers that continuously contribute to the further development of the technology [TOR13]. Comprehensive studies have been carried out in the last 20 years concerning the reducing of the cracking susceptibility, improving the wear and corrosion resistance by improvement of the cladding techniques, parameter optimization or by designing new types of alloys or composite materials, etc.

1.4.1 Parameter optimizations

Laser cladding with powders is an interdisciplinary technology characterized by some dominant key parameters, such as the laser power, powder feed rate and cladding speed, which influence the quality of the cladded layer [RML13], [RRR16], [YYZ18]. Numerous research papers have studied the optimization of the mentioned key parameters for improving the geometry and mechanical behaviour of the cladded tracks [KTG19], [RPS18], [KTG19], [HXS18].
In addition to the main parameters, the laser cladding process depends on numerous secondary parameters that can alter the quality and the repeatability of the process, e.g., the focal distance, powder velocity, cladding head tilting, and preheating of the powder and/or

substrate. According to Tianbiao Yu [TLY18], laser cladding has become a hot spot in the field of materials surface modification. He used the Taguchi DOE applied in a matrix of 25 groups to optimize the laser power, speed and powder feeding rate as function of three response targets (cladding width and height and dilution rate). Using a similar method, statistical analysis and optimization of the cladding process, Sun [SUH12] determined that powder feed rate is the dominant factor regarding the width and clad height, and the cladding speed has a major influence on the molten depth of the substrate.

The key parameters of the laser cladding process were predicted and analysed by the regression method (RA) by Mohammad [MHH17]. A total of 36 laser cladding tracks of WC-12Co powder on AISI 321 stainless were used to determine the influence of the main parameters on the clad high, melt depth and wetting angle.

Further research in the direction of parameter optimization was carried out by Nagulin [NIS18], who used Schlieren imaging and high-speed imaging to visualize the gas and powder flow during multi-jet coaxial laser cladding. In this case, the optical imaging technique allows the optimization of the distance between the workpiece and the nozzle. In addition to the stand-off distance, the tilting angle of the cladding head plays an important role on the geometry profile of the cladded tracks. In a recent study, Hao [HML19] used an analytical model to predict the bead shapes as function of the cladding head tilting angle. The obtained predictive models is a step forward in the building of 3D components by laser cladding.

When taking about the process parameters, an important role is played by the materials used because each powder and base material could have different proprieties in term of the absorption and reflection of the laser beam. For this reason, the process parameters must be fine-tuned for each filler material-base material configuration.

1.4.2 Nickel-based superalloys: Colmonoy and Inconel

The Ni-based powders (Colmonoy, Inconel) have a high resistance to impact, to corrosive environments and generally have good behaviour at high temperatures. NiCrBFeSi, belonging to the larger Colmonoy superalloy family, represents one of the most frequently used and versatile materials in relation to laser cladding, having as advantages a relatively lower price, high hardness and corrosion resistance in comparison to other similar materials [HOH13], [FHC15]. Its high hardness is ensured by the formation of complex carbides and borides, among which the most important are Cr_7C_3, Ni_3B and Ni_2B. However, the formation of these compounds is also responsible for a relatively high cracking susceptibility of the hard coatings,

thus limiting the performance and lifecycle of the material [WLC08]. To date, many studies have involved NiCrBSi alloys for single or multipass laser cladding process investigations. Devojno et al. [DFK18] determined that optimal particle size for the NiCrBSi self-fluxing alloy is in the range of 20 – 80 μm, as larger or smaller dimensions cause a disturbance in the powder flow pattern.

The influence of the scanning speed is investigated by Chen et al. [CLS15], who successfully fabricated a NiCrBSi coating by laser cladding on a substrate of a Ti_6Al_4V alloy. A dilution of 64% and no phase modification were observed at scanning speeds of 5-15 mm/s. Further increasing of the speed (20 mm/s) causes a major decrease of the dilution and modification of the phase constituents. The same material couple, i.e., NiCrBSi and Ti_6Al_4V, was used by Sun et al. [SYG00] to improve the wear resistance of the titanium alloy. The fine particles of TiB_2, TiC and $M_{23}(CB)_6$ emblemed in eutectics of γ-Ni, Ni_3B and silicides produce a 1000 HV hardness on the cladded layer, thus conferring an enhanced wear resistance in comparation with the substrate. The dry sliding wear resistance of the NiCrBSi alloys was also examined by Fernandez et al. [FCG05]. The microcracks that occurred during laser cladding cannot be totally avoided; nevertheless, a hardness of over 850 HV_{300} and good wear behaviour were obtained. The clad presents a thin layer of oxides that acts as a lubricant at lower dry sliding speeds (0.65 m/s). A microhardness improvement of the NiCrBSi was attempted in a recent study by Zhai et al. [ZBZ19]. An electromagnetic field is used during the laser cladding process to modify the microstructure and properties of Ni-based coatings. The content of the CrB hard phase was higher under the electromagnetic field with direct influence of the microhardness, which increases to average values of 700...1000 HV_{02}.

 Another method to improve the hardness of NiCrBSi alloys is the addition of ceramics or carbides, e.g., TiC, WC. Luo et al. [LLG15] fabricated WC/Ni−NiCrBSi composite coatings on Ti6Al4V. The WC/(Ni−NiCrBSi) contributes to the improvement of the wear resistance due to the reinforcement of the Ni matrix with WC and TiC. The microhardness increases with the variation of the NiCrBSi content (0 to 70%), but a decreasing of fracture toughness is simultaneously observed. Luo determined that the addition of 21% Ni into the 30 wt.% WC-NiCrBSi alloy is the optimal ratio for improving the wear resistance of the composite cladding. In another work [OGC17], different ratios of NiCrBSi and spherical WC (10, 20, 30, 40 and 50 wt% WC) were used to examine the distribution of the non-melted carbides in the cladded layer. A dual powder feed was used to independently control the WC and NiCrBSi powder. Using an optical microscope and image processing software showed that 80% of the feed

carbides are present in the coated layer. The carbide content is higher at the bottom of the layer, and it is concluded that the final thickness of the layer after the grinding process is very important for obtaining a certain wear behaviour.

Spherical WC (40–160 μm, 750–1200 μm) and blocky WC (250–400 μm) in conjunction with a NiCrBSi alloy were used by Deschuyteneer et al. [DPG17] to investigate the carbides' shape and size influence on the wear resistance of the composite claddings. The largest spherical WC particle ensured the improvement of the wear behaviour by a factor of 2.

Although WC is the preferable hard particle used for hardening the metal matrix, several other elements can be used for refining the microstructure and to mitigate the cracking susceptibility of the coating. Refining elements with high affinities to Cr and B are used to reduce the dimensions of the chromium boride and carbide phases [JOW15], [LLL15]. Hemmati et al. used 2% and 5% wt. vanadium to refine a NiCrBSiC alloy cladding on S355 carbon steel [HRO13]; the coating presents a lower cracking tendency as a result of VC particle formation but is also accompanied by a significant reduction in hardness. By mixing TC4 and the rare earth oxide CeO_2 with the Ni60 alloy (NiCrBSi), Yanan et al. [YRW19] was able to reduce the cracking sensitivity on Ti811 alloy. The wear resistance and microhardness are improved in the case of a 2 wt.% CeO_2 addition. The addition of Tantalum can also enhance the microhardness by in situ formation of TaC particles in a NiCrBSi matrix. The work of Yu et al. [YDD11] revealed that Ta refines the coarse carbides and improves the abrasion wear resistance of the Ni clads. Wang [13] maintained that the addition of V_2O_5 enhances the toughness, refines the microstructure and reduces the cracking sensitivity of the high Ni alloy coating. In addition to NiCrBSi, many researchers have paid attention to Inconel 718 alloys due to its high application potential. The Inconel alloys are Ni-based alloys with the addition of Cr, Nb, Ta, Ti and more iron. This chemical composition ensures good mechanical behaviour, even at a higher temperature, but the coatings are susceptible to boundary liquidation cracking.

As [ZSL05], [XLL13] stated, the process parameter optimization may provide crack free Inconel layers. Zhang [PRC14] used a continuous wave fibre laser to deposit IN718 powders on IN718 substrates and reports the presence of defects, such as porosity, un-melted powder and metal liquation cracking, in the coating. As [PRC14] reported, the liquation cracks may be healed after a post-clad heat treatment.

In another work, Zhang et al. [ZLN13] investigated the carbide and nitride precipitation during the laser cladding of Inconel 718 on the 1045 steel substrate. The size and amounts of carbide and nitride are related to the cooling rates induced by the scanning speed. After an elaborate

study, Sui et al. [SCM19] declared that lava phases are the crack sources in the case of Inconel 718 laser cladding. A short-time ageing heat treatment of Inconel 718 has good results in term of the stress rupture life. The risk of the appearance of microcracks increases with the thickness of the cladded layer. Therefore, in the case of partially overlapped tracks or of multilayers, a temperature limitation between each layer during laser processing is mandatory. Baldridge et al. [BPF13] used a high power Yb Fibre laser to obtain successful multilayer cladding of Inconel with minimal porosity and surface defects. The defect-free layers were cladded with an optimized laser power, cladding speed, powder feed rate, overlapped degree and optimized preheating temperature.

Numerous studies [SLF09], [NOP14], [OLO05] have reported that optimization of the laser cladding parameters in the case of Inconel alloys is the best method to decrease the liquation cracking susceptibility. Song et al. [SLF09] demonstrated that process parameter optimization and Ni-Cr-Fe-Si-B composition adjustment is a good method to improve the forming microstructure, plasticity and toughness of the cladded layer.

The literature survey shows that for Ni-based alloys, only the right balance between the power, speed and feed rate can mitigate the cracking susceptibility and ensure further enhancement of the clad quality by obtaining a fine and uniform microstructure.

1.4.3 Amorphous coatings

The amorphous, also known as metallic glasses (MGs) have attracted a great amount of scientific interest due to their special mechanical and physical characteristics. The laser cladding process has all the characteristics necessary to obtain amorous coatings, namely, rapid melting and rapid cooling of the melted bath. Numerous studies have revealed the potential for laser cladding in biomedical applications by fabricating bioceramics, hydroxyapatites and bioglass.

The Fe-based MGs have received great interest due to the abundance of the raw materials and the low cost of the alloys. Laser cladding of Fe-based amorphous remains a challenging procedure because of the high cracking susceptibility of the metallic glasses. Lou et al. [LHW18] obtained a crack free $Fe_{37.5}Cr_{27.5}C_{12}B_{13}Mo_{10}$ amorphous coating on a C45 steel substrate by applying a triple laser cladding strategy. First, a rapid laser scanning ensures the substrate preheating; during the second scan, the amorphous coating was cladded; the third laser scan was applied to in situ release the thermal stress. Improved wear capabilities were

obtained in comparation with the traditional crystalline C45 steel. In a recent study, Ibrahim [ISK19] fabricated an Fe-based metallic glass (FeCrMoCB) as a biocompatible coating on a Cronidur30 alloy. The amorphous-crystalline structure (AP) increased the corrosion resistance of the coating and exhibited a non-toxic behaviour, as proved by a cytotoxicity study. FeCrCoNiAlMox [JLJ19], FeCoCrMoCBY [WZG17] or FeCoBSiNb [ZLH12] are other examples of amorphous coatings that have been successfully fabricated by the laser cladding process.

A high entropy alloy (HEA) can also been obtained by laser cladding; also, combining HEA with AP can further confer the special mechanical proprieties of the coatings. In a recent study, Shu [SZL19], fabricated a CoCrBFeNiSi high-entropy alloy (HEA) coating on H13 steel by laser cladding with an SL-80 Nd: YAG laser machine. A different amorphous content was obtained as a function of the cladding parameters, but the best wear and corrosion resistance were attributed to the higher amorphous content. The Fe-to-Co ratio is an important factor that influences the amorphous phases of FeCoCrBNiSi high-entropy coatings, as determined by Shu [SYD18]. Similar studies conducted by Fengyuan Shu [SWZ18], [SLZ18] highlighted the importance of the high-entropy alloy amorphous coatings, which have an extensive potential for industrial applications in nuclear power plants.

In addition to the industrial applications, a special material, namely, Hydroxyapatite (HA) (chemical formula $Ca_{10}(PO_4)_6(OH)_2$), is widely used in medicine for the coating of dental implants and artificial bones. Laser cladding is a good method to obtain metallurgical bonding of HA, with the substrate obtaining partially amorphous coatings that preserve the bioactivity of the original alloy. Hydroxyapatite (HA) and SiO_2-HA laser cladding on Ti–6Al–4V was successfully realized by Yang et al. [YSH11]. The addition of SiO_2 clearly improves the biological behaviour due to a higher rate of cell attachment and proliferation on the coating being observed. Huang et al. [WCM08] synthesized a hydroxyapatite coating by preplaced laser cladding using sodium silicate as the adhesive for the powder mixture and obtained compact HA bio-ceramic coatings on a commercially pure titanium grade Ta2 substrate. Different binders [PWW11], such as water glass or poly (vinyl alcohol), are tested for inter-particle adhesion improvement as well as for improving the bonding between the coating and the substrate. Further improvement of the HA coatings can be obtained by the addition of carbon nanotubes, which increases the microhardness of the functionally graded bio ceramic-layer by 46.8% and almost doubles the bonding strength (28.2 MPa) compared with a pure HA coating [CHH11]. The mixing of HA with another ceramic oxide can increase the low mechanical proprieties of calcium phosphate, which is inherently brittle. Aluminium and titanium oxide, in

the form of dried powder or as a preplaced paste, are commonly used for obtaining high-quality ceramic-amorphous coatings. Chen et al. [CWM13] used spray-dried sintered Al_2O_3-13wt. % TiO_2 to obtain crack-free coatings with fine metallurgical bonding to the substrate. The same ceramic alloy is used [XZZ12] for laser cladding with induction heating to ensure constant heating during the cladding process. Through this method, a temperature beyond 2045 °C was obtained as the aluminium oxide fully melted.

In summary, various types of amorphous coatings have been developed since the laser cladding technology has become available. However, special attention must be accorded when obtaining metallic glasses to prevent the cracking or delaminating of this high hardness material.

1.4.4 Nanocomposites for laser cladding

It is widely accepted that one solution to further improve composite coatings is adding various nanomaterials that can add the specific proprieties of lubrification, hardening or strengthening of the metallic matrix. Thus far, two types of nanomaterials have been employed for embedding in bulk metal phases, namely, ceramic nanoparticles (carbides, nitrides, borides, oxides, and metal sulphides) [CAV14], [RKP16], [SLH03] and carbonaceous nanostructures, such as nanotubes (CNTs) [TYW01], [LSZ14], [NRT17], [HNS08], [CAV14], [SNL12] or graphene oxide [LRC14], [DHS14] with an emphasis on the former type. Currently, in addition to the consecrated synthesis methods, nanomaterials can be produced by a solar synthesis process that uses inexpensive solar energy and is environmentally friendly [PBP16], [PSC18], [SPR18].

A literature survey shows that nanoparticle and carbon nanotube reinforcement of polymer matrices has been studied in detail, but thus far, relatively few studies has been conducted regarding the application of these nanomaterials to improve the mechanical properties of metallic materials [LRC14].

Generally, the following two distinct mechanisms are responsible for the improvement of the coatings, depending on the nature of the metal matrix (1): the carbonaceous nanomaterials react with the metal phase in a molten state, generating carbides with high hardness [LSZ14], [HTS11] or (2): they do not dissolve into the metal phase, providing, in turn, mechanical strengthening, either through the load transfer effect, through refinement of the metal grains (the CNTs are located at the grain boundaries), or through interaction with dislocations at the

atomic level [CAV14], [SAN12]. The former mechanism was reported for titanium [LSZ14], [SNL12], aluminium-copper alloys [BLA10] and silicon-rich metal alloys [TJO13], while the latter was reported, for example, in the case of mild steel [ISM10], pure iron [LRC14], nickel [HNS08] aluminium [KTK13], [ZBK16] magnesium [DIE11] and copper [CJC13], [TYW01], [UMW10]. When embedded in the metal, good interfacial adhesion between CNT and the metal phase has been observed, due to the formation of a thin intermediary layer of metal carbide on the nanomaterial surface, thus avoiding delamination [CRJ06].

While for metal-carbonaceous nanomaterial assemblies, there are several studies focused on bulk materials obtained through powder metallurgy methods (furnace sintering, laser sintering, thermal spraying, consolidation of mechanical-milled composite metal- CNTs powders, and so forth) [BLA10], [TJO13], there are fewer studies involving the obtaining of metal-carbon nanomaterial coatings [CTW03]. These coatings can be obtained through several technologically relevant and up-scalable approaches, among which cladding by pre-placing a mixture of CNTs and metal powder on the metallic substrate in the form of a paste followed by selective melting with a concentrated energy source (continuous-wave lasers, pulsed lasers, focused electron beams) [SNL12], [ISM10], [LSZ14], [DHS14], [HTS11] or thermal spraying of metal-CNT powder mixtures [MKP18] are the most employed. Incorporation of carbon nanotubes in coating presents some limitations because the carbonaceous materials are susceptible to thermal degradation. These limitations are maximized in the case of laser cladding in comparison with other coating processes (e.g., thermal spraying) due to the high temperature generated during the laser processing.

Lei et al. [LSZ18] successfully fabricated a composite laser-cladded layer reinforced with carbon fibres by using a Ni25 alloy as the metallic matrix and 1Cr13 stainless steel as the substrate. The grain refinement and reduction of the content of the precipitated M7C3 and M23C6 carbides was obtained in the CFs/Ni-based coatings. The CFs addition improved the wear and corrosion resistance of the coating. The effect of the carbon fibre content in a CFs/Ni-based coating was also analysed by Shi et al. [SLZ18]. Various fractions of the CFs (0 vol% to 9 vol%) were mixed with C0.8, Cr14.5,Fe15, Si4, B3.5, Ni alloy and deposited by the preplaced laser cladding technique. The results indicate that the best results in term of microhardness and tensile strength have been obtained at a ratio of 6 vol%.

Other studies about laser-cladded metal-CNTs coatings have been conducted on non-ferrous metal powders and substrates (mainly based on copper, aluminium, and titanium) [CTW03], [BSB08]. The nickel- and iron-based coatings reinforced with CNTs, in conjunction with steel substrates, bear a higher application potential but also have limitations due to their relatively

high susceptibility to embrittling and cracking [LRC14], [LIR14]. The literature underlines that nanomaterials in the form of nanoparticles or carbon nanofibre/nanotubes have high potential as a cost-effective approach to fine tuning the coating's mechanical characteristics.

Motivation behind the thesis

Despite the achievements reported above, the laser cladding process is still an emerging technology that requires further investigation. Most of the works accomplished so far share the same results and cover a wide range of scientific investigations, but there are still topics that needs to be further experimentally analysed. In the last five years have been published more than 5000 articles indexed in the Web of Science core collection as presented in figure 1.11.
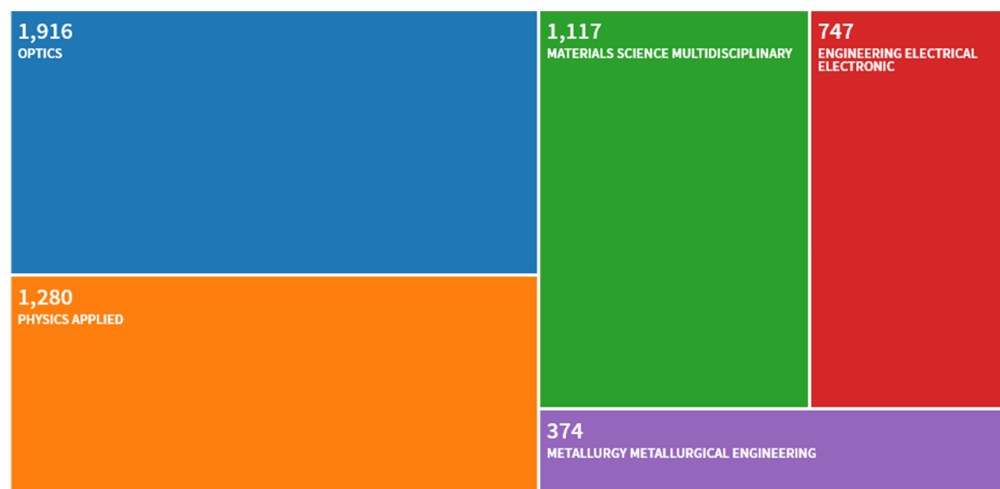

Fig. 1.11 Article related with laser cladding published in the last 5 year according to Web of Science data base [on 14.10.2019].

This habilitation thesis aims to fill some gaps in the field of laser cladding technology by summarizing a collection of my 12 most important articles. The articles interconnect in the following two areas: fundamental and applicative research.

The presented data shows the importance of the fundamental research in the field of laser cladding as being the only method for developing new alloys or laser cladding techniques. In addition, the industrial applicability of the cladding process is revealed by presenting two case studies of worn part reconditioning via laser cladding.

The motivation behind this habilitation thesis rises from the requirements to take the next step in academic career advancement, which involves the tutoring and advising of future doctoral students from the Transilvania University of Brasov.

Cap. 2 LASER CLADDING WITH POWDERS

2.1 Laser cladding versus thermal spraying

2.1.1 Concept

There are numerous technological processes suitable for fabricating coatings to protect or to enhance the proprieties of metallic surfaces. Conventional methods such as submerged arc welding, MIG/MAG or TIG welding, plasma welding or thermal spray coating are successfully used for obtaining of metallic, non-metallic or composite coatings. As previously stated, the continuous evolution of the laser technology led to the emergence of a new technique for coatings, i.e., laser cladding.

Table 2.1 [WIE08] presents the influence of different coating technologies on the fabricated layer proprieties (LC- Laser cladding, MMA- Manual Metal Arc cladding, MIG-Metal Inert Gas cladding, SAW- Submerged Arc Welding, TIG- Tungsten Inert Gas cladding, TS- Thermal Spraying, HVOF- High Velocity Oxy-Fuel, and PC- plasma cladding).

Various techniques for obtaining coatings [WIE08]   Table 2.1.

Process	Thickness	Deposition rate	Tensions	Precision	Dilution	Compactness
	[mm]	[Kg/hour]			[%]	
LC	0.2-2	0.2-7	Low	Low	1-5	High
MMA	1.6-10	0.5-2.5	Low	Low	15-25	High
MIG	1-6	2.3-11	High	Low	15-20	High
SAW	2-10	5-25	High	Low	10-50	High
TIG	0.5-3	0.5-3.5	High	Medium	10-20	Medium
TS	0.8-2	0.45-2.7	High	Low	1-10	Medium
HVOF	0.3-1.5	1-5	Low	Low	Low	Medium
PC	1-5	2.5-6.6	Medium	Medium	Medium	Medium

The main differences between the above coating techniques are related to the precision, deposition rate, dilution and the coat - substrate adherence.

The coating adherence is very good in the case of the welding processes (MIG/MAG, TIG) due to the increased melting of the substrate. It is not the case for the thermal spraying process, where no melting of the substrate occurs and the adherence is a key factor for obtaining a good coating with high delaminating resistance. The main characteristics of coatings fabricated by the laser cladding and thermal spraying processes are presented in Table 2.2 [TKC04], [PHT16].

Main features of the laser cladding and thermal spraying processes   Table 2.2

Features	Laser cladding	Thermal spray
Bonding strength	High	Moderate
Dilution	High	No
Reputation	Moderate to high	Moderate
HAZ	Low	High
Controllability	High	Moderate

Laser cladding and thermal spray coating are the most used coating techniques for reconditioning or for protecting metallic surfaces. A laser beam is used for melting the powder in the case of the laser cladding process and an oxy-acetylene flame forms the fine powder melted particles in case of the flame coating process (Figure 2.1).

Both processes are distinguished by several advantages and disadvantages. First, in case of laser cladding the cladded layer is mixed / diluted with the substrate due to the dilution phenomena induced by the high thermal gradient. This phenomenon did not appear in the case of thermal spraying where the melted powder is projected to the material with no metallurgical changes of the substrate [RPS14]. The main advantage of thermal spraying is the versatility and the possibility to coat large surfaces with a wide range of alloyed powders.
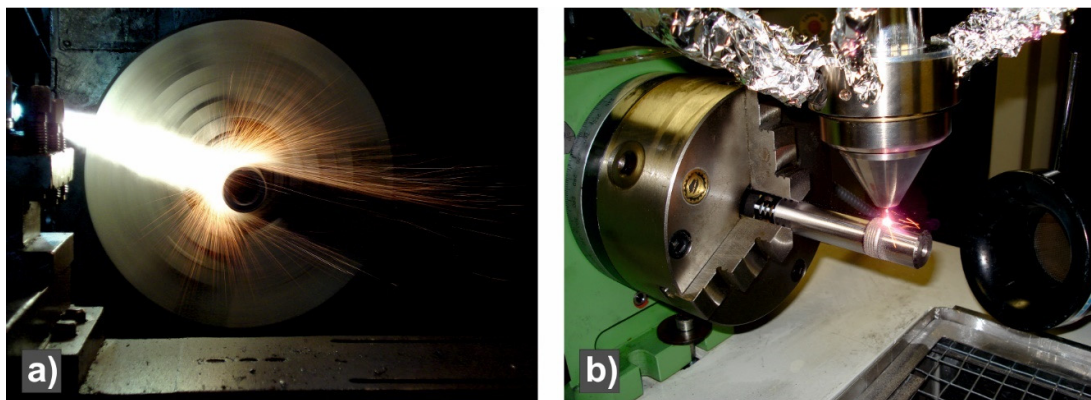

Fig. 2.1. Examples of the thermal spray process (a) and coaxial laser cladding (b) [PHT16].

Comparative studies on the main characteristics of the reconditioning process can be found in scientific literature; however, because those technologies are highly influenced by the process parameters and by the specific experimental set-up, I conducted an experimental study to compare the laser technology and conventional thermal spraying.

A supplementary objective of the study was to determine the behaviour of the powders designed for the thermal spraying process in the case of using them as a filler material for laser cladding. It is an important aspect because the majority of filler materials in the form of powder are specially designed for processes where the powder is only partially melted, e.g., thermal spraying.

For this purpose, the same filler material (powder Metco 15 E) and base material (AISI 5140) have been chosen to obtain a coated layer by laser cladding and by thermal spraying. The test results are disseminated in [PHT16].

The study was performed using a medium alloy steel as the base material, namely, AISI 5140, machined in round bar with the nominal diameter of 22 mm and a roughness of 0.8 µm. The chemical composition of the base material is presented in Table 2.3.

Chemical composition of the base material   Table 2.3

Material	Shape	Element wt. (%) *									
		C	Cr	Si	Ni	Fe	Mn	S	Mo	P	Cu
AISI 5140	Sheet	0.364	0.98	0.223	0.096	97.5	0.65	0.021	0.019	0.013	0.13

*Analysed by SPECTROMAXx Arc/Spark Optical Emission Spectrometry

The Metco 15 E coating material is a commercially self–fluxed gas atomized Ni–based powder that is frequently used for applications where high hardness and corrosion resistance are necessary. According to the manufacturing company, Metco 15 E can produce dense layers with hardness values between 55 and 61 HRC. The chemical composition is presented in Table 2.4.

Chemical composition of Ni based powder [according to Oerlikon Metco® datasheet]   Table 2.4

Power type	Chemical Element (%)						Powder average dimension
	Ni	Cr	Fe	Si	B	C	
Metco15 E	Bal.	17	4	4	3.5	1	5-100µm

2.1.2 Methods, materials and results

The experimental tests were conducted at the Centro Laser department of Universidad Politécnica de Madrid and at the Advanced Welding Ecotechnologies research centre of Transilvania University of Brasov. The laser cladding tests were performed using a Nd:YAG laser of 3.3 kW made by ROFIN (Germany) and a ROFIN cladding head manipulated by a 6 axes ABB robot (ABB IRB 6000). A Sulzer 10C powder feeding device was used for supplying the Metco 15E powder to the cladding head, under an argon (Ar 99%) gas flow. The cladding speed was obtained by means of a rotating device that can ensure constant peripheral speeds of 4.3 mm/s at the surface of the base material bar.

The thermal spraying process was realized using a CastoDyn DS 8000 system with the SSM10 standard metallization module and a mixture of acetylene (0.7 bar) and oxygen (4 bar) as the spraying gas. The sample was positioned and rotated by means of a universal lathe at 110 rev/min. The optimum process parameters were chosen from the previous studies [RPS14], [RIP13], [PII11] of the research team and from the literature related to the laser cladding and thermal spraying technology. The process parameters of the laser cladding and thermal spraying tests are summarized in Table 2.5.

Laser cladding and thermal spraying process parameters   Table 2.5

Laser cladding	Laser power	Cladding speed mm/s	Powder feed rate
Sample 1	780	4.3	6g/min
Sample 2	850	4.5	6g/min

Thermal spray	Module	Distance [mm]
Sample 1	SSM10	200
Sample 2	SSM10	170

Figure 2.2 shows the general appearance of the coating obtained by the laser cladding process and thermal spraying. It can be clearly seen in Figure 2.2(c) and (d) a significant difference in terms of porosity and density between the two deposited layers; the flame-deposited coating is characterized by a higher porosity. The porosity is produced due to the low velocity of the partial melted particle, which cannot ensure a good spread prior to the contact with the substrate.
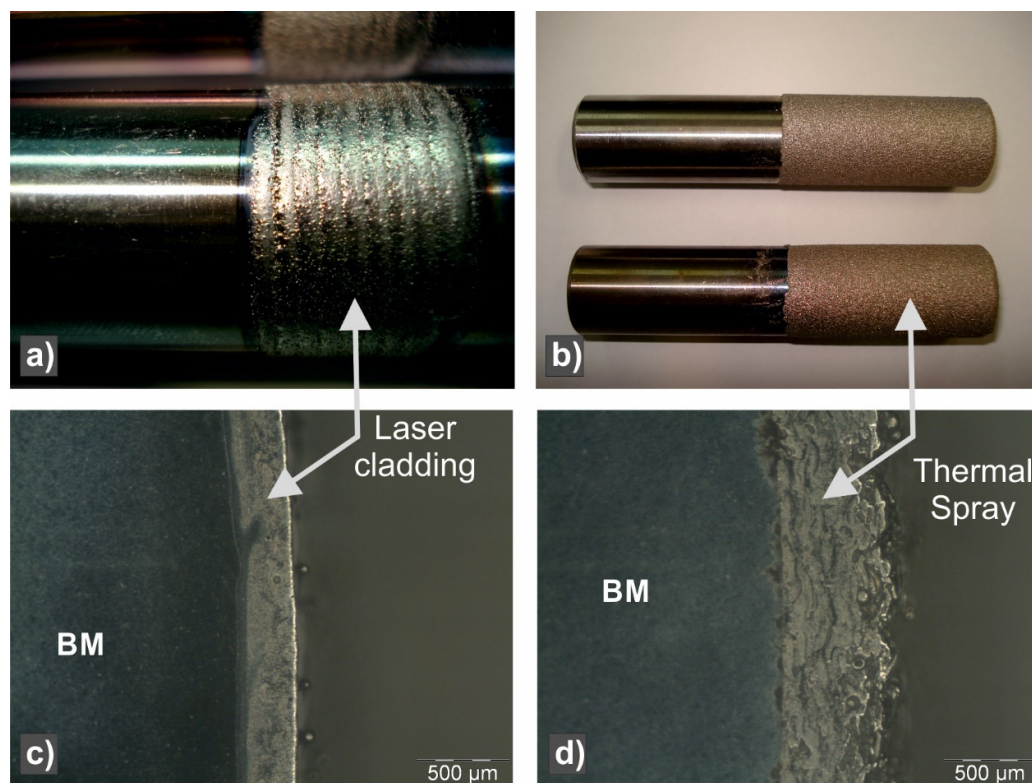
Fig. 2.2. a) and c) laser cladding: appearance and cross-section of the coating, b) and d) thermal spray: appearance and cross-section of the coating [PHT16].

The details from Figure 2.3 highlight the interface zone between the coated material and the substrate for both coatings. The laser-cladded layer is characterized by the presence of a columnar - dendritic structure developed in a matrix rich in Fe and by a well-defined non-interference line between the two materials. It is not the case in the coating obtained by thermal spraying, which is distinguished by the separation line between the materials, the absence of dilution and, therefore by the lack of adhesion to the substrate. The microstructure of the coated layer is composed mainly from hard particles embedded in Ni-based matrix and with large islands of oxide inclusion and pores. The absence of mixing between the materials is highlighted in Figure 2.3(c).

With respect to the SEM analyses presented in Figure 2.4, towards the upper part of the laser cladding (image (a), Figure 2.4), dendritic formations disappear, and the structure is characterized by the presence of rough compounds, carbides and chromium borides embedded in complex nickel-iron matrix. The separation line between the thermal sprayed layer and the substrate is visible in Figure 2.4(b).
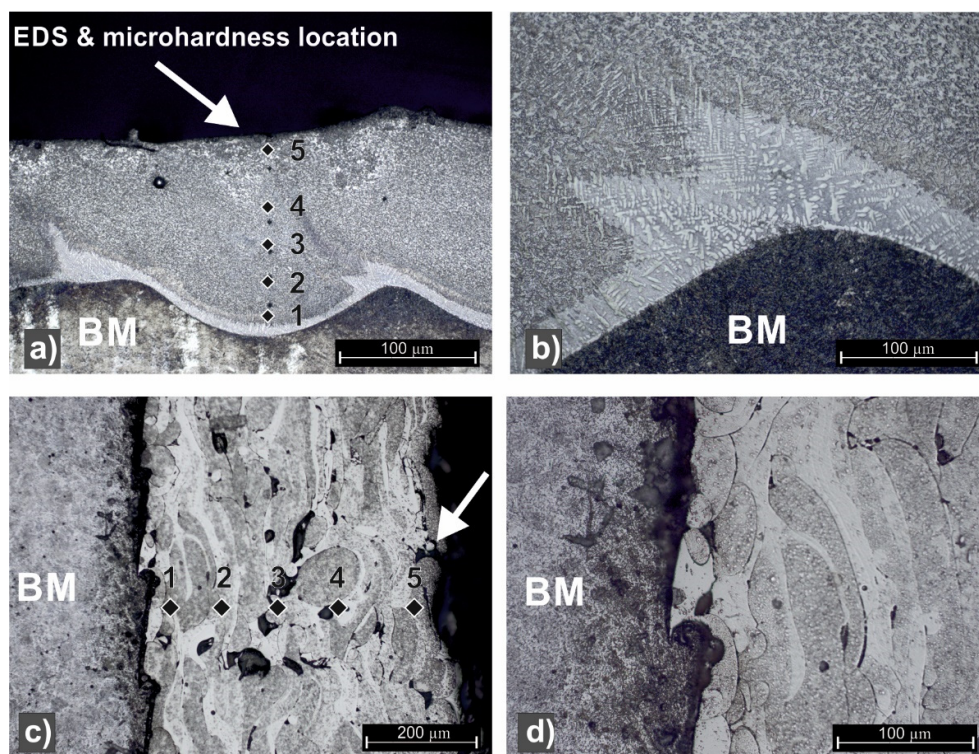
Fig. 2.3. Microscopy of the cross-section of the laser cladding layer (a, b)
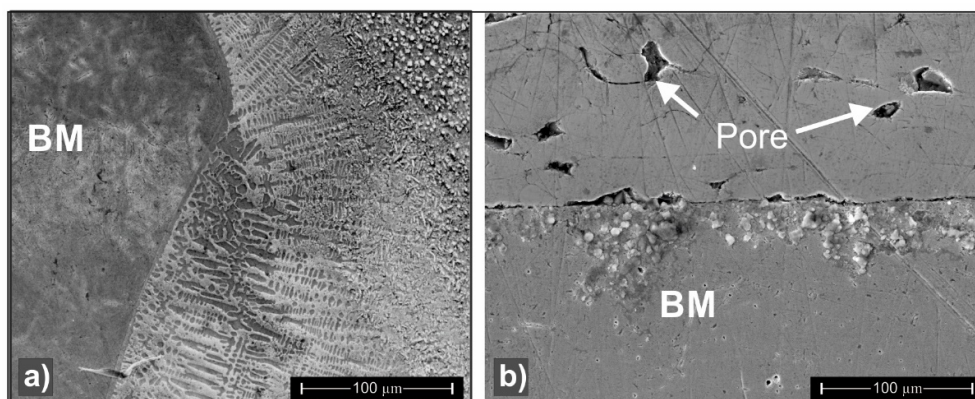and thermal spraying (c, d) [PHT16].

Fig. 2.4. SEM analyses of the laser cladded layer (a) and of thermal spray coating (b) [PHT16].

The hardness profile of the investigated sample is presented in Figure 2.5. In the case of the sample obtained by laser cladding, the microhardness is directly influenced by the dilution percent of the base material and with the amount of iron diffused from the base material into the cladded layer. The chemical distribution from Figure 2.6 reveals that hardness increases as the amount of iron decreases. It is not the case with the thermal sprayed sample, where the dilution phenomena does not appear, and the hardness has a more uniform distribution.
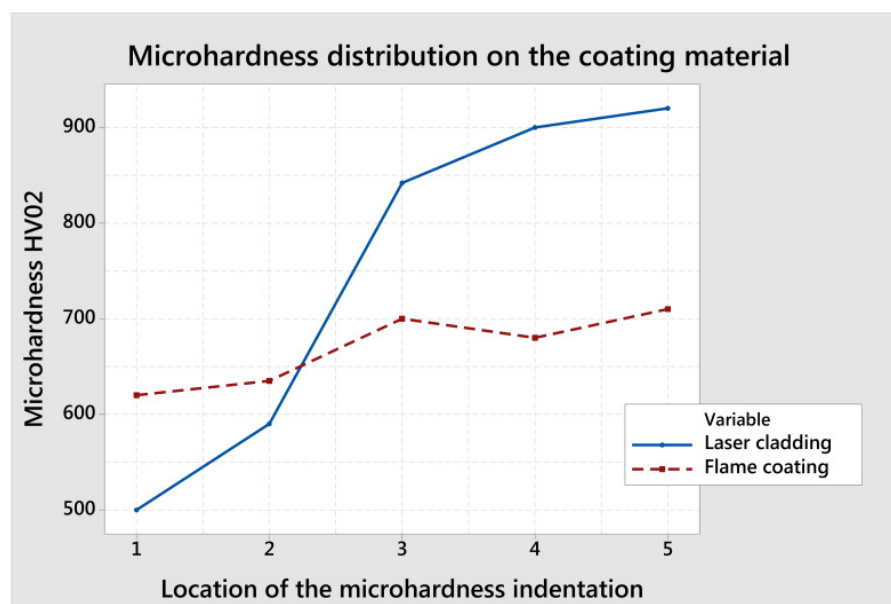
Fig. 2.5 Hardness distributions according with micro-zones from Figure 2.3 (a) and (c) [PHT16].

The chemical analysis realized in the microzones from Figure 2.3 (a) and (c) allowed the identification of the main alloying elements in the coated layers. In Figure 2.6, the distribution of these elements in the cross-section of the samples obtained by laser cladding and thermal spraying is presented. It can be observed that zone 4, which is associated with the upper part of the laser-cladded layer, is characterized by a smaller amount of iron transferred from the base material. As the investigated zones are closer to the interface with the base material, a change in the cladded layer composition emerges due to the diffusion phenomena potentiated by the temperature.

Due to the absence of the chemical mixture with the substrate, the flame-coated layer is characterized by a composition resembling that of the powder.

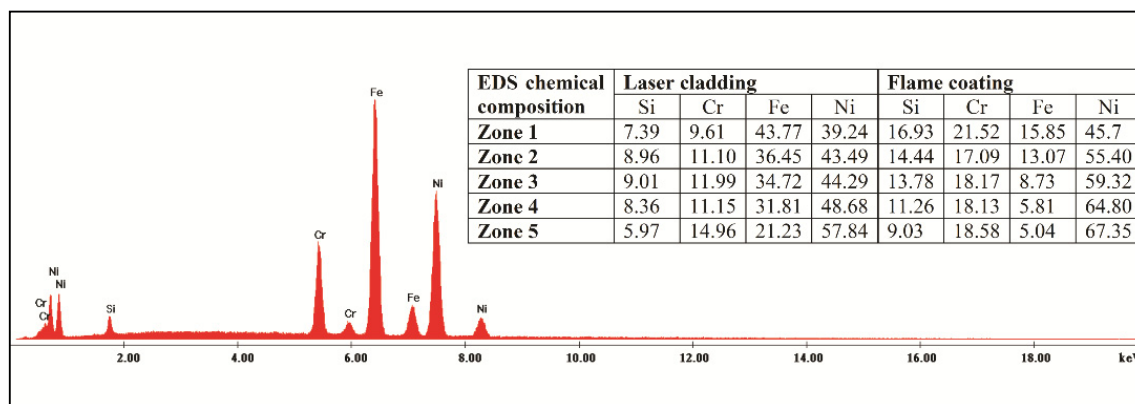| EDS chemical	Laser cladding				Flame coating			
composition	Si	Cr	Fe	Ni	Si	Cr	Fe	Ni
Zone 1	7.39	9.61	43.77	39.24	16.93	21.52	15.85	45.7
Zone 2	8.96	11.10	36.45	43.49	14.44	17.09	13.07	55.40
Zone 3	9.01	11.99	34.72	44.29	13.78	18.17	8.73	59.32
Zone 4	8.36	11.15	31.81	48.68	11.26	18.13	5.81	64.80
Zone 5	5.97	14.96	21.23	57.84	9.03	18.58	5.04	67.35

Fig. 2.6 EDS chemical composition of microzones indicated in Figure 2.3 (a) and (c) [PHT16].

This study [PHT16] demonstrated that laser cladding technique bears several advantages, such as a high layer density, low porosity and very good bonding with the substrate. The disadvantages are dilution with the base material and high cracking susceptibility compared with the coatings obtained by thermal spraying, which are characterized by no dilution and low cracking susceptibility. Nevertheless, delaminating of the thermal sprayed layers remains an actual problem that could be further potentiated by the action of a corrosive environment.

In conclusion, through laser cladding coatings, more homogenous microstructures and increased hardness compared with those coated by the thermal spraying method can be obtained. It must be mentioned that coatings with high porosity and high oxide content may be required in different applications.

In terms of the total cost of the process, the laser technology is far more expensive than other conventional process, such as thermal spraying, plasma spraying and so on. On the other hand, the laser cladding process can be the best technological solution for a wide range of applications, but it is recommended to be used only in the case of high added value components.

This experimental study was the foundation for choosing the laser cladding technology as the main research direction in my scientific activity. The study proves that laser cladding is a superior technology that can be used for high-quality industrial applications.

2.2 Laser cladding of Inconel 718

2.2.1 Concept

According to the previous description, Inconel 718 is an austenitic nickel-chromium-based superalloy. Inconel 718 is a precipitation-hardenable alloy with a high corrosion and oxidation resistance up to 700 °C and good tensile, fatigue, and fracture strength and good weldability. Due to these characteristics, it is frequently used in applications for aerospace (turbine or compressor blades), the chemical industry, pollution control equipment or in nuclear plants [MWZ15], [MVG14], [QID14].

The Inconel grade has been well known in engineering for a long time, but the specialized literature is limited regarding laser cladding of this material.

A solution in this direction has not been established yet because the process parameters are related to the equipment used (e.g., laser wavelength, beam geometry, and focusing optics).

Therefore, the Inconel laser-cladded layers have been enhanced by fine tuning the process parameters and by applying a post heat treatment to further improve the quality and the applicability of this superalloy [PSR17].

2.2.2. Methods, materials and results

A self-fluxing Inconel 718 alloy supplied by Sulzer Metco company, i.e., the MetcoClad 718 alloy, was used to perform the laser coatings on an AISI 5140 steel substrate. This low alloy steel is commonly used in the automotive industry for components subjected to medium wear. The chemical compositions of the materials are presented in Table 2.6 and 2.7.

Chemical composition of the base material   Table 2.6

Mat.	Shape	Element wt. (%)*									
		C	Cr	Si	Ni	Fe	Mn	S	Mo	P	Cu
AISI 5140	Sheet	0.36	0.98	0.22	0.09	97.5	0.65	0.02	0.01	0.01	0.13
		Al	N	Nb	Sn						
		0.026	0.017	0.003	0.008						

*Analysed by SPECTROMAXx Arc/Spark Optical Emission Spectrometry

Chemical composition of the base material   Table 2.7

Material	Element (%) *											Powder dimension
	Ni	Cr	Fe	Mo	Cu	Nb	Ti	Si	Mn	C	B	
MetcoClad 718	Bal	19	18	3	-	5	1	0.2	0.08	0.05	0.005	-90 +44 μm

* According to Oerlikon Metco datasheet

The experimental study was based on fabrication of Inconel 718 single tracks, as well as cladding of multiple overlapped tracks, once the optimal process parameters were determined. The single tracks were used to determine the optimal process parameter window and the overlapped tracks were used to obtain a uniform cladded layer on the surface of the AISI 4140 layer that can be further enhanced by heat treatment [PSR17].

The experiments were carried out using a Coherent F1000 diode laser together with a Precitec WC 50 cladding head manipulated by a CLOOS welding robot (Figure 2.7). The powder was provided to the cladding head with an AT-1200HPHV Termach feeding system and Argon gas was used for shielding and as the carrier of the powder. Tilting of the cladding head by 3° in the cladding direction and defocused the laser beam by 2 mm was used for all the cladding tests. The standoff distance was set at 12.5 mm.
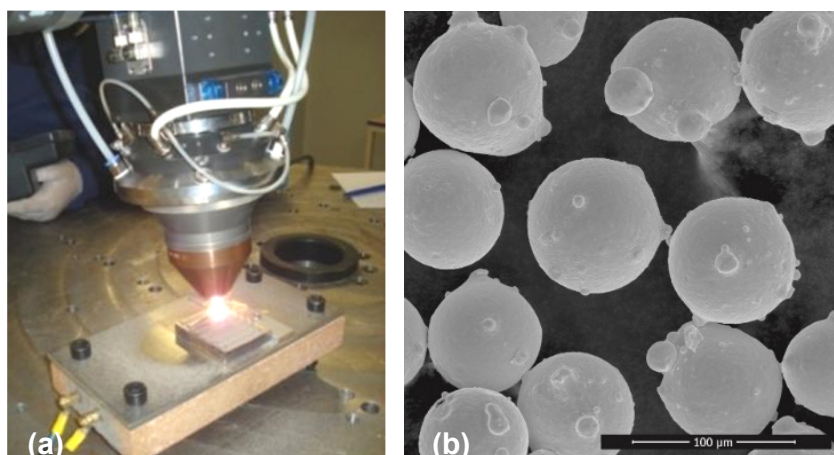

Fig. 2.7. (a) Experimental frame used for the laser cladding, (b) SEM microscopy of the Inconel 718 powder [PSR17].

Altogether, 8 single tracks of 80 mm were cladded with adjusted laser power in the range of 650-950 W at constant scanning speed of 3.5 mm/s and a 4 g/min powder feeding rate [PSR17]. The laser cladding parameters and the main geometrical dimensions are summarized in Table 2.8.

Laser cladding parameters and main geometry dimensions of the cladded tracks   Table 2.8

| Specimen		Sample 1	Sample 2	Sample 3	Sample 4	Sample 5	Sample 6	Sample 7	Sample 8
Parameters	Units								
Laser power	[W]	600	650	700	750	800	850	900	950
Power density	[kW/cm^2]	19.1	20.7	22.3	23.8	25.4	27.0	28.6	30.2
Powder feed rate	[g/min]	4	4	4	4	4	4	4	4
Cladding speed	[mm/s]	5	5	5	5	5	5	5	5
Clad high, (h_d)	[mm]	0.34	0.42	0.38	0.40	0.43	0.52	0.44	0.43
Clad area, (Ac)	[mm^2]	0.38	0.50	0.50	0.58	0.65	0.85	0.73	0.81
Clad width, (L)	[mm]	1.63	1.78	1.91	2.09	2.20	2.32	2.48	2.69
Melt depth, (p_d)	[mm]	0.13	0.15	0.17	0.19	0.20	0.20	0.24	0.29
Molten area, (Am)	[mm^2]	0.19	0.21	0.28	0.35	0.40	0.42	0.56	0.69
HAZ area	[mm^2]	1.21	1.34	1.60	1.82	2.18	2.31	2.54	2.91
Wetting angle(α)	[°]	141	135	145	148	146	138	150	147
Dilution	[%]	33.3	29.6	35.9	37.6	38.1	33.1	43.4	46.0
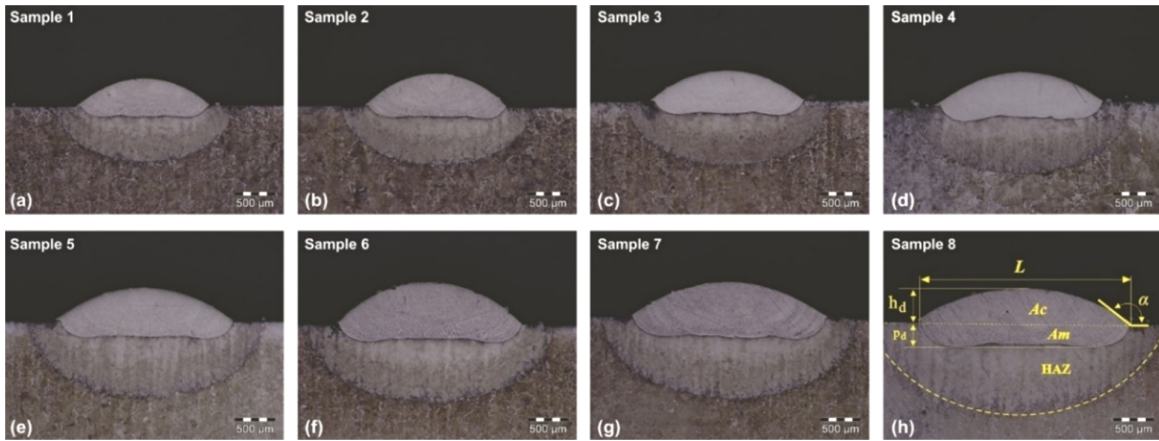
Fig. 2.8 Cross-section of the laser cladded tracks, (h) geometrical profile of the laser cladded tracks [PSR17].

The samples were prepared for metallographic inspection by electrochemical etching in a solution of 10% oxalic acid. The substrate's upper limit was used as a base for all measurements, and the geometrical dilution percent was calculated using formula 2.1.

$$Geometrical\ dilution = \frac{Am}{Am+Ac} \qquad (2.1)$$

were: Am is the molten area and Ac is the clad area according to Figure 2.8 (h).

Figure 2.8 shows the macro appearance of the Inconel 718 individual tracks. It can be observed that all the tracks have the same profile, with small modifications regarding the geometrical dimensions. The height and clad area of the single tracks are characterized by the laser power directly influencing the amount of melted powder. As the laser power increases, more powder is melted. Moreover, the dilution increases at a high power due to the ratio between the clad area and the molten area. By using a defocused laser beam, it was possible to maintain a low molten area and to increase the quantity of deposited powder.
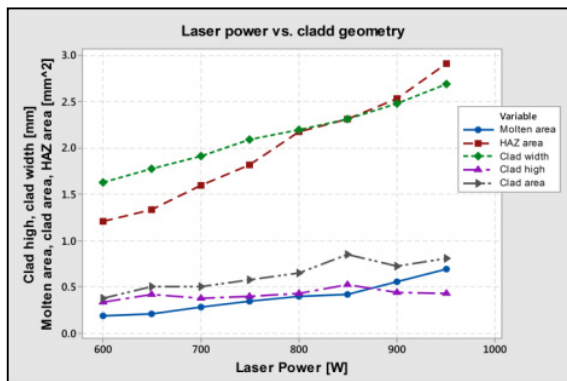

Fig. 2.9 Influence of the laser power on the molten area, heat affected zone area, clad area, clad width and height [PSR17].

With respect to Figure 2.8 and 2.9, the threshold value of the laser power is approximately 900 W; after this value, a sudden increase of the clad profile and heat affected zone occurs. The influence of the power density over the dilution is presented in Figure 2.9. Although the dilution apparently presents high values (29 – 46%), it must be taken into account that in case of partially overlapped tracks, the melted zone area will remain constant after cladding the first layer; then, for the following layers, the cladding thickness will be higher without influencing the melting depth. In this way, the dilution will be considerably reduced, namely, 40-50% dilution values in case of individual tracks will decrease to 10-15% in the case of partially overlapped tracks.

The diffusion line between the two materials can be observed in Figure 2.10 (a) and (c). Dimensionally, the thickness of the diffusion line (non-interference zone) increases along with the increase of the power used, namely, from 1.1 μm at 600 up to 1.9 μm at 950 W. Additionally, at high power densities, the emergence and emphasis of dendrite structures can be noticed.
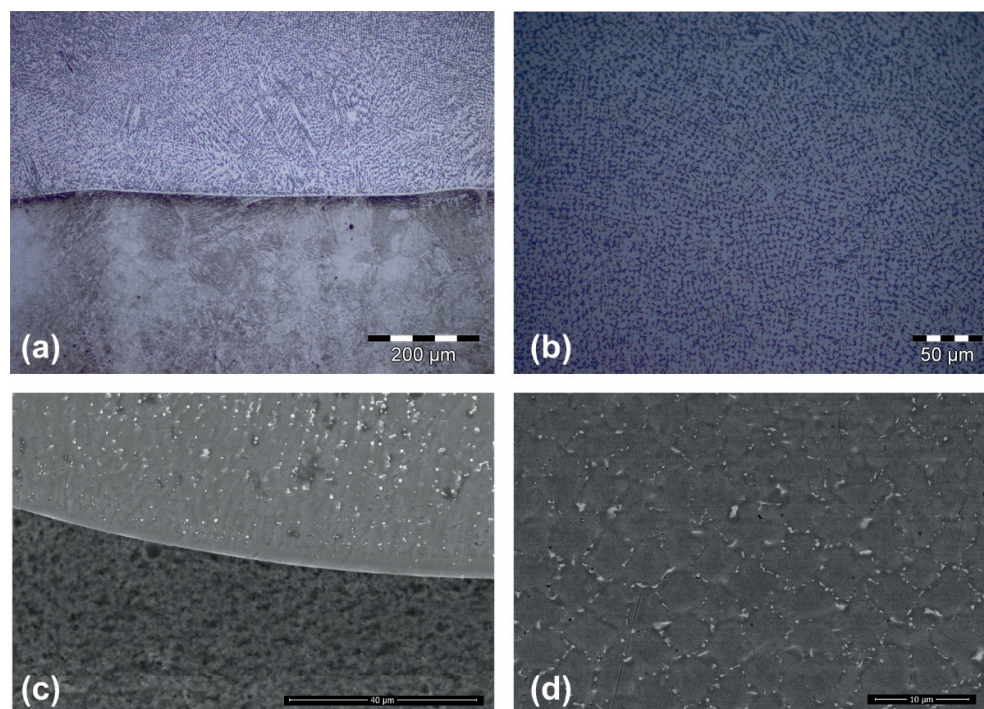

Fig 2.10 (a) and (b) optical and electronically microscopy of the interface zone, (b) and (d) microstructure of the Inconel 718 in the middle of the cladded track [PSR17].

The two materials are separated by a well-defined non-interference line (planar growth). The solidification pattern is determined by the thermal gradient induced by the laser. Therefore, by

varying the laser power, different morphologies of the dendrite and precipitate phases were achieved.

In addition to the thermal gradient, the dilution has a crucial role in the formation of the clad microstructure. According to Figure 2.11 and Table 2.9, it can be seen that nearby the boundary zone there is a higher concentration of iron, which was transferred from the base material. As the investigated area is closer to the upper part of the clad, the chemistry is related to the powder composition. From the EDS analyses of all samples, it was observed that iron is still present in a high concentration in the entire clad area, and the iron concentration in the cladded layers is almost double compared with the powder chemistry. In the upper part of the coating, the iron concentration was found to be 33.5% in the case of sample 3, and 47% in the case of sample 8, which was fabricated with the highest power.
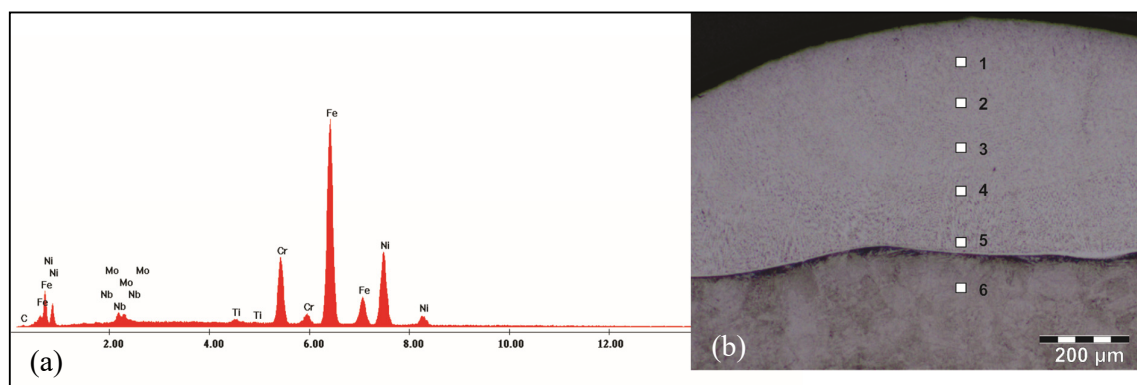

Fig. 2.11. (a) EDS spectrum of microzone 1; (b) distribution of the EDS analysed microzone of sample 3 [PSR17].

Distribution of the alloying elements according to the microzone from Figure 2.11   Table 2.9.

Element	Nb	Mo	Ti	Cr	Fe	Ni
	%	%	%	%	%	%
Microzone						
Microzone 1	6.5	4.7	0.8	15.5	33.5	39.0
Microzone 2	4.8	4.5	1.1	11.3	37.5	40.8
Microzone 3	3.5	2.1	0.6	12.5	47.1	34.2
Microzone 4	1.1	1.5	0.7	8.7	57.4	30.6
Microzone 5	2.1	0.8	0.3	4.3	76.8	15.7
Microzone 6	1.6	0.8	0.1	1.3	93.9	2.3

Inconel 718 is a precipitation-hardenable superalloy. Solidification starts from liquid to eutectic γ and promotes the enrichment of the interdendritic liquid with Nb, Mo, and Ti [QID14], [RRR05]. Because the niobium is a refractory element, it will segregate, forming some laves phase at the end of the solidification process [BRM04], [QLX12].

In Figure 2.12, it can be seen that different precipitated phases are formed in the primary γ Ni solution. This interconnected precipitated phase forms hexagonal patterns that enclose the Ni solution. Round shaped $Ni_3Nb-\delta$, Nb-rich MC carbides and lava phases are present in the hexagonal pattern.

The lava phases are formed due to the Nb segregation and have a typical chemistry of (Ni, Fe, Cr)$_2$ (Mo, Nb, Ti) [LRC14], [QAR09]. This type of brittle lavas segregation has a detrimental impact on the mechanical proprieties of the clads. Moreover, the Nb segregation combined with the rapid solidification occurred at laser processing could promote crack initiation at the grain boundary. This segregation can be partially removed by heat treatment; this process is presented in chapter 2.3.
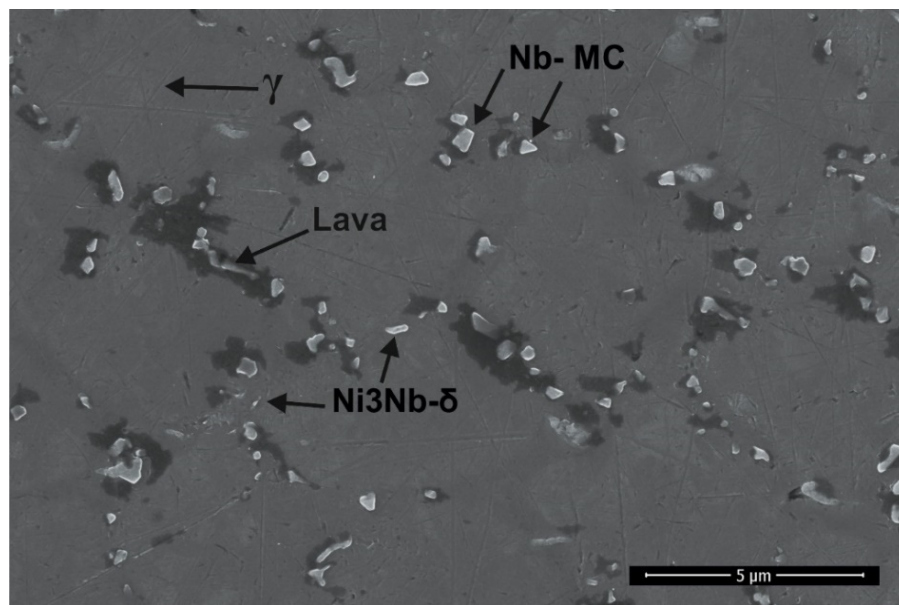

Fig. 2.12 High magnifications of the precipitation formation and lavas phases (sample 3) [PSR17].

Figure 7 shows a severe segregation that is present in all the cladded tracks. This type of grain boundary segregation has not been indicated in other studies regarding Inconel 718 cladding. Increasing the laser power will increase the melt depth and the overall temperature of the cladded track and lead to a high thermal gradient and a high cooling rate. Moreover, it was observed that interconnected lavas phase and hard phase formation were precipitated in a

hexagonal pattern on the entire area of the cladded track. This segregation pattern is more pronounced near the interface with the substrate, were a high amount of iron is transferred from the base material. The segregation pattern remains visible in the entire domain of power used. An in-depth characterization of the Inconel 718 microstructure shows that the precipitations are enclosed in an iron base matrix near the interface with the substrate and form a Ni-Fe solution in the upper part of the cladded tracks.

As seen in Figure 2.13, each Ti or Nb carbide is surrounded by a dark area. The EDS analyses reveal that the irregular shaped particle is rich in Nb, and the surrounding area has a high concentration of iron.
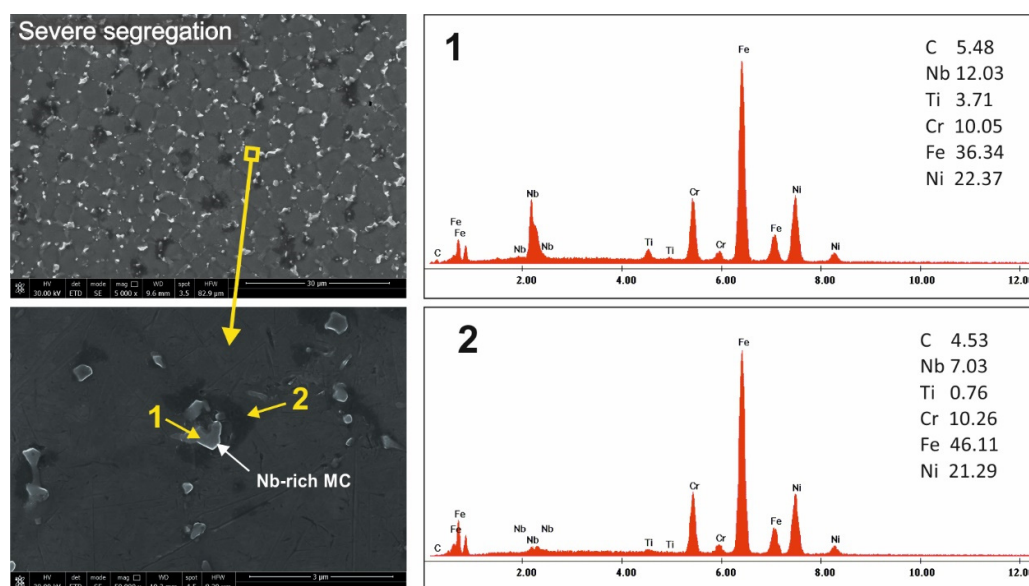
Fig. 2.13. EDS spectrum of the segregated particle and surrounding area, 1-spectrum of the hard phase particle, 2- spectrum of the surrounded region [PSR17].

Both investigated regions have a high amount of iron, which denotes that the laser power used in the laser cladding process is too high and produces a massive infusion of iron from the substrate. A high content of iron assures a good Ni-Fe matrix solution for embedding the hard phases but will also decrease the mechanical proprieties of the Inconel 718 coating. The EDS results are in concordance with the hardness testing results presented in Figure 2.14.

With respect to the graph from Figure 2.14, the hardness decreases along with the increase of the power inserted in the process. The hardness decrease is produced by the dilution percentage between the materials and by the different crystallization and segregation pattern promoted by the gradient temperature. At low laser powers, the powder forms fine and

dimensionally uniform dendrite structures with a small amount of laves and precipitation formation. The overall hardness results for Inconel 718 are good, and the highest hardness obtained is 267 HV_{02}, which could be increased by applying a thermal treatment.
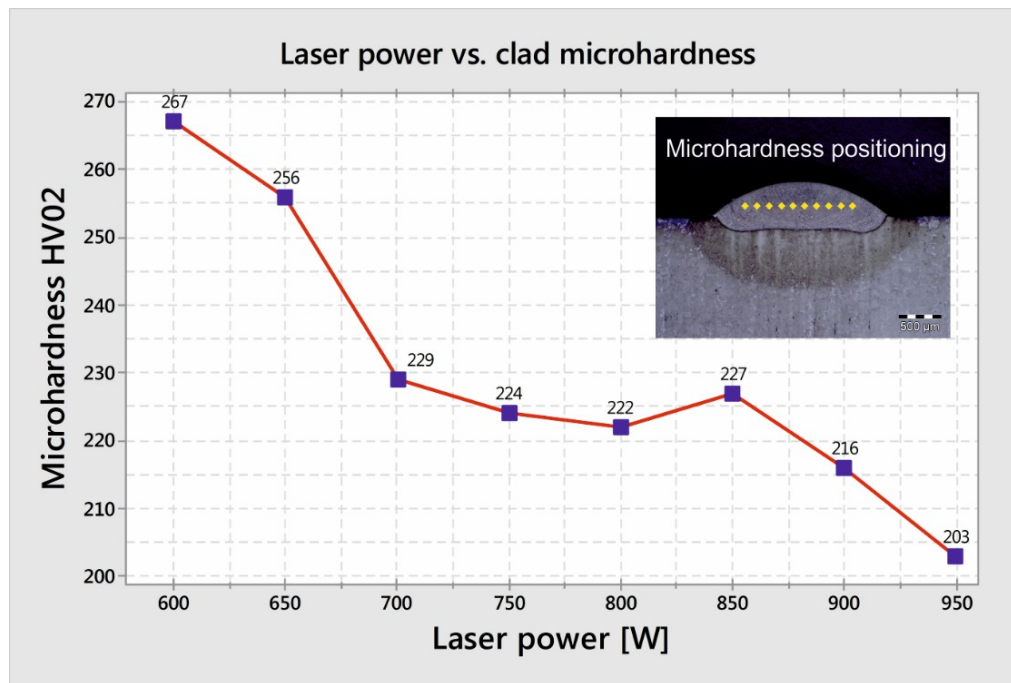

Fig. 2.14 a) Dependence between the laser power and the microhardness of the cladded specimens (Shimadzu HMV 2T microhardness tester: load 200gf and dwell time of 15 sec) [PSR17].

In conclusion, the results show that uniform and defect-free Inconel 718 hard coatings deposited on AISI 5140 substrate can be successfully fabricated by laser cladding [PSR17]. Thus, a comprehensive understanding of parameter influences, especially of laser power, on the cladded track profile and microstructure is necessary to obtain the best results in term of mechanical behaviour. As was demonstrated, the laser power has a direct influence on the clad height, melt depth and on the cladding dilution. Therefore, a low molten area and low dilution increase the quantity of the deposited powder.

As previous demonstrated, temperature plays in important role in the niobium segregation due to the influence on the cooling rate and to the dilution percentage of the cladded layer. The thermal gradient can be influenced and reduced by tuning the laser processing parameters but only to some limits, so further improvement of the Inconel 718 cladded layers should be obtained after the layers are fabricated.

2.3 Thermal heat treatment of Inconel 718 coatings

2.3.1 Concept

After obtaining good results in terms of Inconel 718 laser cladding, I considering that further improvement of the cladded layers can be achieved. For that, refinement of the microstructure and enhancement of the hardness was achieved through a heat treatment (precipitation hardening) of the Inconel 718 laser-cladded layer [PSR17].

Even if the heat treatment process is well known and relatively easy to be applied, it can be quite challenging to heat treat a cladded layer. After analysing the possible option, I decided that heat treatment with concentrated solar energy is the best solution to avoid the heating and degrading of the substrate.

Further, some the results obtained are presented in the project entitled *Residual stress relieve of Ni-based coatings fabricated by laser cladding*, financed through the SFERA II - European Solar Research Infrastructure for Concentrated Solar Power grants– 2015 [PSR17].

Currently, solar energy is the only exhaustless and fully ecological energy source available. Conventionally, solar energy was used to obtain electric energy by photovoltaic panels or by radiant heating. Currently, concentrated solar radiation is successfully used for melting and welding materials, the synthesis of materials/nanomaterials, and also for processes that do not involve melting or evaporation of materials, e.g., heat treatments.

Heat treatment of a coated layer can be realized by local heating only the surface of the coated material while keeping the substrate cold. The process is possible by focalizing the solar energy on the Inconel 718-cladded surface and by active cooling of the substrate. Figure 2.15 shows the schematic representation of the process.
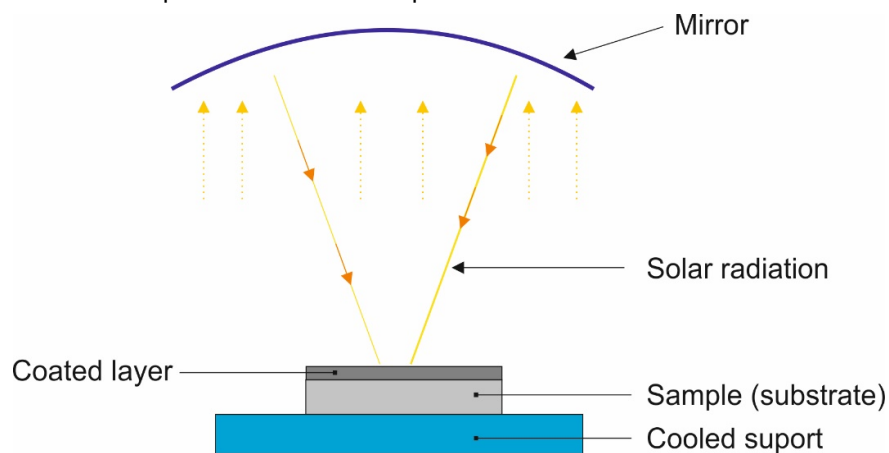

Fig. 2.15 Schematic representation of the solar heat treatment process.

2.3.2 Methods, materials and results

The solar heat treatment was realized at the research unit PROMES-CNRS from Font-Romeu Odeillo, France. The institute hosts a wide range of high and very high flux solar furnaces with modular reactors capable of heating, melting, vapor-condensing or synthesising materials in a controlled atmosphere. The mirrors and concentrators can provide high heat fluxes up to 2 kW. A stable heating and maintaining process was obtained by using a heliotron type reactor with controlled atmosphere and cooled support.

Figure 2.16 shows the principle of the heliotron type reactor. It can be observed that the sample is positioned on a cooled support and coupled to a thermocouple connected to an acquisition and command module that controls the solar flux that reaches the sample surface. During the thermal treatment, the time-temperature-transformation TTT diagram has been respected with the help of an automatic shutter that manages the amount of sun light used for the experiment (~700 ms from 0 to 100% opening-closing of the shutter). Additionally, the variation of the sun irradiation during the experiment was compensated using the same shutter system for opening and closing the shutter blades. A low vacuum-controlled atmosphere of 550 hPa was obtained by using a vacuum pomp and a continuous argon 99% flow rate of 1 l/min. The constant flow of argon is necessary to prevent the deposition of fumes or debris on the interior surface of the reactor, which can lead to overheating and implosion of the Pyrex.
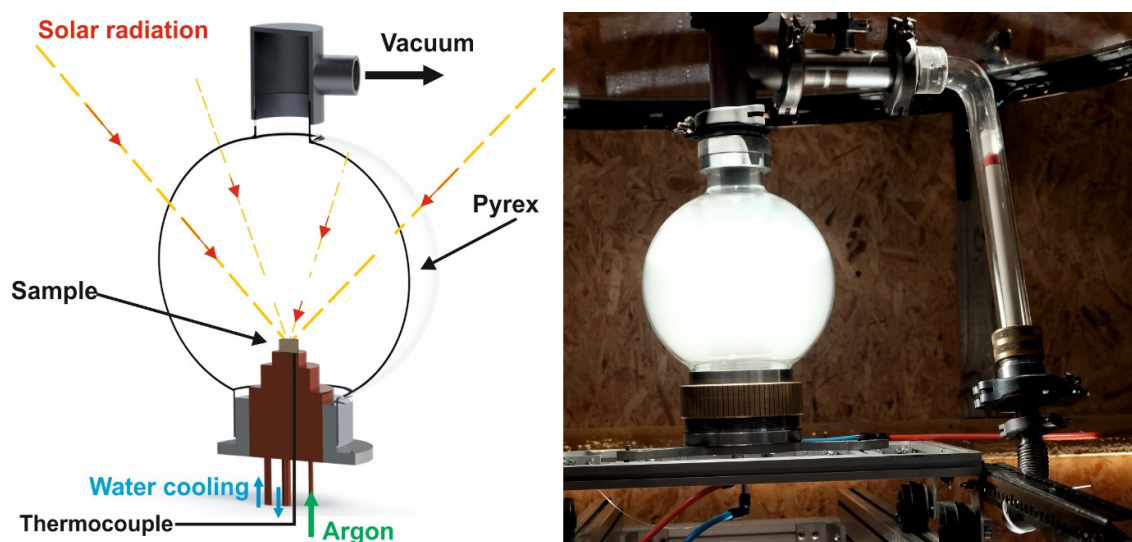

Fig. 2.16 Experimental frame of the solar heat treatment, a) schematic, b) solar reactor [PSR17].

Practical applications of the Inconel 718 alloy imply layers that are uniformly cladded on different surfaces. Considering that implication, I have realized six samples by laser cladding in partially overlapped tracks with Inconel 718.

It must be mentioned that same experimental frame as for the cladding of single tracks was used (cap. 2.2.2, page 44). The optimal parameters for this samples have been determined from the previous tests and are summarized in Table 2.10.

Laser cladding parameters of partially overlapped tracks   Table 2.10

Sample	Power [W]	Speed [cm/min]	Powder feed rate [g/min]	Overlapping degree [%]	Stand-off distance [mm]
ASC (as cladded)	750	22	5	45	12

The solar heat treatment was performed on 4 samples and 2 were kept as reference. The samples were positioned on the water-cooled plate to maintain a low temperature of the base material (200 – 250 ℃). The temperature was measured and controlled by means of two k type thermocouples, one coupled with the substrate and one with the cladded layer.

The heat treatment was carried out according with the time-temperature parameters presented in Table 2.11.

Parameters of the solar heat treatment   Table 2.11

Parameters	Temperature	Time	Environment	Cooling	Pressure
Inconel 718 STT (after solar heat treatment)	980	3.5 h	Ar – 1 l/min	In air 300°C / hour	Pressure of 550 hPa with an constant Argon flow of 1l/min

The readers should know that solar energy received from the sun is not constant due to the rotational movement of the earth and to the impredicative methodological condition. Over several days, numerous tests and trials were performed until the correct temperature was maintained during the heat treatment.

After the solar heat treatment, the samples were prepared and investigated by mean of optic and SEM microscopy. The samples have been analysed in cross-section and also on the top surface after removing by grinding 1/3 from coating surface as illustrated in Figure 2.17.
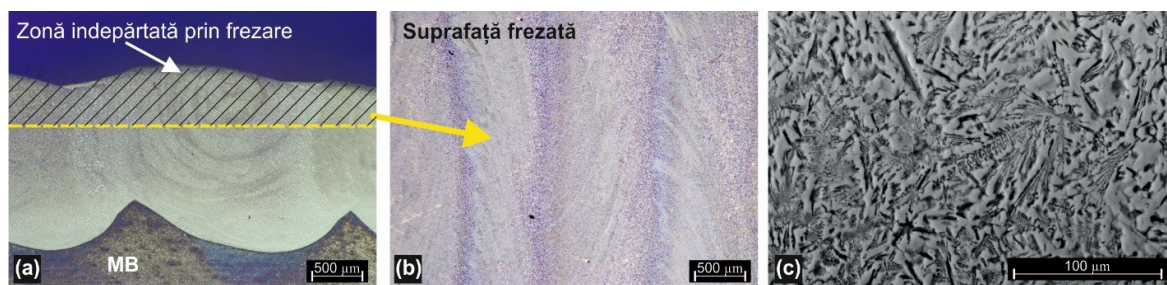
Fig. 2.17 Laser cladding in partially overlapped tracks, a) macroscopic profile, b and c general view and detail of the top grinded surface [PSR17].
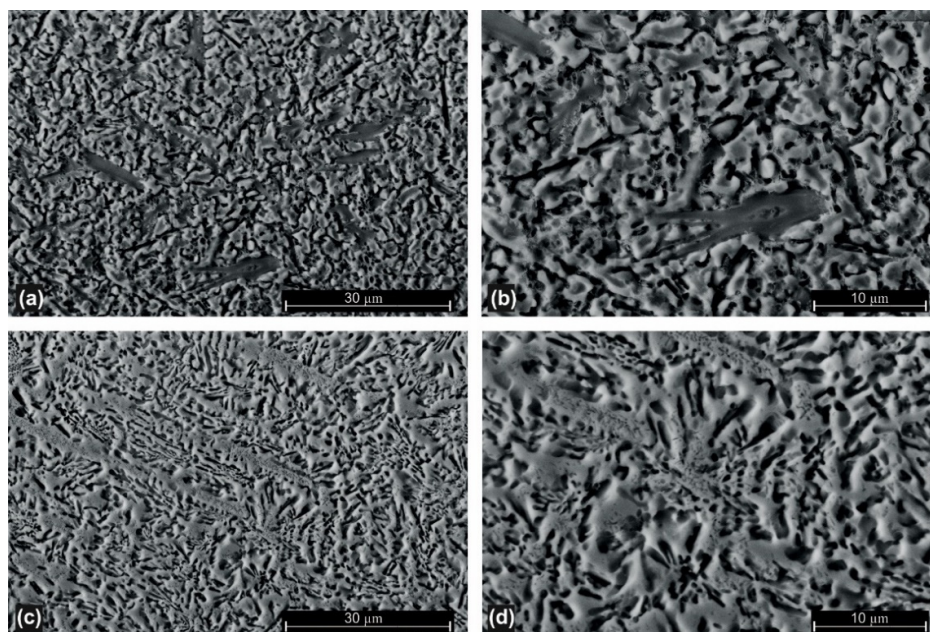

Fig. 2.18 SEM microscopy of the grinded surface of Inconel 718 layer. a) and b) SEM microscopy before the solar heat treatment, c) and d) SEM microscopy after the solar heat treatment [PSR17].

The images from Figure 2.17 underline the laser cladding aspect after removing a third part of the cladding upper part (Figure 2.17 (b) and (c)). It can be noticed the aspect of the dendrite structures and precipitated formation that are sectioned on their increase direction as presented in Figure 2.17 (c).

Less lava phases and reduction of the segregation pattern was observed after the solar heat treatment. As can be seen in SEM image from Figure 2.18, the microstructure refinement was occurred during the solar thermal treatment (STT) by the partial dissolution of the lava phases and also the enrichment of the precipitation particles with Ni resulted from the diminished of lava formation. This phenomenon normally occurs at $960 - 980$ °C and was potentiated by the STT temperature of 980 °C [PSR17].

The common microstructure of Inconel alloys after the solar heat treatment is formed by coarse and fine dendrite at the interface with the substrate and lava phases precipitates in interdendrite spaces. Besides the microstructure refinement, after the solar heat treatment the strength of Inconel 718 layer was increased. As presented in Figure 2.19, the HV02 hardness of the STT sample increase with 100% compared with the as-cladded material.
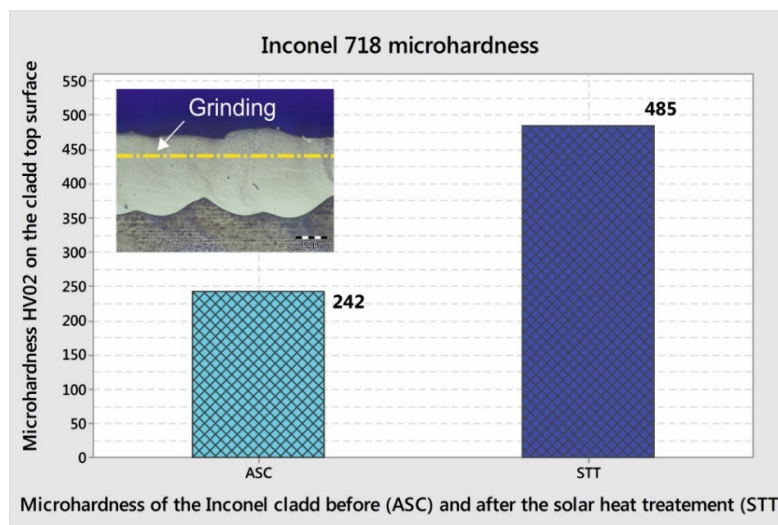

Fig. 2.19 Microhardness before and after the solar heat treatment.
(Shimadzu HMV 2T microhardness tester: load 200gf and dwell time of 15 sec) [PSR17].

The reported data and discussion demonstrate that post heat treatment using solar radiation can be used for diminish the laves formation and segregation pattern and to sequential improve the plastic characteristic of the laser cladded material [PSR17].

The mechanical proprieties of the cladded layer were modified and hardness increasing from 242 HV_{02} to 485 HV_{02} on the grinded surface of the Inconel 718 laser cladded layer was obtained. This hardness increasing occurs mainly due to the precipitation hardening phenomena and due to the reduction of the lava phase from the metal matrix.

Inconel 718 is one of the most widely used material in the aerospace industry so the possibility of using it as the coating for the repair processes presents many benefits in terms of reducing waste and cost reductions. The presented study [PSR17] successfully demonstrates that laser cladding with Inconel alloys is a viable solution for improving the corrosion and mechanical performance of metallic surfaces. Additionally, further enhancing the Inconel 718 coating quality can be obtained by post heat treatments.

The applicability of the Inconel 718 coating can be extended, as will be highlighted in the following section of the habilitation thesis.

Chapter 3. ADVANCED LASER CLADDING TECHNIQUES

3.1. Gradient materials

3.1.1 Concept

The increasing demand for high-performance materials that possess improved physical, chemical, mechanical and technological characteristics has motivated extensive research in the field of hard coatings with improved corrosion and wear resistance. Usually, an increased wear resistance coating is obtained by means of a hard-metallic matrix or by the addition of hard carbides as reinforcement for a softer matrix. Both methods have limitations due to the higher cracking susceptibility of these high hardness claddings.

The readers should know that it is almost impossible to obtain a high hardeness coating, which is usually brittle and having in the same time a low cracking susceptibility. In addition to the mechanical proprieties of the material, the laser cladding process is rapid and induces thermal stress that will produce cracks if the strength limit of the material is exceeded. Thus far, no solution to this problem exists.

Therefore, I propose a method [SPT16] to overcome the abovementioned issues by using a dual-layer coating formed by a buffer layer and a hard coating (Figure 3.1).
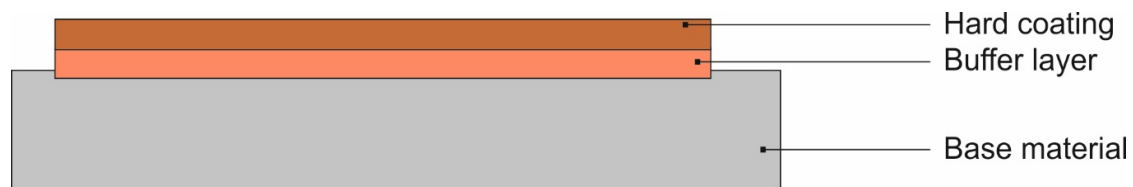

Fig. 3.1. Schematic of the dual-layer coating.

An alternative method for obtaining a Metco 16C-NS NiCrBSi-based hard coating on AISI 5140 steel by using an Inconel 718 alloy as a buffer material between the base material and the coating is proposed [SPT16]. The buffer layer approach has also been used in the literature to obtain graded layers, but no studies have been reported that have applied Inconel 718 and NiCrBSi together as functionally graded materials.

The advantage of this alternative method is twofold. On one hand, it could provide hard coatings with lower cracking susceptibility than those presented in the reference literature, with lower dilution, which is responsible for the higher hardness, wear resistance and

corrosion resistance values obtained in comparison with the reference material. On the other hand, the presented composite coating approach, through combining both the advantages of Inconel 718, such as its low cracking susceptibility and good corrosion resistance and those of Metco 16C-NS, i.e., high hardness and good wear resistance, could provide the required characteristics for the high added-value components used in special-purpose civil engineering, energy and maritime applications. This method could greatly mitigate the risk of potential occupational hazards generated by a potential unexpected failure of the hard coating, the interlayer being able to protect the base material against an aggressive environment, e.g., in the case of hydraulic riser tensioners and piston rods used in offshore oil and gas drilling platforms, as well as in the case of large hydraulic cylinders working in an extremely corrosive marine environment [***ARM], [TGM11]. In these cases, the presence of a corrosion-resistant buffer layer can be a major advantage in preventing damage to the hard coating layer [***ARM], extending the life cycle of the components and could constitute a more cost-effective alternative to manufacturing the entire component from stainless steel or highly alloyed corrosion-resistant steel.

3.1.2 Methods, materials and results

To validate the proposal, I have performed an experimental study [SPT16] consisting of making a comparation between a coating obtained by fabricating the hard coating directly on the base material and by adding a buffer layer.

AISI 5140 grade steel specimens with 60x25x12 mm dimensions have been used as substrate for the cladding tests. Prior to cladding the base steel specimens have been polished to a final 0.8 μm average rougness. The hard wear-resistant upper layer was fabricated by using Metco 16C-NS (Ni 17Cr 4Si 3.7B 3.0Fe 2.5Cu 2.5Mo 0.6C) powder (Sulzer Metco®, Switzerland). A self-fluxing Ni-based Inconel 718 (Ni 19Cr 0.2Si 18Fe 3Mo 5Nb 1Ti 0.08Mn 0.05B 0.05C) powder (Sulzer Metco®, Switzerland) has been used as the buffer layer between the base material and the Metco 16C-NS layer.

Laser cladding tests have been conducted using a COHERENT 1000F diode laser (λ= 975nm) and a PRECITEC YC50 water-cooled cladding module, with a 15 L/min flow rate of argon carrier gas. A CLOOS seven-axis welding robot has been employed in the positioning of the cladding head. A 3.2° tilting angle in the cladding direction of the cladding unit was required in order to protect the laser optical system. The tests have been performed at room temperature (24°C). A laser spot with a diameter of 2 mm and stand-off distance of 12 mm was used for the

experiment. For the reference sample one layer of partially overlapped tracks consisting of Metco 16C NS has been cladded on AISI 5140 steel substrate, using the parameters depicted in Table 3.1.

Laser cladding process parameters   Table 3.1

Parameters		Power	Energy density	Scanning speed	Powder feed rate	Overlap degree
		[W]	[J/mm^2]	[mm/s]	[g/min]	[%]
Single coating (*reference sample*)	(Metco 16C NS)	740	92.5	4	5.2	45
Dual coating	(Inconel 718)	800	100	4	5	45
	(Metco 16C NS)	700	77.7	4.5	5.2	50

The dual coating laser cladding has been obtained in two steps. First, the intermediate Inconel 718 powder has been cladded in 12 partially overlapped tracks. After the sample was cooled to room temperature, the second layer consisting of Metco 16C NS was cladded on top of the Inconel 718 layer. The process parameters are summarized in Table 3.1. Three identical samples consisting of both sample types have been obtained to test the reproducibility of the experiment.

For the optical microscopy and scanning electron microscopy analysis, the samples have been cross-sectioned, polished and etched in two steps. First, the Inconel 718 layer was electrochemically etched in a 10% wt. solution of oxalic acid, followed by the etching of the Metco 16C-NS layer in a 1:3 vol. HNO_3: HCl solution.

Regarding the reference sample, obtained by cladding Metco 16C-NS layer directly on the steel substrate, Figure 3.2 reveals the presence of macro- and micro-cracks on the cross-section of the sample, the majority of which could be ascribed to the cold crack domain. It can be seen that most of these cracks are formed starting from the interface between the clad and the substrate with an upper vertical development into the structure (Figure 3.2 (b-d), (f)) and are mainly due to a combination of both thermal expansion mismatch stresses that occur due to the difference in variation of the thermal expansion coefficient with temperature of the hardcoating Metco ($7 \cdot 10^{-6}$ to $10.6 \cdot 10^{-6}$ K^{-1}) in comparison with AISI 5140 steel substrate ($12.6 \cdot 10^{-6}$ to $14.9 \cdot 10^{-6}$ K^{-1}) and thermal plasticity modifications of the cladding material

during solidification, as it has been evidenced by the specific cracking sounds produced during the cooling of the cladding.
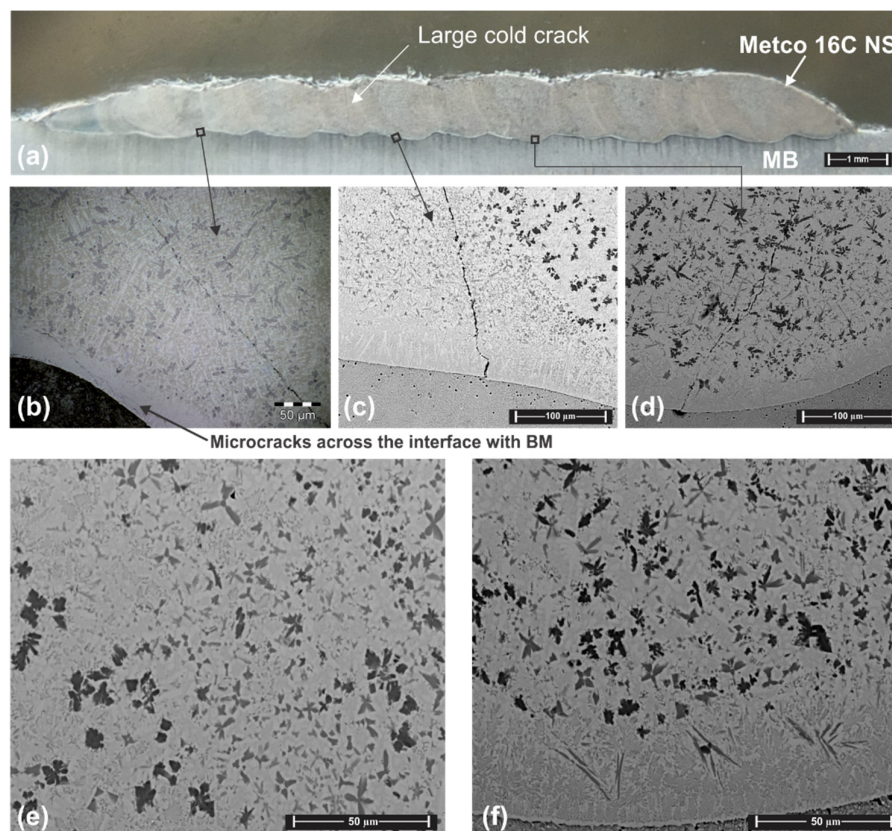

Fig. 3.2. Laser cladding without interlayer: (a) general profile of the Metco 16C-NS coating on the steel base material; (b), (c) and (d) cracks at the interface between the buffer layer and the substrate; (e) hard phases distribution in the middle zone of the cladded layer; (f) diffusion zone between the coating and substrate [SPT16].

Only one crack could be identified as being formed due to the possible segregation of Ni+Ni$_3$B eutectic with lower thermal conductivity at the grain boundaries, thus producing a discontinuity in the metal matrix and promoting the hot cracking mechanism. The bulk of the cladding is composed mainly of irregular precipitates with an average diameter of 4.8 μm dispersed in the Ni eutectic matrix (Figure 3.2 (e)). Since during the cladding process the local surface temperature increases and then decreases rapidly with the passing of the laser, the thermal gradient difference generated in the bulk of the cladding leads also to the appearance of in-plane tensile stress. Since the laser power is kept constant, it could be assumed that the amount of generated stress is mainly due to the thermal regime, dictated by the dissimilarities between the thermal conductivity variations with temperature of the cladding and base material. The thermal conductivity of Metco 16C NS has a pronounced decrease with

temperature (0.7 to 0.02 W/m·K), in contrast with that of the base material (44.6 to 30 W/m·K). This contrasting behavior could generate a significant thermal gradient and stresses during the rapid heating-cooling cycles that occur when cladding multiple tracks, due to the local concentration of heat at the surface of the cladded material, since at high temperatures Metco becomes practically a thermal insulator. This pronounced temperature gradient in the original melted Metco is also responsible for producing precipitates with 6% lower diameter at the surface of the cladding, then at its base, thus generating an inhomogeneous structure with a high dispersion in hardness values and other useful properties. Furthermore, this inhomogeneity and the presence of cracks could have a significant influence on the wear and corrosion resistance behavior of the cladded materials.
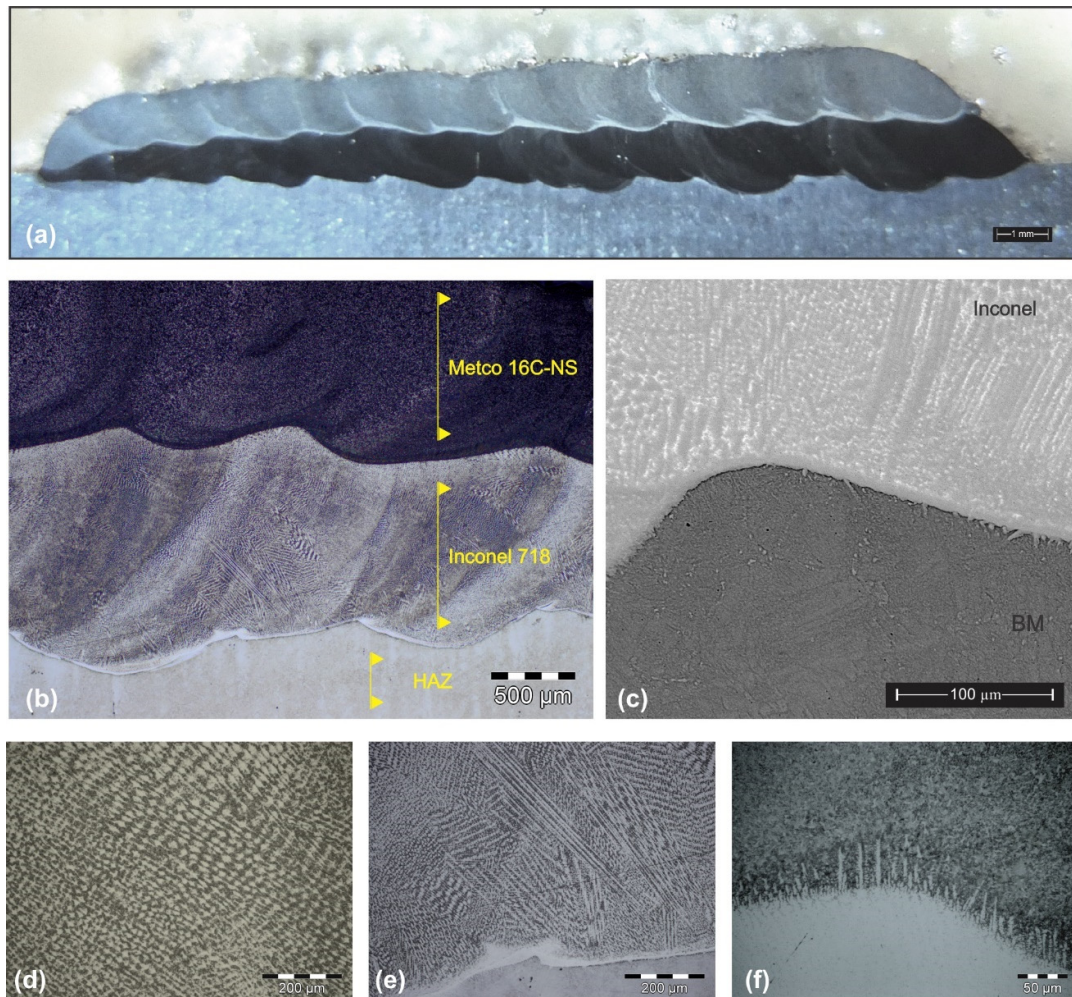

Fig. 3.3. Laser cladding using Inconel 718 intermediate layer: (a) and (b) general profile of the double coating on the steel base material; (c) SEM microscopy of the interface between the buffer layer and the substrate; (d) dendrite pattern in the middle zone of the Inconel layer; (e) dendrite growth near the boundary zone with the substrate; (f) diffusion zone between the Inconel layer and the Metco 16C-NS cladding [SPT16].

Regarding the dual-layer configuration sample, the two claddings can be easily distinguished due to their different chemical composition (Figure 3.3(a) and 3.3(b)). Another aspect to be remarked is the compactness of the two cladded layers and the absence of cracks, as it could be remarked from the micrographs presented in Figure 3.3(b-f). The absence of cracking in this case could be due to both the enhanced metallurgical compatibility of the layers and the relatively similar variation of the thermal expansion coefficient with temperature of the Inconel 718 buffer ($12.8 \cdot 10^{-6}$ to $16.4 \cdot 10^{-6}$ K^{-1}) in comparison with the substrate, which could contribute firsthand to expansion stresses diminishing. On the other hand, the Inconel buffer layer could act better as a heat sink through favoring the diminishing of the thermal gradient in the Metco melt than in the case of AISI 5140 steel alone, due to its increasing thermal conductivity with temperature (9.8 to 22.8 W/m$\cdot$K). Also, the lower variation of the relative thermal expansion coefficient with temperature of the Metco powder in comparison with that of Inconel buffer could generate in this case compressive thermal stresses that do not contribute to cracks formation, but in contrast favors the obtaining of claddings with increased compactness. Both cladded layers have an average thickness of 1 mm.

The cumulative variation of the cladded tracks height and width ($\pm$ 0.23 mm) could be related to the progressive increasing in accumulation of heat in the substrate onto which the new layer is cladded (from left to right, as it can be visually observed from Figure 3.3(a), favored also by the higher values of the average specific heat of Inconel (0.56 J/g$\cdot$K) and Metco (0.7 J/g$\cdot$K) in comparison with the base material steel (0.5 0.7 J/g$\cdot$K). Due to its improved compatibility with the substrate, the Inconel layer presents a well-defined interface at the contact with the base metal as well as a minimal dilution, as it can be observed from Figure 3(c). Further insight into this interface zone reveals an unalloyed band between 3 and 12 μm wide. Near this zone, due to the more pronounced thermal gradient, the microstructure is composed of coarse columnar dendrites rich in Fe and Ni, exhibiting branch tree growth (Figure 3.3(e)). The superior zone of the Inconel 718 layer is mainly composed of finer and more uniform equiaxed dendrites as it can be observed from Figure 3.3(d). The zone adjacent to the interface between the hardfacing layer and the buffer layer is highlighted in Figure 3.3(f). There is no separation line between the materials, indicating a good compatibility between the two layers. The dilution effect between the two layers is indicated by the formation of a dendritic structure extending from the buffer layer to the upper layer [SPT16].

Three distinct regions could be observed at the interface between the Metco and Inconel cladding, as shown in Figure 3.4(a). The lower region (towards the steel) is characterized by

the presence of fine dendrites and interdendritic Laves phases, consisting of an interconnected grid of complex brittle niobium phases, resulted due to the segregation of niobium from the metallic bath during solidification, as it could be observed from Figure 3.4(c). The distribution of the Laves phases is similar to the equiaxed dendrite structure in the upper part of the Inconel layer and the columnar dendrite structure near the diffusion zone.
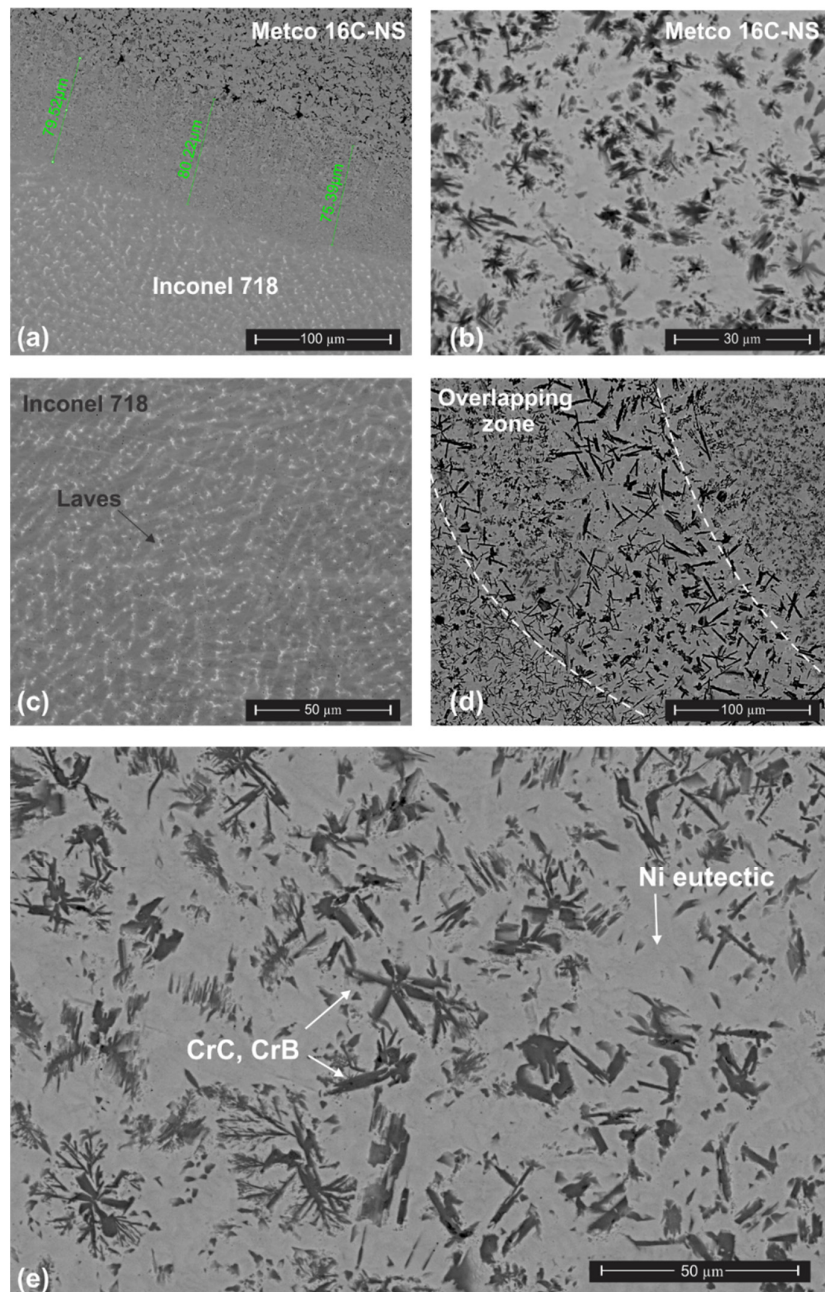

Fig. 3.4 Microstructural analysis of the dual coating: (a) Diffusion zone between interlayer and upper layer; (b) distribution of the hard phases in the Metco 16 C NS layer; (c) segregation of the chemical elements into the Inconel 718 layer; (d) microstructural changes in the tracks overlapping zone; (e) detail of the chromium carbides and borides [SPT16].

The microstructure of the intermediate zone (the boundary area between the Inconel and Metco claddings) is composed of free-precipitation dendrites. In the overlapping area of the hard coating, the chromium boride precipitates are coarser and have a needle-like appearance due to their dilution with the intermediate layer (see Figure 3.4(d)). In this zone, the presence of coarse precipitates has a negative impact on the cracking susceptibility and on the hardness of the metallic matrix, as it can be seen from Figure 7. In the sample without an interlayer (see Figure 3.2), all the cracking was located near the overlapping interface between the cladded tracks. Therefore, limiting the degree of overlap in the cladding is important to reduce the dilution and to avoid coarse carbide precipitation.

The EDS analysis of the hardfacing (Metco 16 C-NS) microstructure, as presented in Figure 3.5, reveals the presence of precipitates, i.e., chromium borides, dispersed in the Ni-based eutectic matrix enriched in molybdenum, similar to the structure observed in Figure 3.2, and consistent to the data found in the reference literature [HOH13].
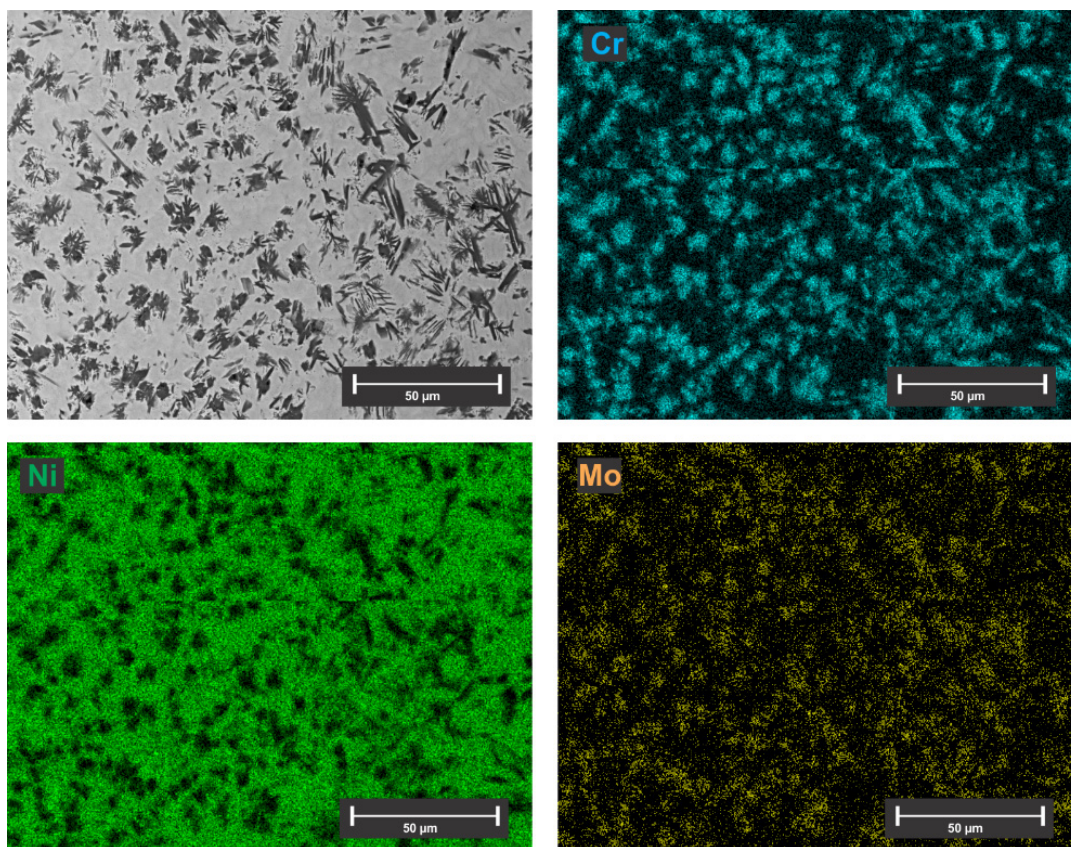

Fig. 3.5. EDS elemental mapping of chromium, nickel and molybdenum; position: middle region of the Metco 16C-NS hard coating present in the double layer configuration [SPT16].
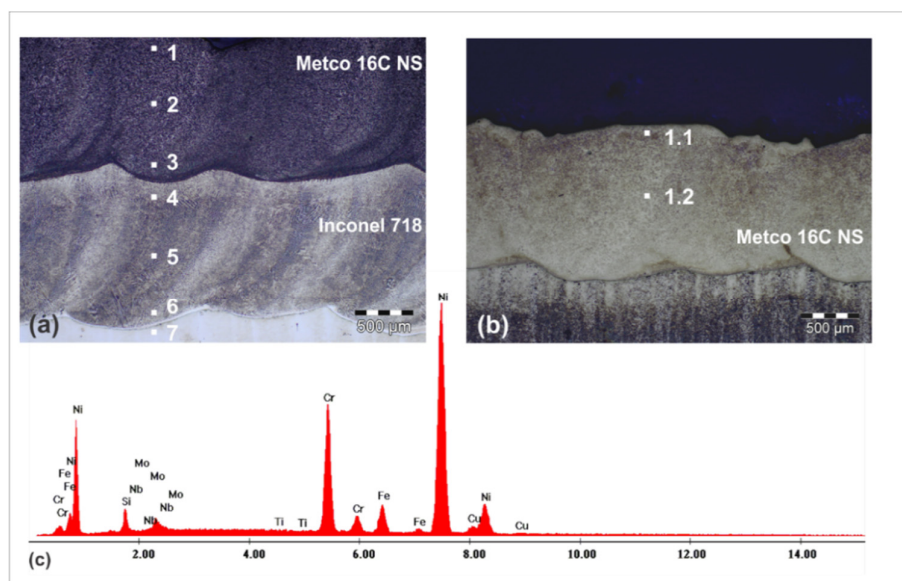
Fig. 3.6. Chemical distributions along the coating cross section. (a) (b) EDS location on the sample fabricated with and without interlayer; (c) EDS spectrum of the microzone 3 of the dual coating [SPT16].

EDS chemical composition of the areas from Figure 3.6   Table 3.2

Area Wt %	1.1	1.2	1	2	3	4	5	6	7
Si	2.87	2.10	3.48	2.58	7.26	2.91	0.31	0.34	0.24
Nb	-	-	0.29	2.14	6.30	5.73	2.09	0.97	-
Mo	2.24	1.94	2.38	5.62	4.81	3.56	1.69	0.82	0.10
Ti	-	-	0.07	0.16	0.82	0.85	0.63	0.04	-
Cr	14.07	11.61	24.88	21.09	17.42	15.85	18.00	3.89	1.62
Fe	15.47	33.19	6.06	9.24	12.80	25.05	42.13	77.38	93.92
Ni	63.24	50.12	62.67	57.23	49.47	45.63	64.96	16.5	42.12
Cu	2.11	1.04	1.17	1.94	1.12	0.43	0.11	-	-

The chromium carbides formation mechanism implies the more complex $(Fe,Cr)_{23}C_6$ Mo-favored destabilization under the intense heat treatment, so it is expected that iron content has a great influence in determining the shape, distribution and dimensions of the chromium borides and carbides phases. At higher iron contents (towards the base of the Metco layer), the carbide/boride phases have an average diameter of 6% higher and are more compact than towards the surface, where the iron content is with 50% lower, as determined from EDS analysis (Figure 3.6) and Figures 3.4(b) and 3.4(e). The presence of the buffer layer leads to a more uniform distribution of the hard refractory phases in the Metco coating, than in the case of cladding it directly to the base material, having as result a more uniform mechanical stress

distribution potential, thus generating a hardcoating with an improved structural integrity and improved mechanical properties.

As with the majority of mono-layer claddings presented in the reference literature, the dilution effect of the cladding with the substrate is rather difficult to be controlled. My proposed method [SPT16], through using an intermediate buffer layer acting as a barrier between the hardfacing coating and the base material, offers a better control on the mechanical properties and on the corrosion resistance of the obtained material, through an improved dilution control as it could be noted from the EDS analysis presented in Figure 3.6 and Table 3.2.

High iron content towards the surface of the material has detrimental effects on the hardness, wear resistance and corrosion resistance of the cladding. Based on the EDS analysis performed in the middle area of the hard coating for both reference and dual-layer cladding sample, at the same distance from the surface of the materials, it resulted that iron content is 30% higher in the sample cladded without an intermediate layer compared with the sample fabricated with the intermediate layer.

Consequently, the diffusion of chemical elements in the interface area between the Inconel and Metco claddings is higher due to the high surface area contact between the two layers, but this does not have a detrimental influence on the hardfacing coating properties. One of the major advantages of using a high alloy buffer layer such as Inconel 718 is the possibility of enriching the hardfacing layer with elements such as Ni, Cr, Nb, or Ti, which can further improve its hardness and wear resistance. The data from Table 2 demonstrate that, in the case of the dual coating, the middle region of the upper layer is enriched with elements such as hard-phases forming Nb and Ti. The diffusivities of the chemical elements during the cladding process are related to the corrosion resistance and the mechanical behavior of the coatings. The data presented in Figure 6 indicates that the dual-layer configuration sample is more resistant to corrosion, having a 20% lower corrosion rate than the reference sample, obtained using similar operational parameters.

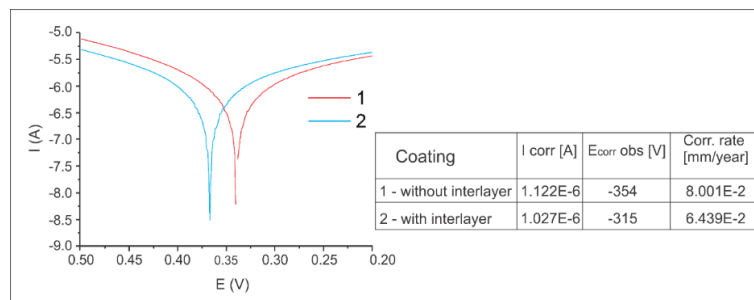| Coating	I corr [A]	Ecorr obs [V]	Corr. rate [mm/year]
1 - without interlayer	1.122E-6	-354	8.001E-2
2 - with interlayer	1.027E-6	-315	6.439E-2

Fig. 3.7. Linear polarization curves of the dual-layer cladding and reference samples.

This improvement could be due to the enriching of the surface of the dual-layer configuration sample with elements such as Ti and Nb, as well as through maintaining a lower amount of diffused Fe in the upper part of the cladding exposed to the corrosive environment, in consistence with the EDS data from Figure 3.6 and microstructural information from Figures 3.3-3.4

The high content in Ni and Cr, as well as in a more uniform distribution of hard and wear-resistant intermetallic compounds generates a structure with a higher surface hardness (as it can be seen from Figure 3.8) and lower wear coefficients (Figure 3.9) than the reference sample.
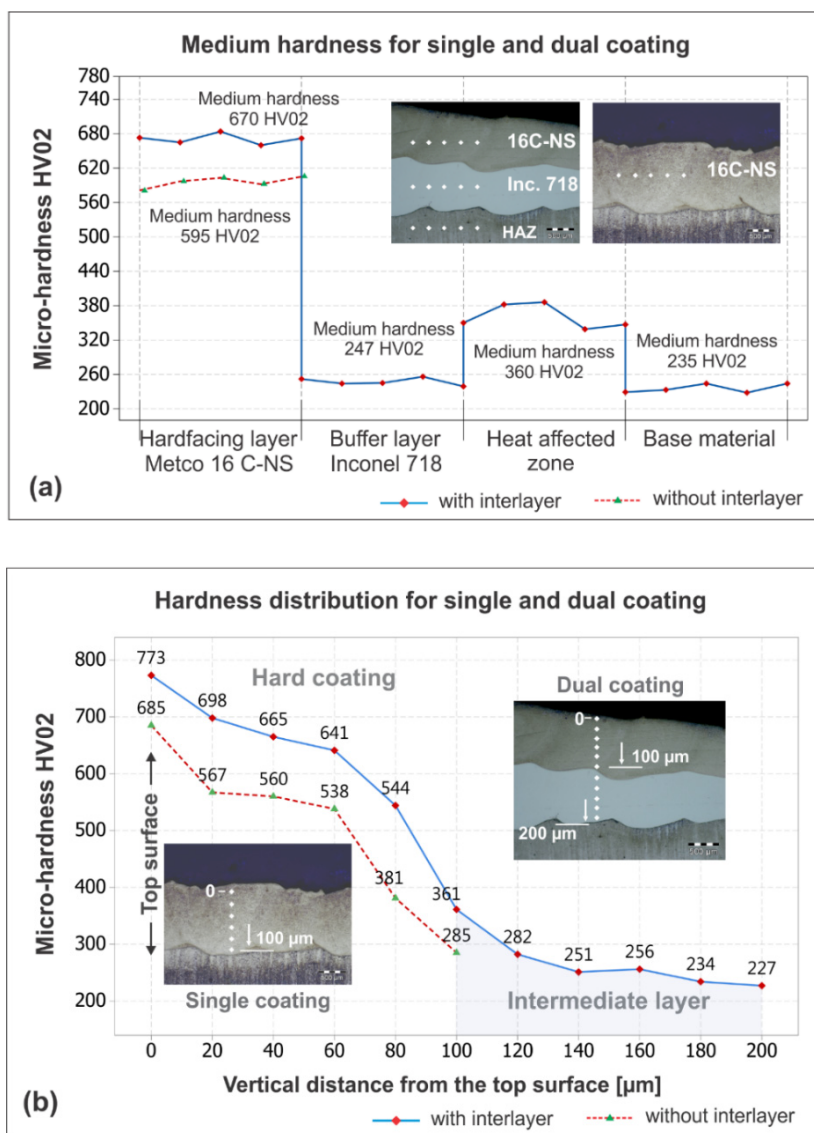
Fig. 3.8. Microhardness distribution on samples cladded with and without Inconel 718 buffer layer: (a) microhardness values for the main areas of the cladded sample; (b) microhardness evolution as a function of the distance from the cladded top surface [SPT16].

Analyzing the microhardness distribution on the cross-section of the cladded layers, the data show that the hardness increases from 247 $HV_{0.2}$ in the buffer layer up to 670 $HV_{0.2}$ in the middle area of the hardfacing layer, while the microhardness of the sample coated in a single layer is limited to 595 $HV_{0.2}$. Without significant differences between the maximum hardness of the two samples, the data indicates that the hardness measured in the middle of the hard coating is nearly 14% higher when an intermediate layer is used, probably due to its dilution limiting effect, thus preventing the enriching of the hard coating with more ductile iron. The hardening effect in the heat-affected zone of the base material could be due to the ferrite-pearlite ductile microstructure phase transformation to a hard martensite-based one.
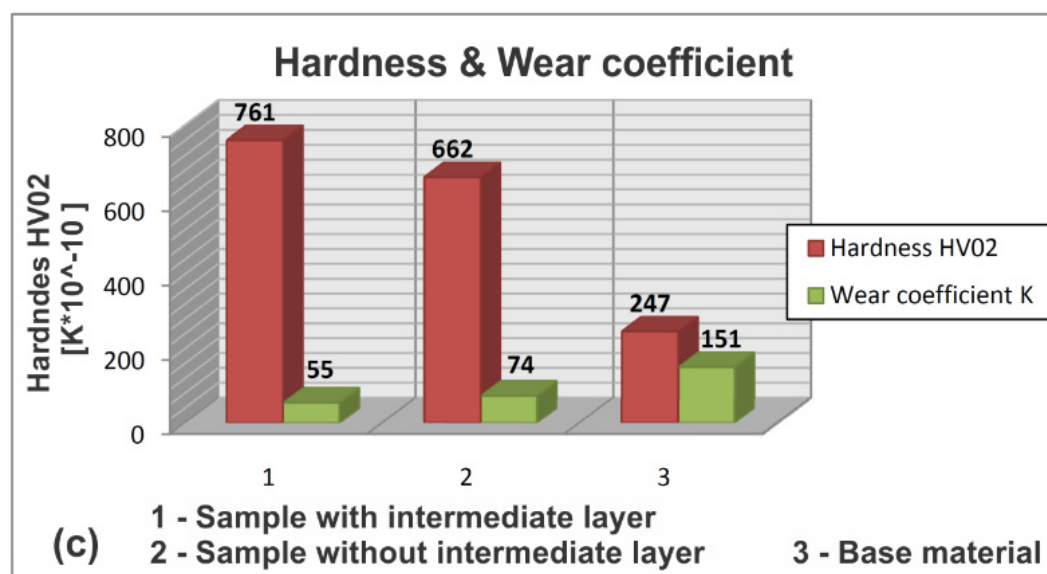

Figure 3.9. Wear results: (a) CSM Calowear testing equipment; (b) microscopy of the wear mark obtained after the analysis; (c) hardness and wear coefficient values for the analysed samples [SPT16].

 The diffusion limiting effect of the buffer layer is responsible for a uniform surface and bulk distribution of the hardness values when comparing to the reference. The same effects responsible for the hardness increase (across the section and at the surface) determine a wear coefficient decrease of 7% for the dual-layer cladded sample, in comparison with the reference sample (Figure 3.9(c)).

As demonstrated, it can be concluded that intermediate Inconel 718 layer is able to reduce the internal stress that develops during the solidification process of the cladding therefore decreasing the cracking susceptibility of the hardfacing and acts as a barrier to the dilution of the substrate, preventing the diffusion of iron, chromium, boron and carbon.

In addition, good compatibility between the Inconel 718 and Metco 16C-NS has been observed. A homogenous microstructure of the Metco 16C-NS hard coating has been noted in the presence of the intermediate Inconel layer, consisting of complex carbides and borides embedded in a metallic matrix of iron enriched with nickel and chromium. Thus, minor segregation effects have been noted at the grain boundaries in the Inconel layer due to the high thermal gradient.

Compared to other alternative methods of cracking susceptibility reduction such as substrate preheating or induction heating during cladding, the presented approach which uses an intermediate layer between the hard-coating and the substrate has two benefits: (1): the improvement of metallurgical compatibility between materials with different thermal coefficients and (2): preserving the chemistry of the hardfacing by minimizing elemental dilution, resulting in improvement of the corrosion resistance with 20%, as well as increasing of the surface hardness and wear resistance with 7% in comparison with the reference material, obtained without an interlayer [SPT16].

Improving the quality, safety and the life-cycle of the hard-coated materials designed for use under extreme environmental and operational conditions could overcome the method potential disadvantages, such as its higher cost and higher processing time and could constitute a viable alternative to other traditional technologies, especially in the case of materials with long-term exploitation periods, where access to components and regular maintenance is difficult.

3.2. Composite / ceramics coatings fabricated by laser cladding

3.2.1 Concept

As was previously stated in subchapter 1.4.3, laser cladding can be successfully used for the fabrication of ceramics coatings. It is well known that ceramics are a good thermal barrier and have high dielectric strength and are used in biomedical, aerospace, solar energy and other applications.

The efficiency of solar-thermal conversion systems mainly depends on the optical properties and thermal stability of the spectral-selective materials used as solar radiation absorbers. An efficient solar-absorptive layer is defined as having high absorptance values (in ideal cases, the solar absorptance coefficient α_s= 1 in the 0.3-2.5 μm spectral range).

Among the spectrally selective surfaces, such as semiconductor-metal tandems, multilayer absorbers, ceramic-metal composite coatings (cermet) and textured surfaces, the ceramic-based ones are the most promising in terms of performance and versatility and are well studied. However, despite all the advantages, ceramic coating applications have been restricted due to poor adhesion and high cracking susceptibility.

In the light of above, I proposed a new composite ceramic coating that uses hydroxyapatite as the absorptive material. HA combined with other ceramics materials can be used in a narrower field of application, e.g., solar applications, due to the specific optical proprieties, the good IR absorbance and the visible light reflectance.

Through the presented study [PSS17], a solar-absorptive coating has been obtained on a copper substrate by laser cladding, starting from a mixture of aluminium and titanium oxides, with metallic aluminium added into the composition to improve the adhesion of the coating to the substrate and hydroxyapatite (HA) as IR-absorptive ceramic and glass former.

3.2.2 Methods, materials and results

The materials used for obtaining the ceramic coating are Metco® 131VF powder comprising of aluminium oxide in a mixture with titanium oxide $Al_2O_3+TiO_2$, (Oerlikon Metco, USA), pure aluminium powder Al (Sigma-Aldrich, USA) and hydroxyapatite $Ca_{10}(PO_4)_6(OH)_2$ (Sigma-Aldrich, USA). All the reagents used were of analytical purity. Rectangular electrolytic copper (99.99% purity) plates with dimensions of 30x80x3 mm were used as the coating substrate for the

experiments. The Cu plates were cleaned by grinding on a P 600 grit paper and were degreased in ethanol prior to use. The PVA binder decomposes at ~ 400 °C, and it is expected that during the coating fabrication, a typical temperature of 1000-1500 °C is achieved; therefore, no organic phase remains.

It must be noted that in this case, the ceramic coating was obtained by a two-step process, namely, pre-placement of the ceramic starter and laser melting of the powder mixture, as described in the following paragraphs [PSS17].

The ceramic starter mixture has been obtained as a thick paste through mixing of the ceramic/metal powders with an aqueous solution of poly (vinyl alcohol). The mass ratio of the powders used in this study was 50% wt Metco® 131 VF, 25%Al and 25%HA. The mass ratio between the powder mixture and the organic PVA binder has been kept at 3:1. The obtained paste has been applied on the surface of the copper plates by using the Dr. Blade [MBS04] technique, in an approximate thickness of 0.5 mm. The coated specimens were dried on a heating plate for 30 min. to evaporate the excess solvent and to form a continuous polymeric film, binding the particles together.

Laser cladding was carried out using a Coherent F1000 diode laser together with a Precitec WC 50 welding head manipulated by a CLOOS welding robot, Argon was used as shielding atmosphere surrounding the preplaced powder. A 2 mm spot laser spot diameter was used and 12 partially overlapped tracks were realised on the sample with a scanning speed of 8mm/s and a laser power of 680W. Three identical samples were fabricated to validate the tests. Etch sample was precision cut and prepared form microstructure investigation by grinding polishing and etching with a metallographic reagent representing a weight ratio mixture of $FeCl_3$: CrO_3: HCl 37%: distilled water = 5:1:1:20.

The copper plate with the pre-placed glass-ceramic starter powder used in this study [PSS17] and the glassy coating obtained through laser cladding is illustrated in Figure 3.10(a). It can be clearly observed from Figure 3.10(a) that the addition of poly (vinyl alcohol) aqueous solution as binder in the composition of the powder mixture contributes to the obtaining of a ceramic-starter paste with high surface energy, which contributes to a uniform spreading on the copper substrate and improves the homogeneity of the mixture, by impeding the gravimetric separation of the particles. The overall dimension of the powders used in the starter-paste composition is 1-3 μm, with the hydroxyapatite particles having a higher average diameter (3-6 μm). The uniformity of the pre-placed ceramic coating starter could be also evidenced by the EDX elemental composition depicted from the surface of the coating (Figure 3.11), which

comprises all the main elements (Al, Ti, O, Ca, P) in an approximate ratio similar with the gravimetric fractions of the components in the prepared powder mixture receipt.
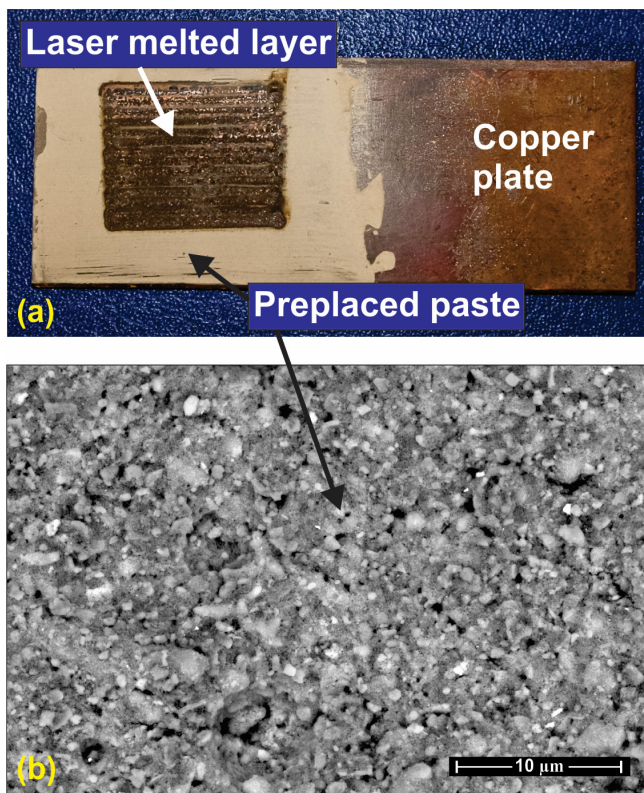

Fig. 3.10 a) Sample appearance after the laser melting, b) the SEM images of the preplaced powder before laser processing [PSS17].
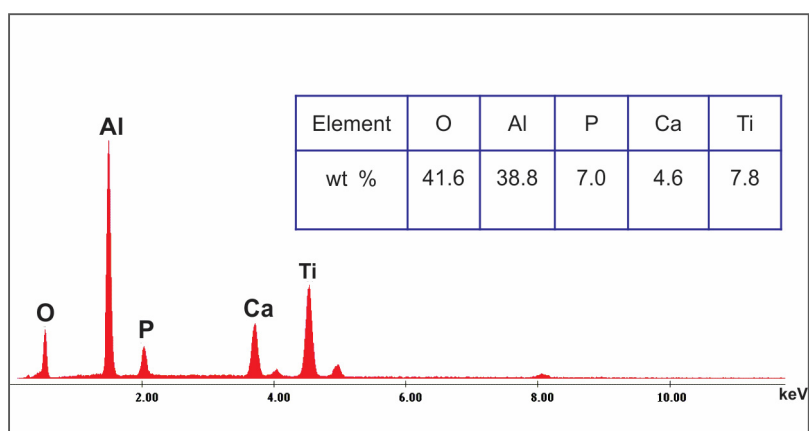

Element	O	Al	P	Ca	Ti
wt %	41.6	38.8	7.0	4.6	7.8

Fig. 3.11 EDX analyses of the pre-placed powder before the laser processing
(EDS set-up: kV: 30.00 Tilt: 0.00 Take-off: 2.92 AmpT: 12.80) [PSS17].

Optical microscopy of the samples shows that a 15 to 40 μm glassy-ceramic layer was coated on the surface of the cooper substrate. The coated layer is not uniformly deposited on the copper surface and presents no visible transition line between the materials.

Figure 3.12(a) illustrates the geometrical appearance of the layer and the heat affected zone. The copper substrate has visible heat affected zone (Figure 3(b)) where a dynamic recrystallization up to 300 µm from the surface occurs due to the intense thermal gradient induced by the laser radiation (Figure 3.12(b)). The recrystallization phenomena lead to the substrate hardness increasing from 63 $HV_{0.05}$ to 86 $HV_{0.05}$ in the proximity of the coated layer (Figure 3.20). The laser cladding using a starter pre-placed paste lead to the formation of a glassy-ceramic coating on the surface of the copper plate, as it can be observed from both optical (Figure 3.12(a)) and SEM micrographs (Figure 3.13 and 3.14).

The glassy-coating formation could be due to the synergistic action of three factors, namely: a) the high local temperatures reached through laser beam directional focusing on the surface of the sample; b) the high temperature gradients arising from the rapid cooling of the oxidic-HA melt and c) the presence of HA as glass forming agent, which impedes the crystallization of the oxides as ceramic.
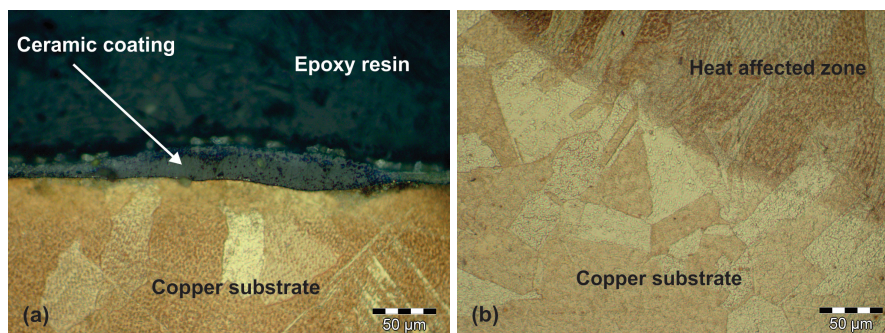

Fig. 3.12 (a) Optical microscopy of the ceramic coated layer and (b) the heat affected zone [PSS17].
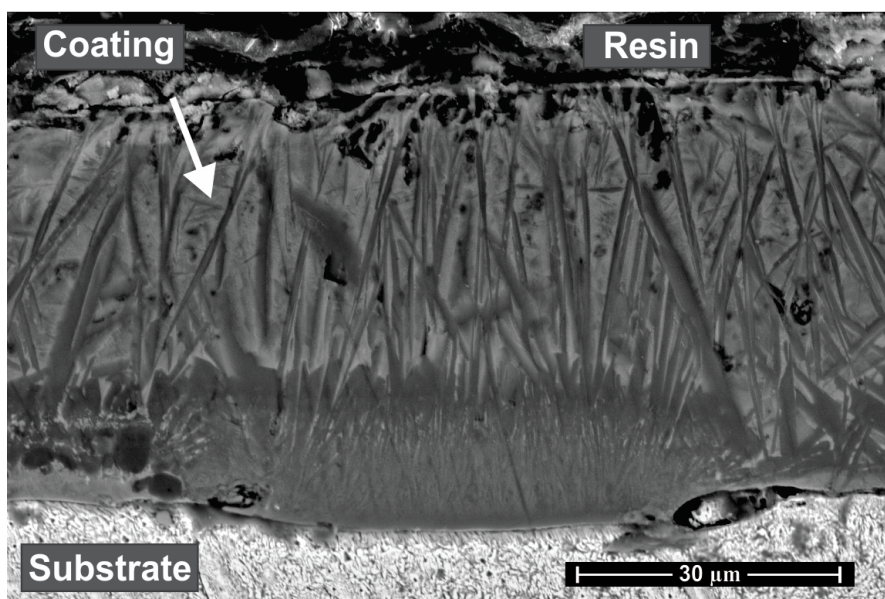

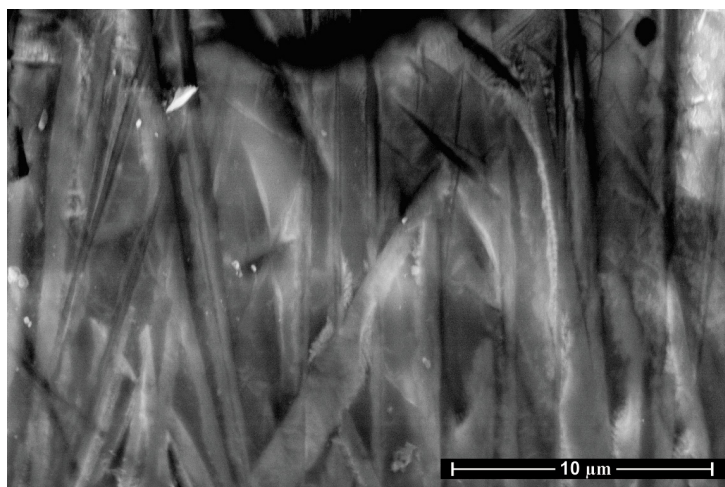Fig. 3.13. SEM image of the ceramic coated layer [PSS17].

Fig. 3.14 Detail of the $(Al_2O_3+TiO_2)$/Al/HA amorphous coating fabricated by laser cladding [PSS17].

SEM microscopy from Figure 3.14 reveals further insight on the microstructure of the obtained coating. As the oxidic-HA melt in contact with the base material (as copper can uniformly distribute and radiate heat) cools at a lower rate than the melt from the top of the material, in contact with the atmosphere, the bottom part of the coating is richer in crystalline ceramic phases entrapped in a dominatingly amorphous glassy matrix, while in the upper part, the glass phase is predominant [PSS17]. Throughout the glass phase, several columnar-shaped crystalline phases could be observed, almost perpendicular to the surface of the base material.

The dominatingly amorphous (glass) phase presence in the coating is also confirmed by XRD diffractogram data from Figure 3.15 (the broad reflection peak from ~ 20.15°; 23.84° and 25.18°). The overall crystallinity of the coating, calculated as the sum of the peak areas of the crystalline phases, reported to the overall area under the diffractogram is 47.83%.
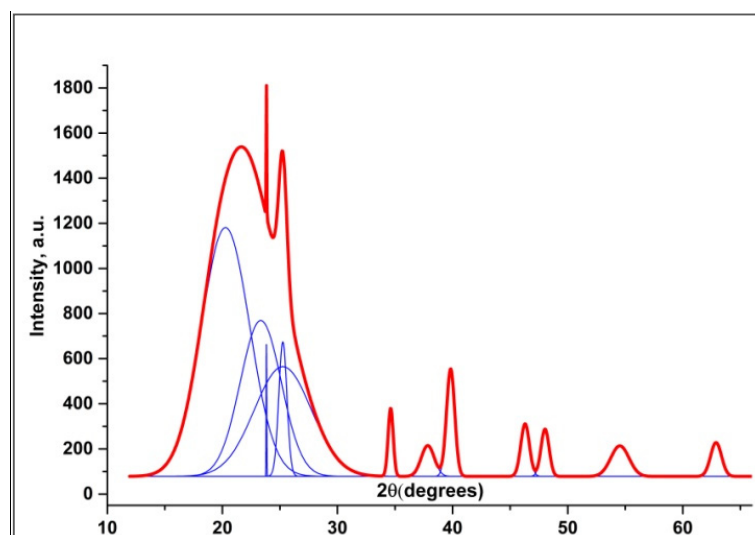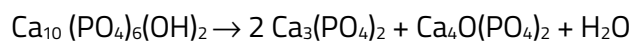

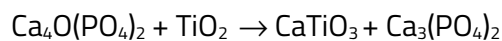Fig. 3.15. XRD diffractogram of the obtained coating [PSS17].

From the diffractogram, the presence of several crystalline phases could be noted, coming from both compounds found in the original ceramic-starter powder, such as hydroxyapatite Ca_{10} $(PO4)_6(OH)_2$ (23.87°; 39.86°); α-Al_2O_3 (34,78°); TiO_2-rutile (54,57°), intermediary hydroxyapatite decomposition, such as β-$Ca_3(PO_4)_2$ (25.17°) or copper oxidation (CuO, at ~37.83°) products as well as new phases, such as Al_2TiO_5 (46.27°) and $CaTiO_3$ (~62.86°). These new phases could be embedded in both crystalline form in the glass-matrix, or they could form glass on their own, with the HA, decomposed HA-resulted TiO_2 and Al_2O_3 components. Due to the presence of several reflections of the amorphous phases, it could be suggested that the glass matrix could be multiphasic, determined by the different diffusional processes of the glass-forming compounds in the laser-generated melt.

The role of HA could be therefore concluded as hard-phases generator (through forming IR-absorptive ceramic titanates) and as glass forming agent, either as calcium triphosphate, or mixed with Al and Ti oxides.
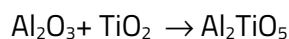

- Glass/ceramic forming compounds

Ca_{10} $(PO_4)_6(OH)_2 \rightarrow 2\ Ca_3(PO_4)_2 + Ca_4O(PO_4)_2 + H_2O$

- Ceramic forming compound

$Ca_4O(PO_4)_2 + TiO_2 \rightarrow CaTiO_3 + Ca_3(PO_4)_2$

- Mixed Al/Ti oxides (glass/ceramic forming)

$Al_2O_3 + TiO_2 \rightarrow Al_2TiO_5$

The study approach through determining a combined embedding and/or formation of IR-absorptive components into a glassy matrix, protects the assembly from degradative factors, as well as ensuring a mechanical-resistant coating [PSS17].

The presented method eliminates the disadvantages of the traditional solar collectors obtaining, related to low economic efficiency (sequential processing) or environmental risks (potentially toxic precursors), through using an integrated laser-processing approach.

Also, by using glass in molten state, a more efficient covering of the substrate metal could be achieved than in the case of traditional spray pyrolysis techniques, due to the good wetting properties of molten glass. The presence of CuO, as depicted also from the XRD diffractogram could act as a compatibilizer between the base metal and the coating.
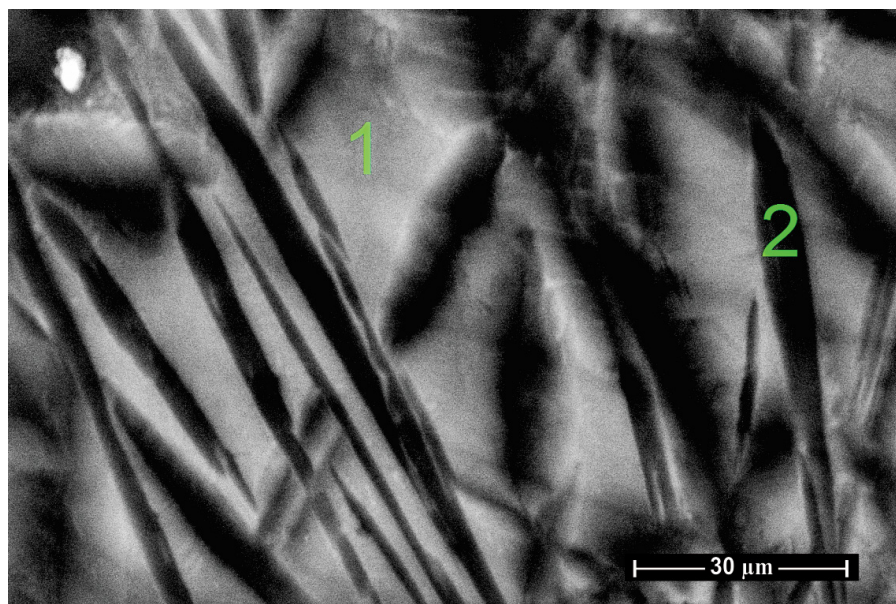
Fig. 3.16. Localization of the EDS spectrum realised on the glassy coating, white area, and dark area [PSS17].

Element	O	Al	P	Ca	Ti
wt %	40.05	40.67	0.66	8.79	9.84

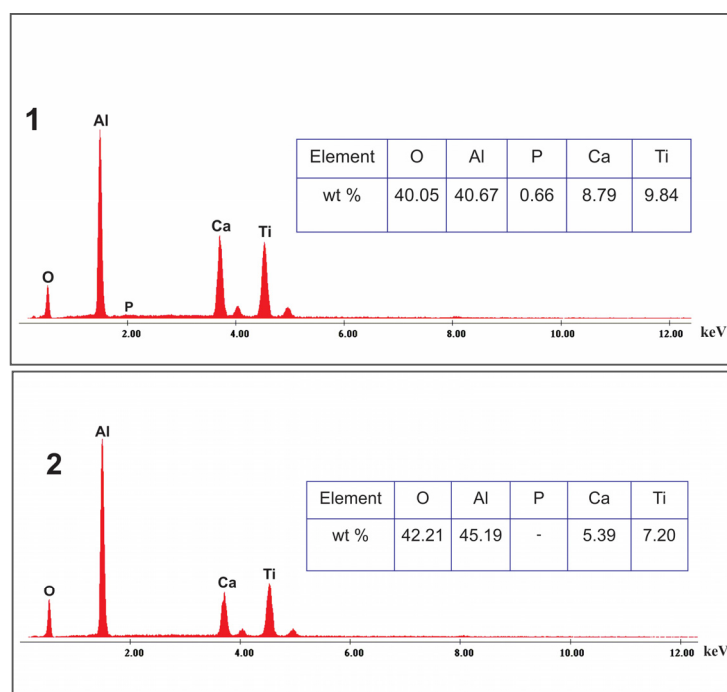| Element	O	Al	P	Ca	Ti
wt %	42.21	45.19	-	5.39	7.20

Fig. 3.17. EDX spectrum of the white (1) and black (2) area indicated in Figure 6 (EDS set-up: kV: 30.00, Tilt: 0.10 Take-off: 5.45, AmpT: 12.80) [PSS17].

EDX spectrum (Figure 3.17) on the glassy region of the coating reveals the presence of all the initial components from the powder mixture used for laser cladding (zone 1 from Figure 3.16). The darker crystalline areas depicted in Figure 3.16 (zone 2) contain a higher amount of aluminium, while containing no phosphorus. They could be formed by large oxides/mixed

oxides crystallites, which play an important role in tuning the optical properties of the assembly, as well as in contributing to the hardness (Figure 3.20) and mechanical stability to the assembly.

From the cross-sectional EDX elemental distribution illustrated in Figure 3.18 it could be observed that the surface of the coating is richer in Ca, Al, O and P, which are efficient glass-forming elements, while the coating in proximity to the base material is richer in Ti, a crystalline ceramic-forming element.
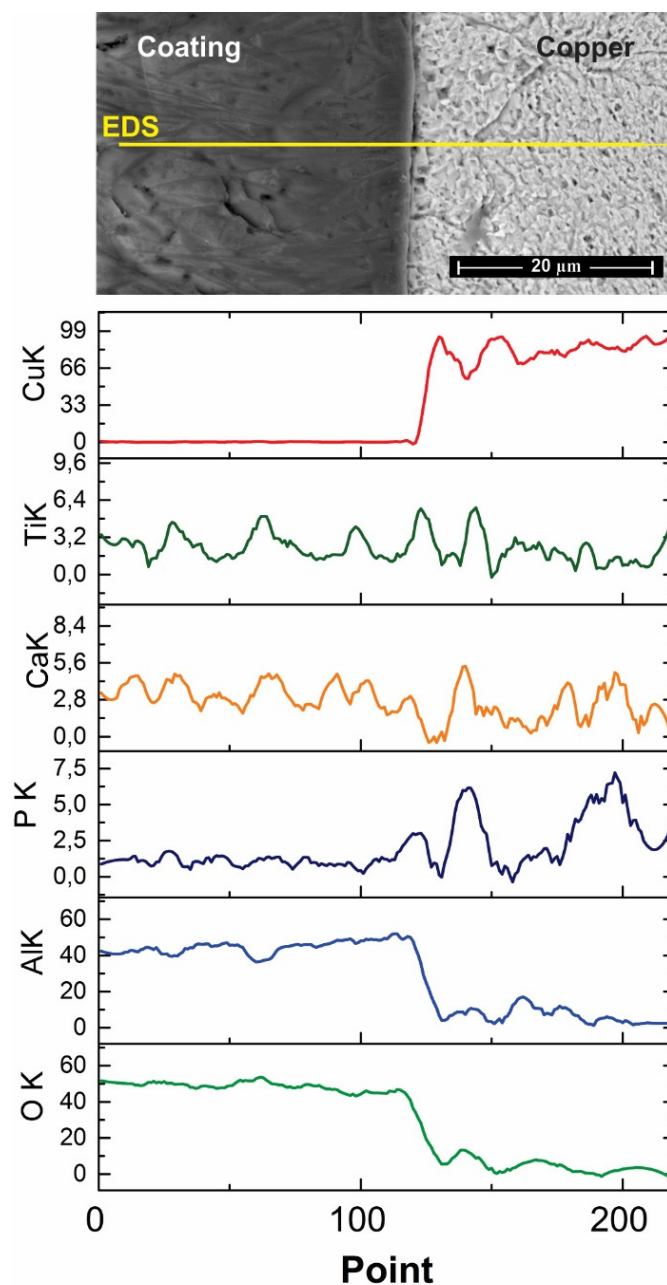

Fig. 3.18 EDS line spectrum analyze in the cross section of the specimen (Kv 20.0, Mag 7000, Tilt 0.0 Averaging 16) [PSS17].

With the respect of Figure 3.19(a), the obtained coating presents good transparency in the 550-800 nm domain, reflecting the wavelengths corresponding to the copper substrate. This is particularly important in the field of designing non-black solar absorbent materials.

The NIR spectra of the coating presents several absorption bands, such as those centered at ~1262 nm ascribed to -OH groups overtones (from HA or hydrated ceramic compounds); ~1862 nm, ascribed to P-O groups vibration overtones; ~1585 nm, ascribed to Ti-O vibration modes in TiO_2 and/or TiO_3^{2-} and 949 and 1075 nm, ascribed to Al-O bonds from Al_2O_3 and/or aluminates.
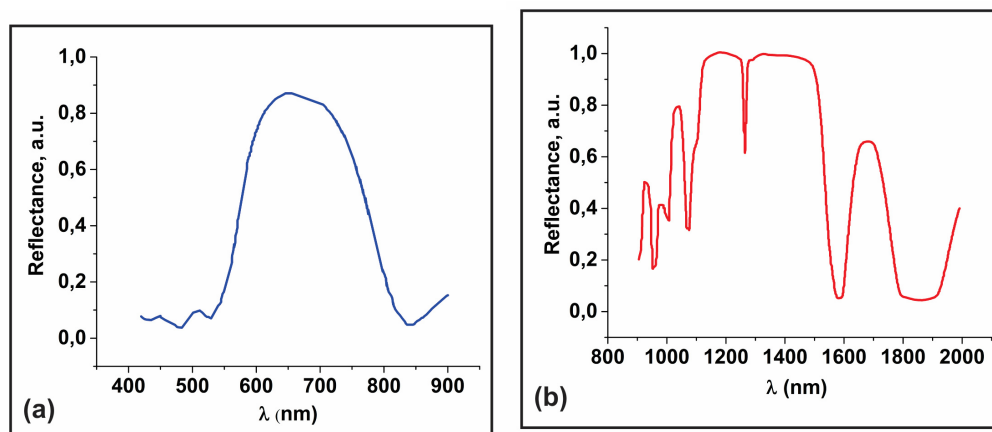

Fig. 3.19 (a) VIS and (b) NIR reflectance spectra of the ceramic coating [PSS17].

The solar absorptance (αs) of the material, theoretically defined as weighted fraction between absorbed radiation and incoming solar radiation in the wavelength interval 0.4– 2 μm, has been determined using equation 3.1[16].

$$\alpha_s = \frac{\int_{0.4}^{2} I_s(\lambda)(1 - R(\lambda))d\lambda}{\int_{0.4}^{2} I_s(\lambda)d\lambda}$$

(3.1)

where $I_s(\lambda)$ represents the solar spectra irradiance for a given mass of air, according to the ISO standard 9845-1 (1992) and $R(\lambda)$ represents the reflectance of the coating in the specified wavelength interval.

The value of the solar absorptance of the glass-ceramic coating obtained by presented laser cladding method on copper substrate is α_s=0.816, comparable to other Al_2O_3 or Al_2O_3-MO_x systems (where MO= NiO, TiO_2, WO_3 and so forth) which fell in the range of 0.7-0.9.

The average hardness value of the coating is up to 16 times higher than that of the substrate, proving the formation of hard glassy/ceramic phases, but also with brittleness low enough to prevent the cracking of the sample during analysis. Further studies are needed to improve the

bonding with the substrate and to characterize the thermal emittance of the glassy-ceramic coating, as well as its stability to degradative factors (metal ions leaching from the glass matrix, wear resistance). Also, by tuning the operational parameters such as the ratio between the components from the glass/ceramic starter powder and the laser cladding regime, materials with improved optical properties (high absorptance and low thermal emittance coefficients) can be obtained using this method.
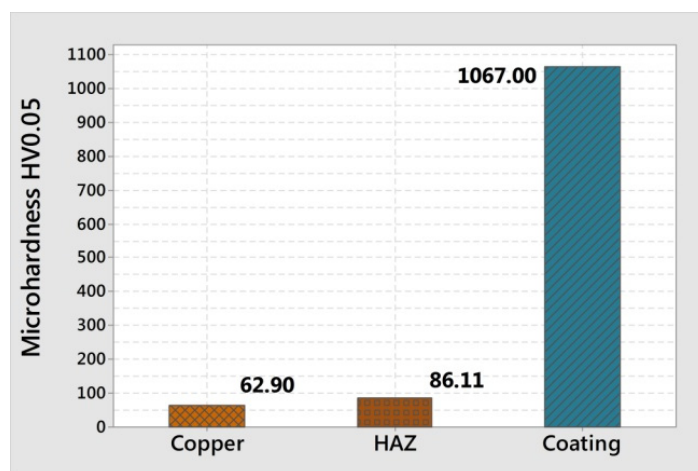

Fig. 3.20 Microhardness of ceramic coating, copper substrate and heat affected zone [PSS17].

In conclusion, a glass/ceramic Al_2O_3-TiO_2 composite coating has been obtained through laser cladding directly on the copper substrate, without the addition of a buffer layer. The addition of hydroxyapatite in the composition of the glass/ceramic starter lead to the obtaining of a crack-free glassy matrix, in which several titanate/aluminate columnar-shaped hard crystalline phases could be observed, almost perpendicular to the surface of the base material [PSS17]. The glassy/ceramic coating presents high hardness values.

The assembly presents promising potential as use in non-black solar-collectors designing. The solar absorptance coefficient of the coating is 0.816, comparable with other Al_2O_3-based materials, and the transparency of the coating is optimal in the 500-800 nm domain.

By using the presented laser cladding approach [PSS17], novel IR-absorptive coatings could be designed in a one-step procedure, eliminating traditional sequential processing (deposition of powders starting from precursors, annealing and so forth) while being more environmental friendly. The high price of the laser treatment method could be overcome by the obtaining of efficient, corrosion-resistant coatings. Thus, further studies are needed to assess the chemical and environmental stability of the obtained coating, as well as for fine tuning the composition of the ceramic starter, to obtain materials compatible to a sustainable development of the society.

3.3. Carbon nanotubes composite coating by laser cladding

3.3.1 Concept

Carbonaceous nanoscale additives present pronounced influence on the mechanical properties of both metallic and plastic materials. The obtaining of durable metal coatings with improved mechanical strength, wear, and corrosion resistance represents both a milestone and a focal point of the research conducted in the last decades in the field of materials development. Shifting the technological barriers in the field of metallic coatings to further levels, dictated by the need for "greener" and cost-effective technologies, for lighter metallic materials, and by the overall increasing trend in the price of alloying elements and dispersion phases, has led to a growing interest in embedding nanomaterials (with an emphasis on carbon-derived nanomaterials) into the metal phase. The high aspect ratio of nanomaterials, coupled with their remarkable mechanical properties, chemical stability, and higher available surface area for interacting at the atomic level with the embedding host material, has led to the obtaining of materials with unique properties not found otherwise when using ordinary micro- and macroscale materials.

The results presented in this habilitation thesis aim to improve the quality of the cladded layers by fine tuning the process parameters, by microalloying and heat treatments of the coatings or by using the gradient coating technique. However, it is clear that a new direction must be approached to improve the mechanical proprieties of the coatings.

Therefore, I designed and proposed a pulsed laser cladding method [PSC19] to obtain nickel-based hard coatings on a mild steel substrate, starting from a pre-placed commercial NiCrBSiFeC powder, mechanically blended with single-walled carbon nanotubes (SWCNTs), for improving the microstructure, hardness, tribological properties and corrosion resistance of the obtained cladded layer.

3.1.2 Methods, materials and results

The commercial Metco 12C powder used for the cladding test (SULZERMETCO 12C) was purchased from Sulzer Metco Inc., with the following elemental composition (wt. %, according to producer specifications): 84.5%Ni; 7.5% Cr; 1.7%B; 3.5% Si, 2.5%Fe; 0.25% C, the balance representing the Ni base. The SWCNTs have been purchased from Sigma-Aldrich and were of

>85% purity and average diameter distributions between 1.3 and 2.3 nm and median length >5 μm.

AISI 5140 (EN 10083-1, grade 37Cr4) steel has been used as a substrate for coatings deposition. Workpieces with dimension of 60 x 25 x 8 mm have been fabricated by milling from the same raw material in order to prevent any structural or morphological variation between the samples. Before coating, the substrate surface was polished to a 0.8 μm grit and washed several times with ethanol (98% wt.), to remove trace of organic contaminants.

The NiCrBSiFeC powder and SWCNTs (0.2% weight SWCNTs reported to the metallic powder) were mechanically blended by using a FRISTCH Planetary Micro Mill PULVERISETTE 7 with hardened stainless-steel grinding spheres. The optimum metal powder/SWCNT weight ratio reported in this paper has been chosen based on preliminary studies which indicated high susceptibility to cracking for the composite coating with higher SWCNTs loadings. The milling time was 40 minutes at 450 rpm speed, ensuring optimal embedding of the SWCNTs into the metal phase, based on prior experimenting of milling time optimization. The temperature of the grinding bowls was kept below 70 °C to prevent any morphological changes of the powder. In the Figure 3.21 is presented the powder morphology after the mixing process with CNTs. The spherical shape of the powder is maintained after the rotational ball milling and only minor deformation can be observed due to the impact with the steel balls. The SEM analyses emphasize a good adherence of the CNTs to the particle of NiCrBSiFeC (Figure 3.21(d)).
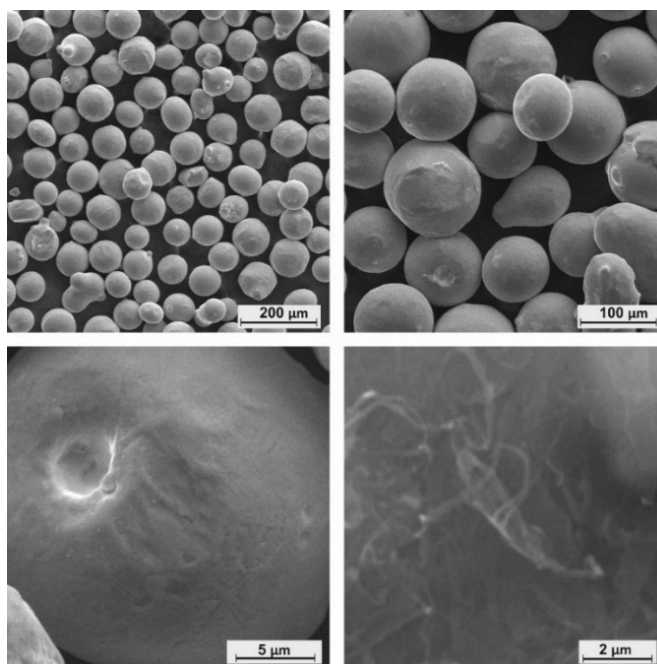

Fig. 3.21. SEM micrographs at different magnifications of NiCrBSiFeC powder milled with SWCNT [PSC19].

The mechanically-blended powder was mixed with a 12% wt. poly (vinyl alcohol) (PVA) (purchased from Sigma-Aldrich, the average polymerization degree of 900 and a hydrolysis degree of 98.5%) aqueous solution until the obtaining of a homogenous and free-flowing viscous paste. The paste has been pre-placed on the steel substrates, kept at room temperature for 4 hours until complete water evaporation, ensuring a final thickness of 2 mm for the mixture.

A Nd:YAG TRUMPH TruPulse 556 laser system (λmax=1064 nm) and a Precitec YC 50 cladding module manipulated by a 6-axes CLOOS robot has been used for the laser cladding experiments. Argon of 99% purity at 18 l/min flow rate was used as shielding gas for the preplaced powder. The cladded layer was fabricated by laser cladding of 12 partially overlapped tracks on the base material with the following parameters: 1500 W laser power, 1.3 mm spot diameter, 3J laser energy, pulse duration 2 ms and 90 Hz frequency, deposition speed: 27 cm·min-1, as summarised in Table 3.3. The overlapping degree was 45 %.

Three sample batches of samples 1 and 2 have been obtained following the procedure as mentioned above, to ensure the repeatability of the results. Reference sample (sample 1), without SWCNTs in the composition have been obtained following the same procedure [PSC19].

Parameters of the laser cladding process   Table 3.3

Powder	Sample	Parameters				
		Laser power [W]	Laser Energy [J]	Pulse [ms]	Frequency [Hz]	Speed [cm/min]
NiCrBSiFeC	Sample 1 Reference (without CNTs)	1500	3	2	90	27
	Sample 2 with CNTs	1500	3	2	90	27

The microstructure of the cladded specimens has been studied both on the surface of the coating (the surface was levelled, the top 1/3 of the coating being removed) and in cross-section. The samples (on both surface, and cross-section) were ground, polished to 0.5 μm, and finally etched for 5 s with 3:1 (vol:vol). HCl:HNO$_3$ reagent (aqua regia). A Leica DM ILM

inverted microscope (50 $\times$, 200 $\times$, 500$\times$) and a VegaTescan LMHII scanning electron microscope (SEM) was used to acquire the micrographs of the cladded assemblies.

The samples have been analysed in cross-section and on the top surface that was previously machined. The coatings-substrate interface is characterised by a good bonding and a geometrical dilution (η) of 20 and 25 % between cladded layer and the substrate. The base material presents an ferito-pearlitic structure with lamellar pearlite that was transformed during laser processing into a martensite or austenite structure in the heat affected zone.

Figure 3.22 shows the cross sections for the reference sample and the CNTs-fabricated sample with the addition of carbon nanotubes. The only difference between the samples, meaning compositional and laser processing, is the addition of single-walled carbon nanotubes in the composition of sample 2. In both cases, the cladded layer is free of cracks and pores and has a typical structure, common to both powder metallurgy and laser cladding processes (Figure 3.22(a) and 3.22(b)).

The bottom part of the coating contains a typical powder metallurgy feature, resulted from the coalescence of the uniformly-melted metal particles, namely a 5µm-thick planar crystal, as represented also in the principle mechanism form Figure 3.23. Due to the verticality of the heat gradient and to the high cooling ratios, the individual melt pools above the planar base crystal tend to crystalize in long primary dendrites (Figure 3.22(c) and 3.22(d)). The subsequent passing of the laser beam in adjacent regions determines the re-melting of the tops of the dendrites, with the formation of equiaxed crystals, which can be found near the top of the coating (Figures 3.22(e) and 3.22(f), and the principle mechanism scheme from Figure 3.23).

To quantitatively assess the microstructural grain refinement that the CNTs promote in the coating, the ImageJ software (with the *Analyse Particles* plugin) was used to automatically compute the grain boundaries from the selected optical micrographs, i.e. Figures 3.22(e) and 3.22(f) and plot the histogram of grain areas frequency, following the contrast enhancement and binarization of the images [PSC19].

CNTs addition determines a more uniform distribution of grain dimensions and a higher proportion of equiaxed crystals, as it can be seen from Figure 3.22(g), probably due to their confining effect on the melted metal particle (being concentrated in the walls of the initial spherical metal particles that expand during melting) and, subsequently, presenting high thermal conductivities they could act as local heat gradient disruptors, leading to the preferential formation of uniform crystals, rather than dendrites, as is the case with the reference powder.
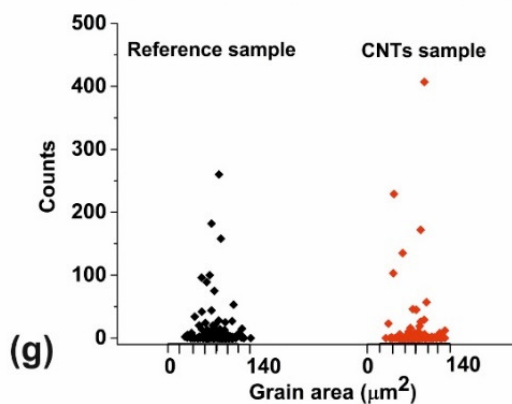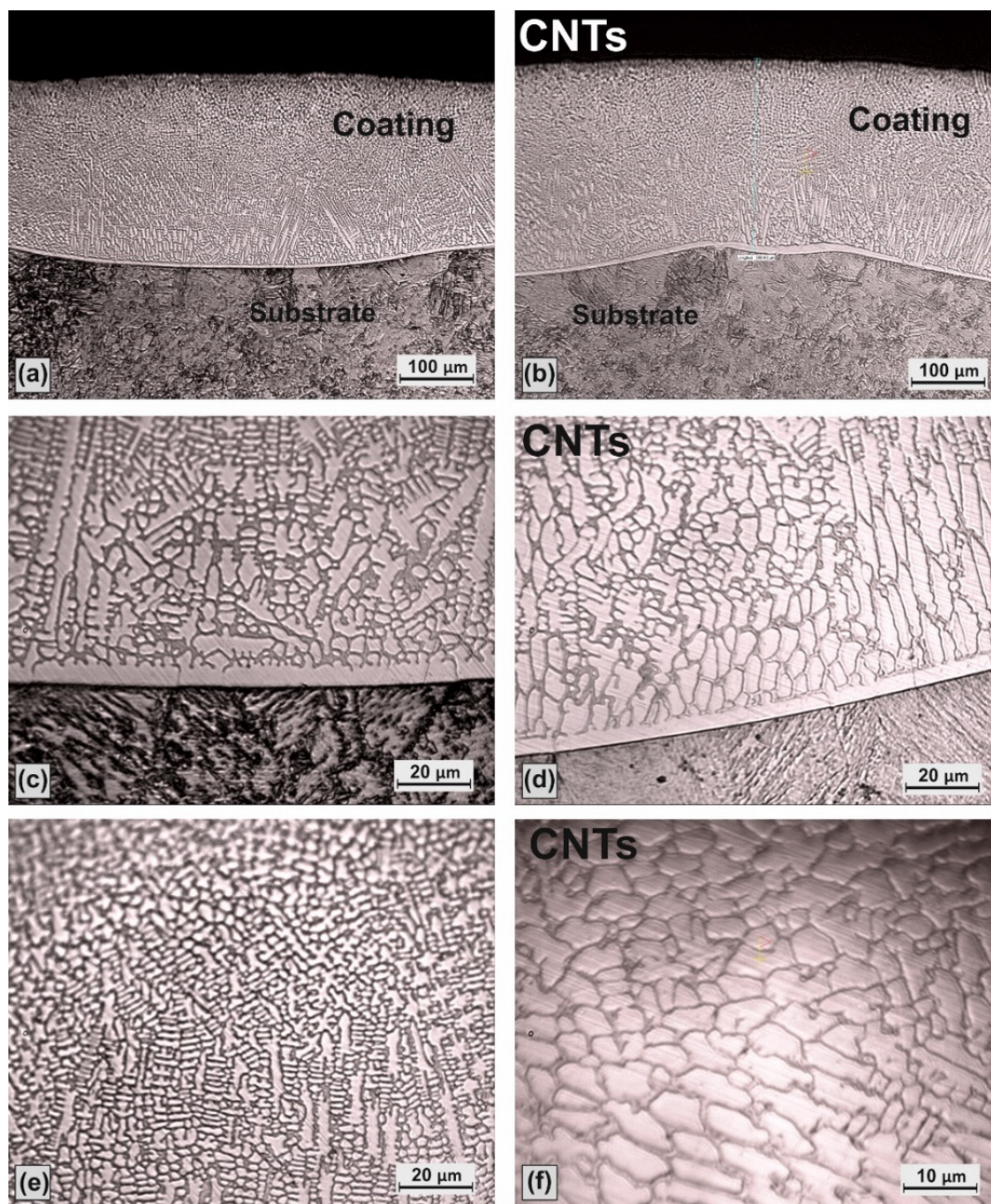
Fig. 3.22. Cross-section microscopy of the cladded layer of the reference sample 1 (a), (c), (e) and sample 2 with CNTs addition (b), (d), (f); (g) show the grain area distribution histograms [PSC19].
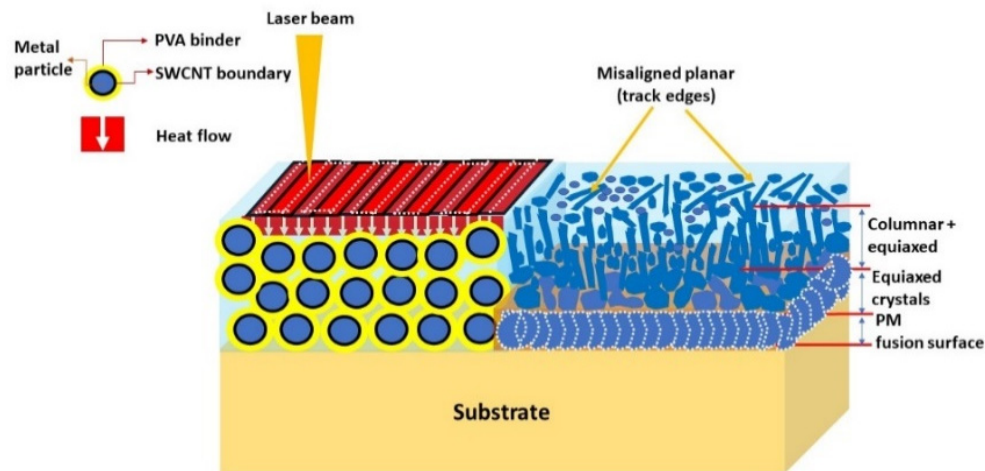
Fig. 3.23. Schematic representation of the growth mechanism of dendrite structure [PSC19].

Due to the localised micro-strains occurring in adjacent melt pools boundaries, the dendrite growth does not occur entirely in the direction of the heat gradient. In this respect, misalignments could be observed, as illustrated in Figure 3.24, for both reference and sample fabricated with CNTs. Higher misalignments could be observed in the case of the sample fabricated with CNTs, probably due to the local disruption in the heat gradient and due to grain growth hindrance [PSC19].
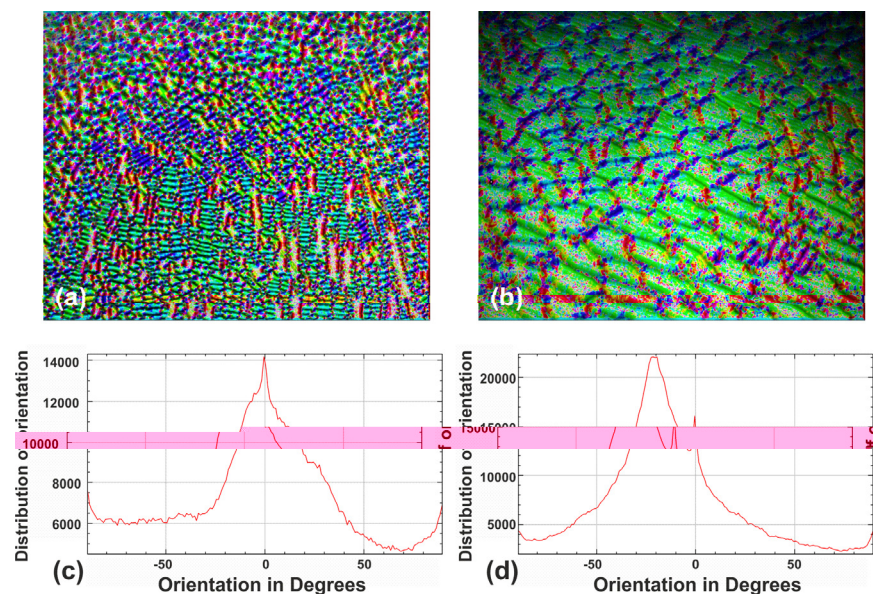

Fig. 3.24. Grain orientation angle mapping and plot (obtained by ImageJ software – Orientation J plugin) [PSC19].

Similar microstructural patterns can be found on the machined-levelled surface of the coatings. In the Figure 3.25 is presented the microstructural appearance after the 1/3 from

the top of the coatings was removed showing the dendrite structures which are sectioned in their growth direction.

Very long dendrite arms are observed in the region of the tracks overlapping area (Figure 3.26) and more uniform structure in the middle of each cladded track. Therefore, can be assumed that high growth rate of dendrite structure is increased during the re-melting that occurred during the partial overlapping of the tracks.
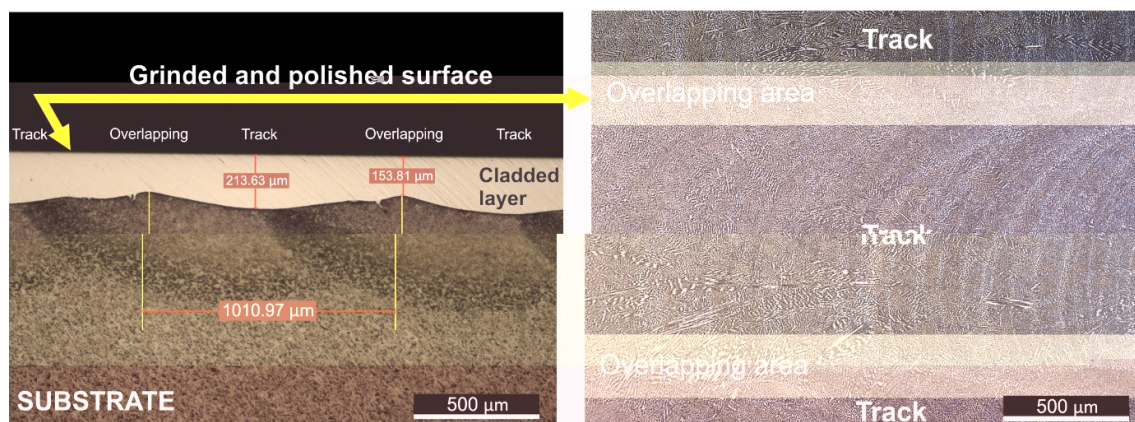
Fig. 3.25. Top surface profile of the reference sample after 1/3 was removed [PSC19].
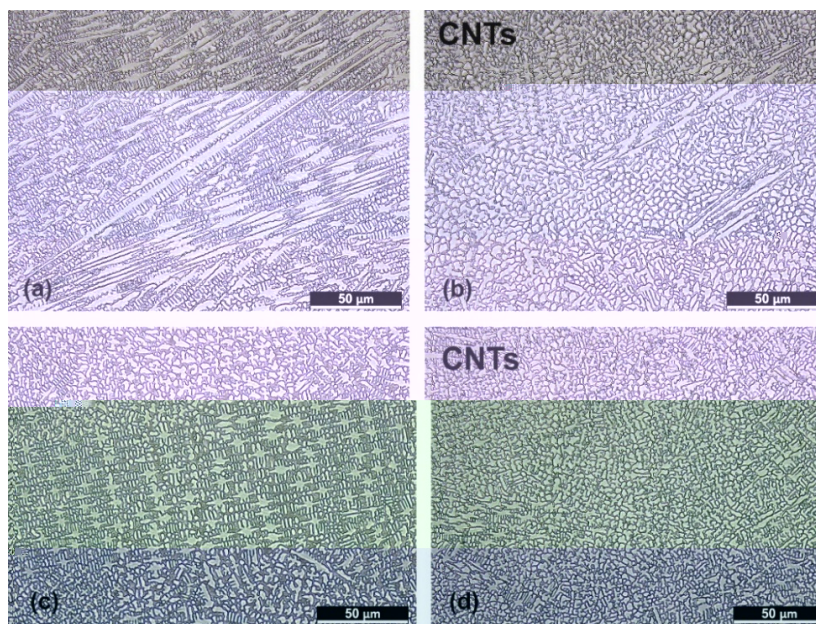
Fig. 3.26. Microstructure of the machined top surface, (a) and (c) reference sample, (b) and (d) CNTs composite coating [PSC19].

Figure 3.26 reveals the differences of the grown pattern of the columnar dendrite with and without the addition of CNTs. The CNTs additives determine the refining of the grains microstructure and homogeneity. As indicated in the Figure 3.26, the sample 1 has a large

variety of dendrite shapes from equiaxed to elongated with dimensions between 2 µm up to 400 µm. The grains dimension is smaller in the case of the cladded layer obtained with the nanotubes addition as showed in Figures 3.26 (b) and (d). The CNT addition influences the growth of mainly equiaxed dendrite. Due to the high thermal conductivity of the CNTs determines a non-preferential growth direction of the dendrites while in the case of the reference sample the crystallization is orientated along the heat flow produced during the laser processing.
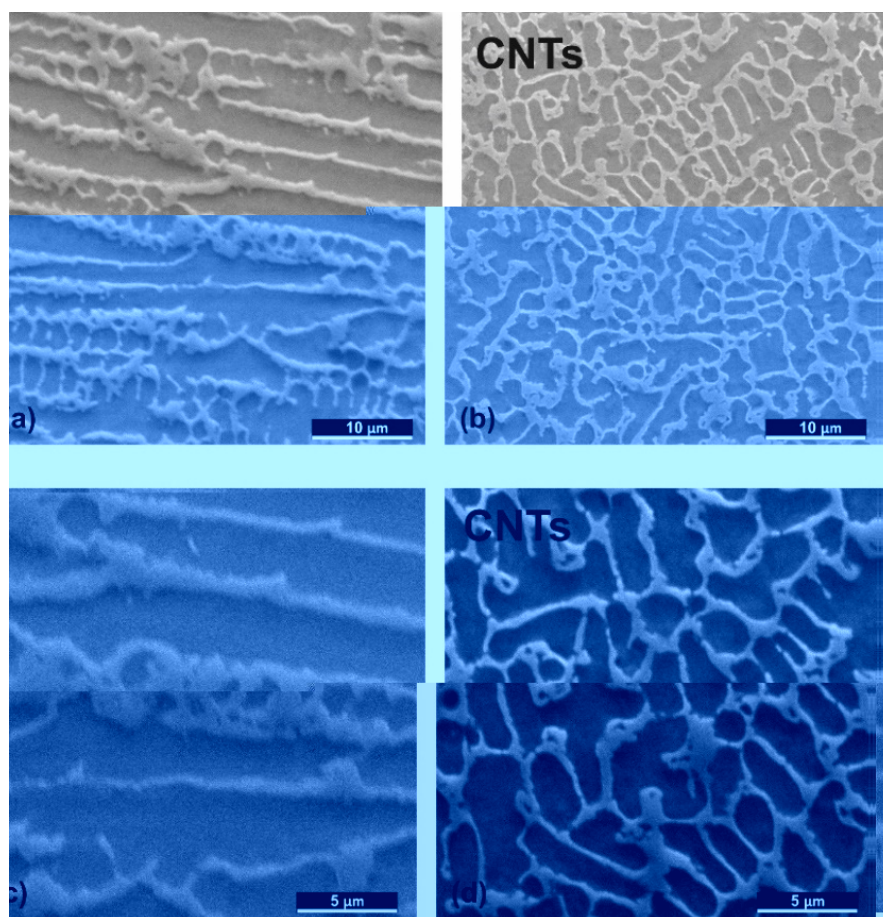
Fig. 3.27. SEM microscopy of the machined top surface, (a) and (c) reference sample, (b) and (d) CNTs composite coating [PSC19].

The SEM overall appearance of the dendrite structure agree with the optical microscopy presented in Figure 3.27. The grains are well fused into the matrix without any defects such us pores, inclusions or microcracks. The nanotubes could be included at the grain boundaries (the lighter colors indicate the higher rigidity/hardness of the structure). The CNTs that have not been decomposed during the laser cladding process can be found as interstitial solid solution with the nickel and iron and possible monodispersed hard phases with chromium and

boron. The hard phases (with the possible remainder of carbon nanotubes) are segregated at the grain boundaries which is in the accordance with the AFM images from the Figure 3.28. The AFM cantilever is influenced by the Young elastic modulus of the material (i.e., hardness, rigidity). Therefore, the soft and hard phases of the material can be distinguished by using the cantilever vibration movement. The processed image indicate with lighter color the areas with an higher hardens-rigidity domain (e.g. carbides and intermetallic compounds) and with darker color the surfaces with a lower hardness.
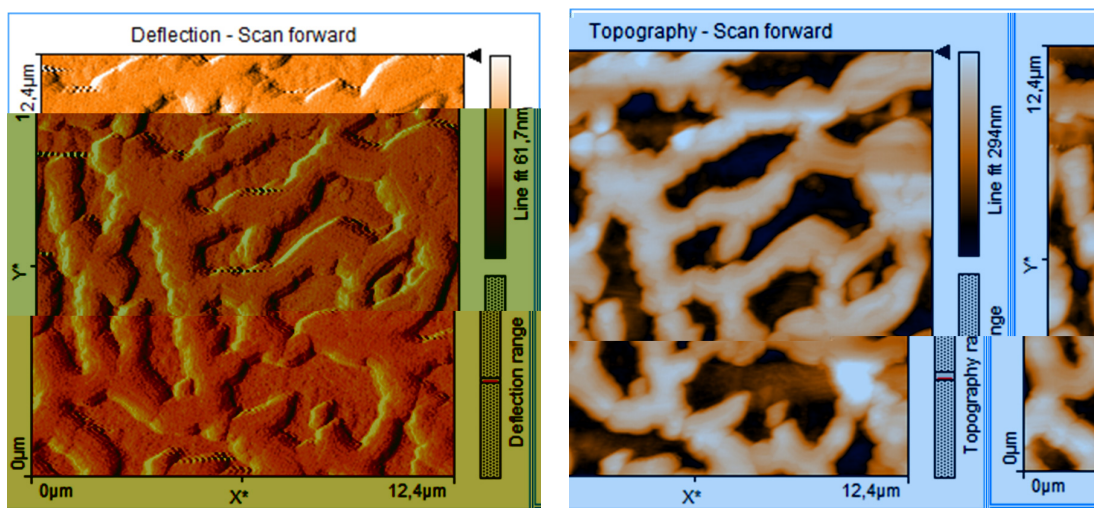

Fig. 3.28. Atomic force microscopy on composite sample using deflection and topography scanning mode [PSC19].
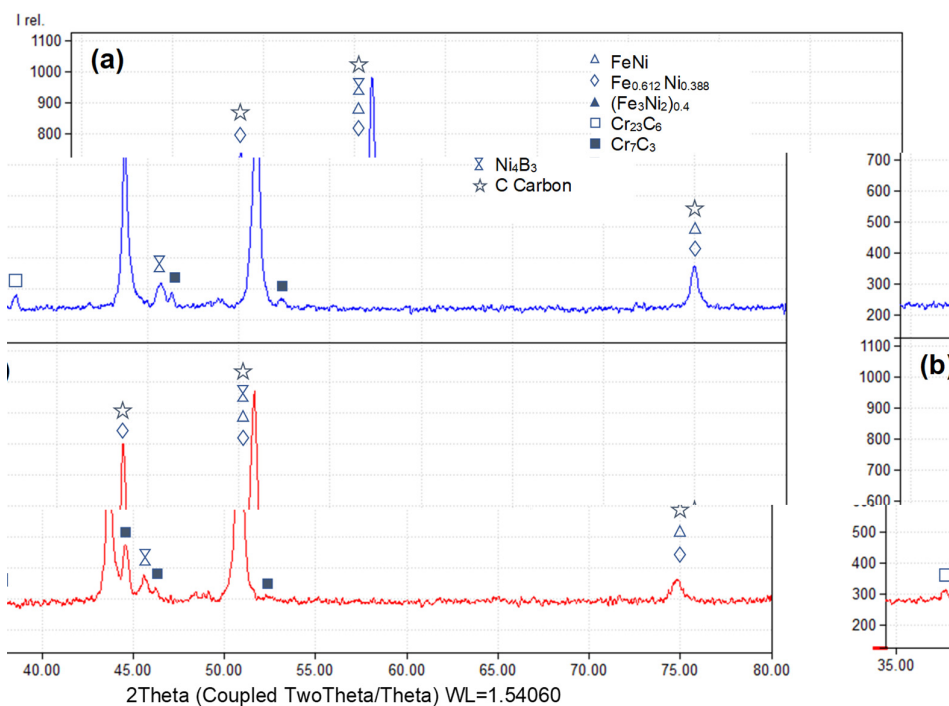

Fig. 3.29. XRD diffractogram of the reference sample (a) and CNTs composite coating (b) [PSC19].

The crystalline structure of both samples was analysed by XRD. The diffractograms indicate that the cladded layer is composed of a complex mixture of borides and carbides (Cr23C6, Cr7C3, Ni4B3) arranged in an iron nickel (FeNi) matrix.

It can be observed that the main phases identified, namely FeNi, Cr23C6, Cr7C3, Ni4B3 and C are similar for both samples. The main difference between the samples is observed at 44.58° where a high intensity peak identified as Cr7C3 appears in the case of CNTs composite coating. The coatings fabricated with the Metco 12 C powder (NiCrBSiFeC) are characterised by a low hardness (370 HV_{03}) with the benefits of a very low cracking susceptibility and a good machinability. The testing shows that composite coatings have a 364 HV_{03} microhardness compared with the reference sample characterised by a microhardness value of 342 HV_{03}. The microhardness testing on the sample cross-section show a decreasing from the top of the coatings to the bottom of the coating due to the iron diffusion from the base material.

The microhardness testing on specific dendrite and interdendrite structure is a useful tool to compare the microhardness of the coating with and without the addition of CNTs. Due to the low loading (0.5 gF) the indentations can be located exactly on the interface line with the substrate and on the dendrite arms. Figure 3.30 shows the results obtained on the reference sample being obvious that inter-dendrite areas (Ni matrix) has an almost double microhardness compared with the dendrite arms.

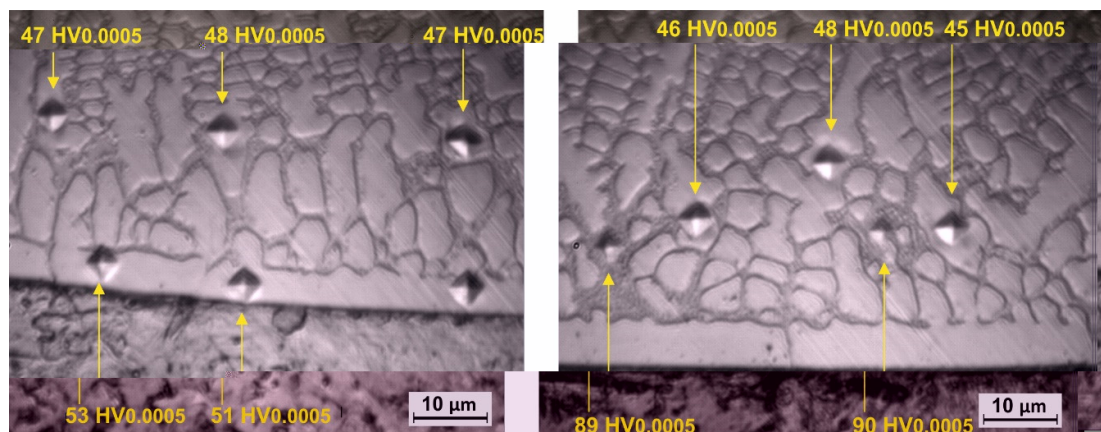Fig. 3.30. Micro indentation on the dendrite arm and on the interdendrite area of the cross–section of sample 1, Loads 0.0005 kgF [PSC19].

Addition of CNTs has no major influence near the interface with the substrate, where a microhardness between 50 $HV_{0.0005}$ and 59 $HV_{0.0005}$ has been recorded mainly because in this zone the cooling rate is too high and the grain dimension is not reduced.
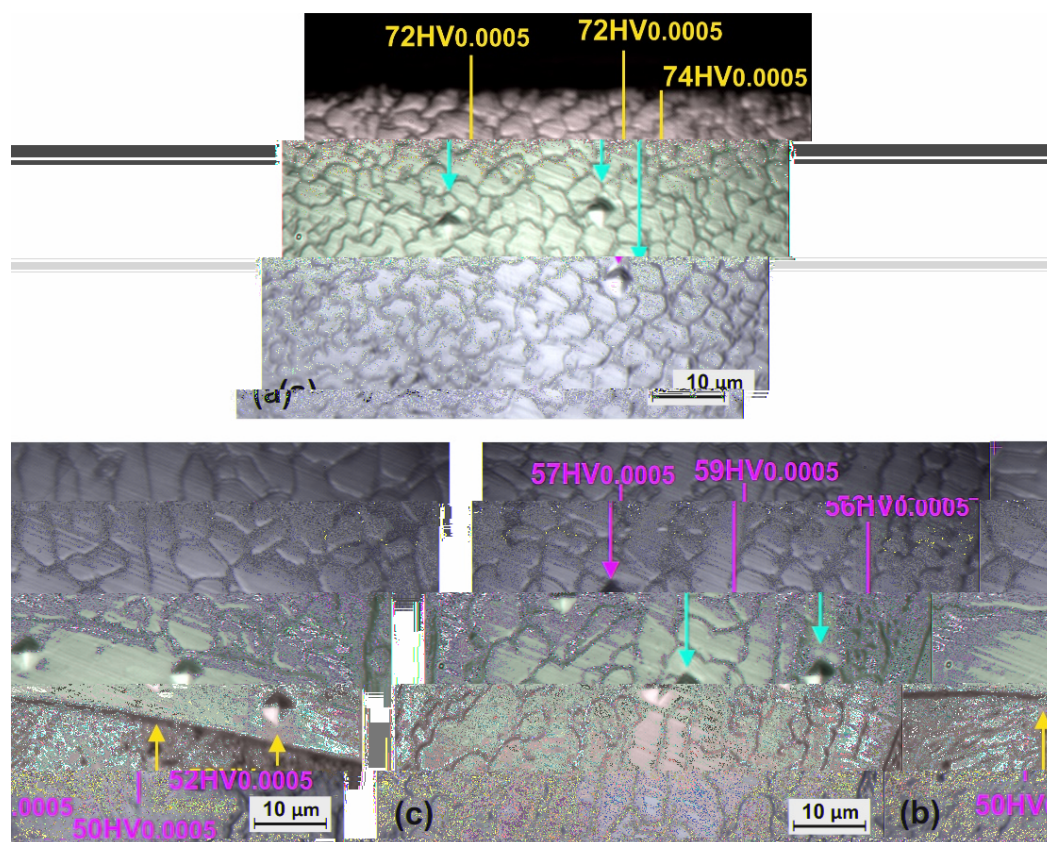
Fig. 3.31. Micro indentation on the white dendritic formation on the cross-section of sample 2, Loads 0.0005 kgF [PSC19].

The microhardness improvement in the case of sample 2 occurs in the top part of the composite coatings (Figure 3.30(a)) were the microstructure refinement produce better intergranular adhesion and reduces the dislocation density. According to Figure 3.30 and 3.31 the microhardness tested on the dendrite formation increase from 59 $HV_{0.0005}$ to 74 $HV_{0.0005}$ in the case of sample 2.

The corrosion rate was measured trough the intensity of the corrosion current and respectively the Tafel plots presented in Figure 3.32. It has been determined that sample 2 fabricated with the addition of CNTs has a better corrosion resistance than the reference sample (sample 1). As presented in Table 3.4, the value of corrosion current density (Icor index) and the corrosion rate decreases in the case of the CNTs composite sample [PSC19].

The potential of the CNTs is much higher than of Ni compounds and chromium / boron hard phases resulting and improved corrosion resistance of the composite coating. Moreover, the addition of the CNTs into the Ni based matrix determines the microstructure refinement which is beneficial in the case of corrosion resistance. An almost 40% lower corrosion rate compared with the reference sample is obtained by the addition of CNTs.
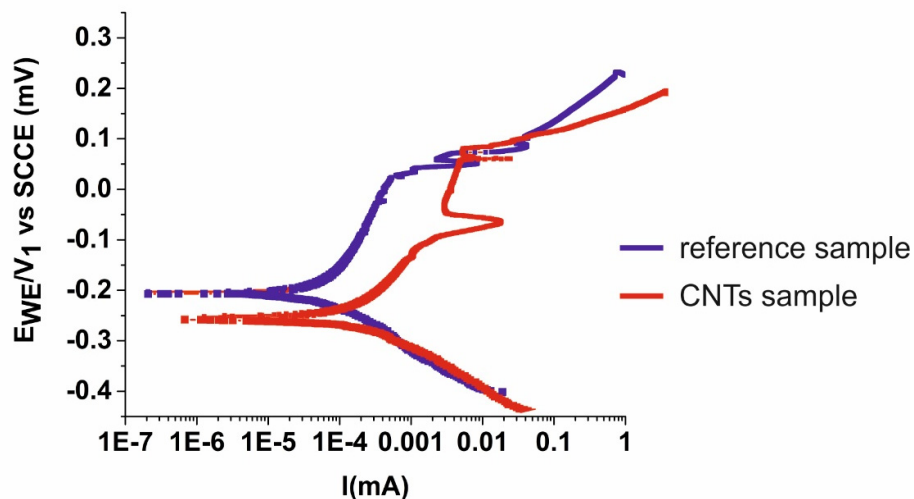
Fig. 3.32. Polarization curves of the reference sample (sample 1) and of the CNTs sample (sample 2) [PSC19].

Corrosion test parameters and results   Table 3.4

Operational parameters	Sample 1 (reference)	Sample 2 (CNTs)
Ecorr	-207.373 mV	-256.253 mV
Icorr	0.073 µA	0.036 µA
Bc	99.1 mV	76.2 mV
Ba	271.2 mV	161.9 mV
Chi²	3 872.35	134.92
Corrosion rate	0.228 134 e-3 mmpy	0.138 091 e-3 mmpy

The ball on disk testing with similar conditions for both samples has been carried out for determine the wear behaviour of the composite coating. The tests results show no significant differences between the two samples, noting only a slightly better wear resistance of the CNTs composite coatings. Also, the coefficient of friction of the composite layer is 10% higher (sample 1:0.59µ and sample 2:0.66µ) compared with the reference sample (Figure 3.33, (c) and (d)). It is well known that carbon nanotubes are a good lubricant material but, in this case, the CNTs addition promote the formation of hard phases (Cr_7C_3) with an increased hardness, as determined by the micro-harness testing and the XRD diffractogram. Therefore, the higher coefficient of friction has no direct influence on the wear rate of the composite coatings.
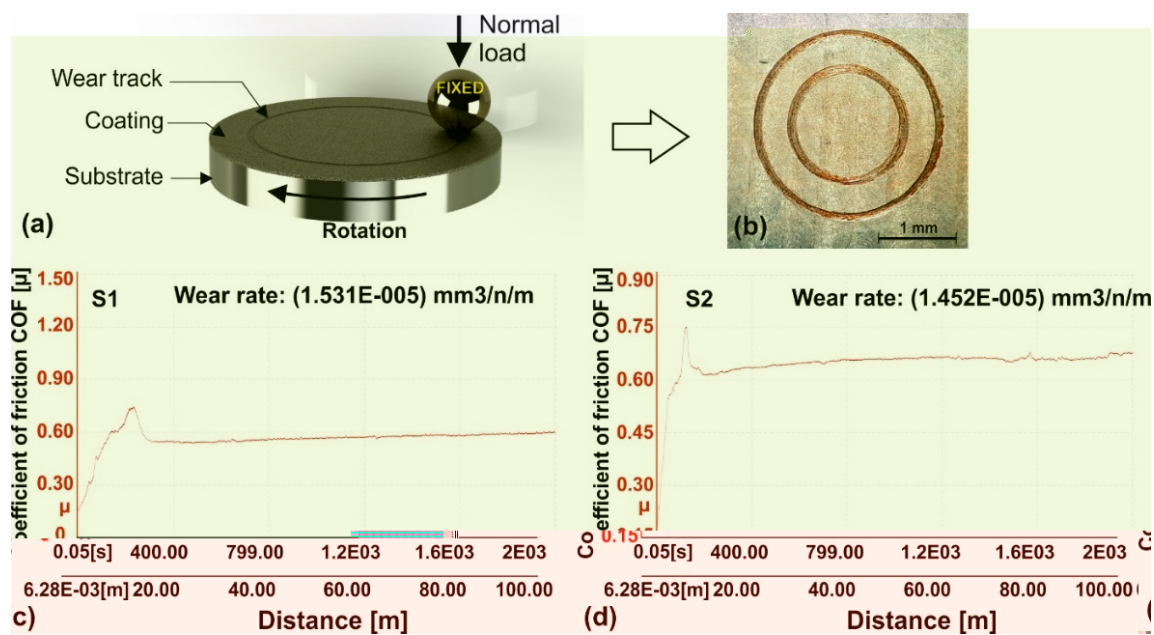
Fig. 3.33. Wear results, (a) schematic representation of the ball on disk testing, (b) wear tracks on the surface of sample 1, (c) and (d) plot of COF vs distance of sample 1 and sample 2.

With the respect to the presented results [PSC19], improving of mechanical behaviour and corrosion resistance of nickel-based coatings was realized by the addition of single-walled carbon nanotubes. Crack-free coatings have been fabricated by the preplaced laser cladding method on a low carbon steel substrate.

The addition of CNTs determines the different crystallization patterns in the laser-cladded coatings, with a more uniform distribution of the grain shape and dimensions, through the local disruption in the thermal gradient direction and growth hindrance. The morphology of the coatings consists of misaligned dendrites, without second- and higher-order hierarchies, along with epitaxially grown crystals separated from the steel substrate by a 5 um-thick planar crystal. The CNTs addition refines the microstructure and promotes the formation of hard phases, such as Cr_7C_3, resulting in an improvement of the corrosion resistance of 40% and a microhardness improvement of 25%, as well as the enhancement of the wear resistance of 5.5% in comparation with the reference sample realized without the addition of CNTs.

Overall, even if the improvement percentages are not impressive, it can be concluded that the obtained morphology has a positive influence on the microhardness, corrosion and wear resistance of the assembly, leading to the obtaining of improved value-added materials at minimal carbon nanotube addition [PSC19].

Chapter 4. INDUSTRIAL APPLICATION OF THE LASER CLADDING TECHNOLOGY

This section briefly describes the concepts behind the applications of the laser cladding technology in various industrial fields. This chapter addresses the reconditioning of worn components by laser cladding technology, as laser cladding is a modern and efficient technological solution to repair wear parts and to save natural resources and energy consumption.

Reconditioning of carbon steel moulds/dies and of titanium compressor jet engine blades are two case-studies presented that emphasis the applicability of laser cladding for a diverse range of industries [PSR19].

4.1 Reconditioning of moulds and dies

4.1.1 Concept

Currently, the laser cladding process is well known as the preferred repair technology for pistons, shafts, mouldings parts and so forth. Compression or injection moulding and die castings are the most used technology for fabricating small parts of metal and non-metal alloys, polymers, thermoplastics and composite materials. Unconcerned with the materials used, the forming process is characterized by repeatably cycles of fast heating and cooling of the moulds, which cause a premature wearing of the moulds' cavities and active parts. The durability of the die-casting moulds and injection moulds is directed influenced by different factors, such as the following: thermal stress due heating and cooling, abrasion wear, impacts, corrosion wear, and adhesion wear during the casting extraction [LGV15], [CZR14], [SHY08]. All these factors have a negative impact to the lifetime of the casting/injection moulds, with direct consequences on the quality and production rates of the components and to the final production costs.

Almost 80% of the moulds and dies used in the automotive industry will be repaired/reconditioned during the production lifespan. In the automotive industry, up to 15% of the total production cost of components fabricated by moulding and casting is related to the durability and the lifespan of the moulds and dies. Moreover, an unexpected failure of a

mould/die can produce many under-quality casted pieces and production delays with further increasing of production costs.

Today, the fast production requirements of the automotive industry require new methods to improve and to repair the mould and die components from the production lines.

Laser technology, through its characteristics of local fast heating and cooling, is used for surface re-melting, laser cladding, laser alloying and laser heat treatments with minimal heat affected zones of the processed component. As presented in the previous chapters, laser cladding with injected powder has the most potential for the reconstruction of complex 3D active parts and cavities of worn moulds and dies.

Responding to a requirement from an industrial company from Brasov, I have developed a viable technology for reconditioning various compression moulds used for the manufacturing of rubber sealings in the automotive industry [PSR19].

After some unpredicted failures of various compression moulds used by Hutchinson company, a study was initiated to investigate the feasibility of the laser cladding reconditioning process for the active edges of several specific compression mould. The moulds are fabricated by MOULD STEEL 1.2738 (AISI P20+Ni).

4.1.2 Methods, materials and results

The moulds and dies used in the automotive industry are subjected to premature wear due to the repeated moulding cycle time, heating-cooling and ejecting the piece. Fatigue, thermal shocks, corrosion and abrasion are several sources of damage for the moulds. Even mistakes in manipulation, overheating or using of tools to remove sticky parts can be sources of major mould damage. Figure 4.1 exemplifies two compression moulds with medium signs of wear on the active edge.

Fig. 4.1. Examples of compression mould with signs of wear [PSR19].

It must be noted that for local reconditioning of the compression mould, the coated material, besides metallurgical compatibility with the base material, must have low cracking susceptibility, low melting temperature in order to not overheat the entire mould and good machinability after the deposition. For this reason, it was be chosen an alloy with lower hardness but with very good milling proprieties necessary for remanufacture the active sharp edges. The coating material for reconditioning the P20 steel was Metco 15 E. The chemical composition of the powder and base material are presented in Table 4.1.

Chemical composition of the powder and base material   Table 4.1

Material	Element wt. (%)									
	C %	Ni%	Cr%	B%	Si%	Fe%	Mn%	Mo%	P%	S%
P20 + Ni *	0.44	0.98	1.94	-	0.28	94	1.32	0.17	0.01	0.02
Metco 15 E**	1	Bal	17	3.5	4	4	-	-	-	-

*Analysed by SPECTROMAXx Arc/Spark Optical Emission Spectrometry

**According Oerlikon Metco data sheet

The experimental reconditioning of the compression moulds has been realised using an CW diode LASER, Coherent 1000, with a maximum output power of 1000 W. The laser beam was focused (200 mm focal length) by a Precitec YC 50 cladding module manipulated by means of a robotic arm CLOOS synchronized with a rotation Table. The powder was preheated (70 °C) and delivered through a Thermatech AT-1200HPHV feeding device. Depending on the wear signs and the desired clad geometry have been used different parameters for each ring edge (table 4.2).

Laser cladding parameters used for the reconditioning process   Table 4.2

	Laser power	Power density	Cladding speed	Powder feed rate
	[W]	[kW/cm²]	[cm/min]	[g/min]
R1 (ring edge 1)	450	14.33	24	4.5
R2 (ring edge 2)	450	14.33	22	4.5
R3 (ring edge 3)	450	14.33	20	4.5

After the reconditioning process, the moulds have been sectioned and prepared for metallographic analyses by grinding, polishing and etching with 1:3 HNO_3 / HCl reagent.
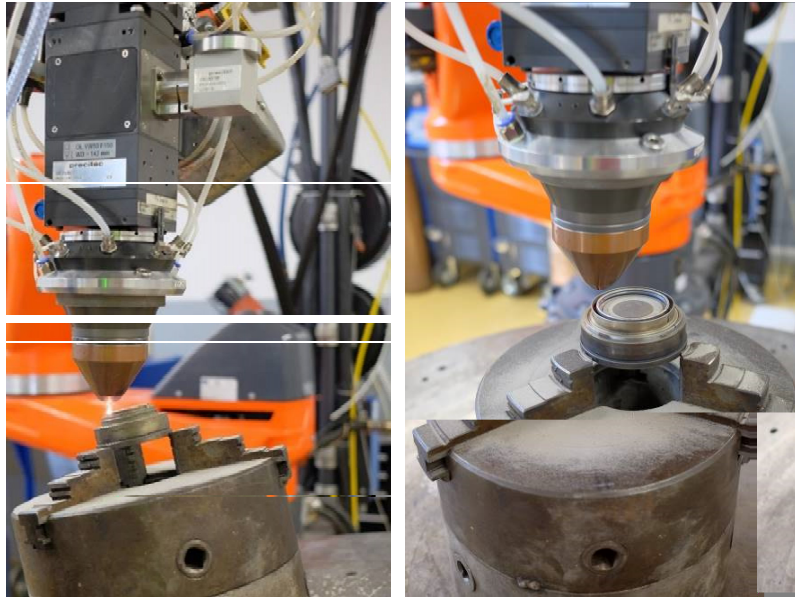
Fig. 4.2. Compression mould during the reconditioning process [PSR19].

The laser cladding capability to repair compression moulds is demonstrated by partially or complete repair by laser cladding of four compression moulds used for manufacturing of caliper piston ring gasket. These types of moulds are used in the hot compression mouldings process designated for the automotive industry. As previously stated, the active edge of the mould is subjected to impact and adhesion wear due to the open-close cycle of the moulding process.
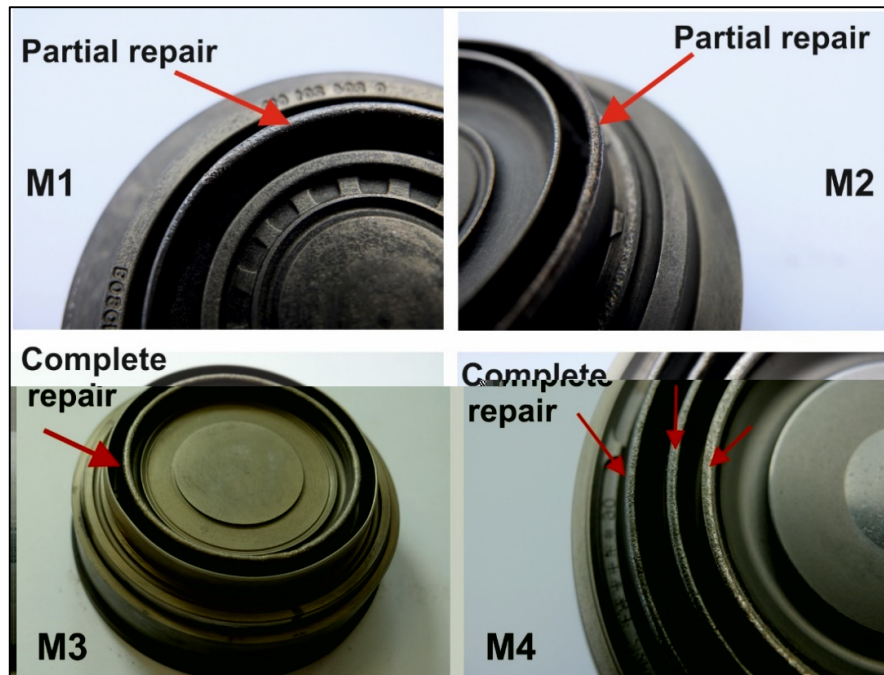
Fig. 4.3. Compression mould after the reconditioning process [PSR19].
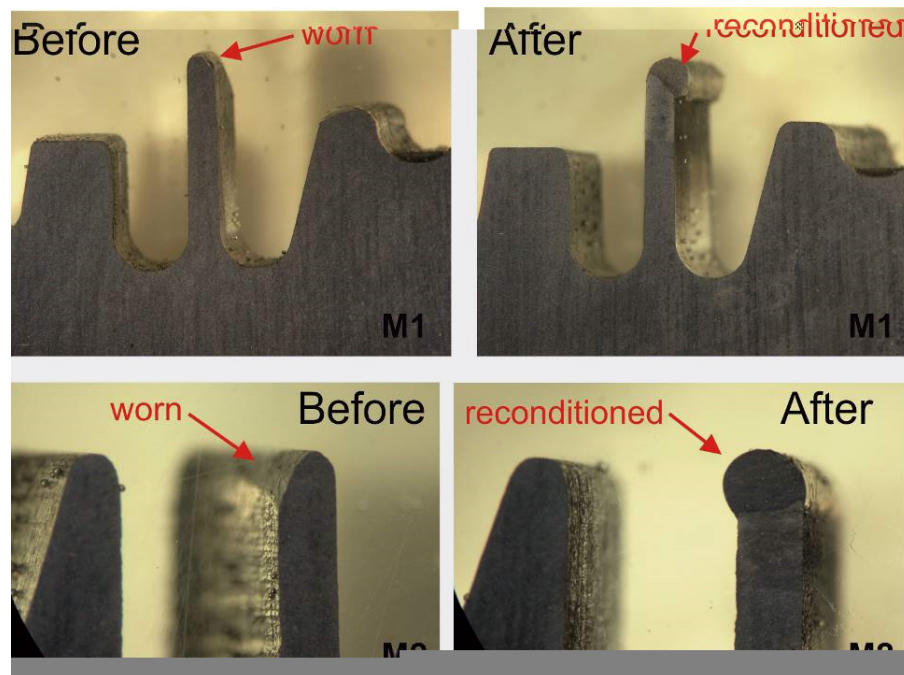
Fig. 4.4. Cross section of moulds M1 and M2, **Before** and **After** the reconditioning process [PSR19].
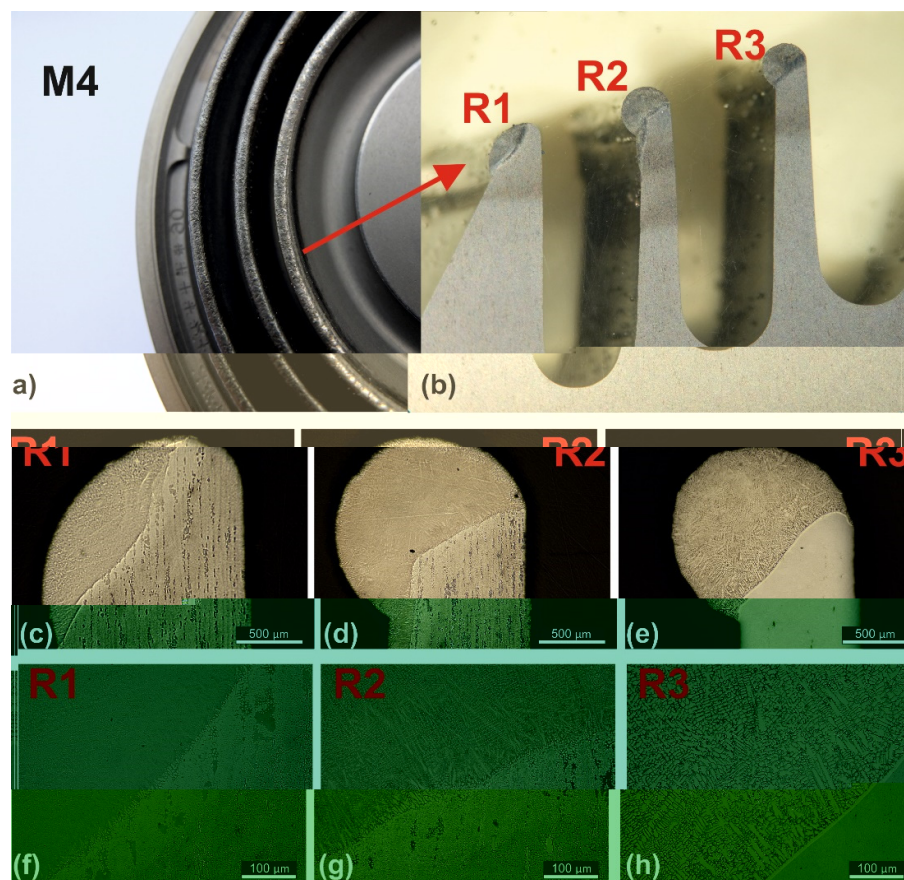
Fig. 4.5. Cross section of the reconditioned ring edge of mould M4 [PSR19].

Figure 4.3 presents different compression moulds (male and female side) after the laser cladding reconditioning process. In the case of M1 and M2 moulds only a partial repair of the active edge was necessary and moulds M3 and M4 were reconditioned on the entire ring edge. The cross-section profile of the reconditioned edge of moulds M1 and M2 are presented in Figure 4.4

For better understanding of the reconditioning process, the M4 mould will be further analysed and discussed in this thesis. One single track has been laser cladded on each ring edge of M4 mould and as it can be seen in Figure 4.5, the coated material is uniform without visible defects or unmelted powder particles. Cladding speed of 20, 22 and 24 cm/min was chosen in order to not overheat the ring edges but, in the same time, to obtain a good adhesion with the substrate.

Each ring edge has been repaired with adapted speed in accordance with the ring shape geometry and depth of the worn marks [PSR19]. Figure 5.5 shows at different magnifications the cross-section profile of the three edges, R1, R2 and R3, that have been repaired. The cladded layer is free of cracks having a good bonding with the mould substrate. The coating is dense and have a typical Ni based superalloy microstructure composed of columnar dendrite with the growth direction perpendicular on the base material. Only in the case of R3 edge, a well-defined non-interference line (planar growth) between the two materials is visible. This edge was repaired using a lower speed therefore a higher temperature and thermal gradient was created during the laser processing producing the planar growth at the bottom of the melted pool (Figure 5.5 (h)) [PSR19].
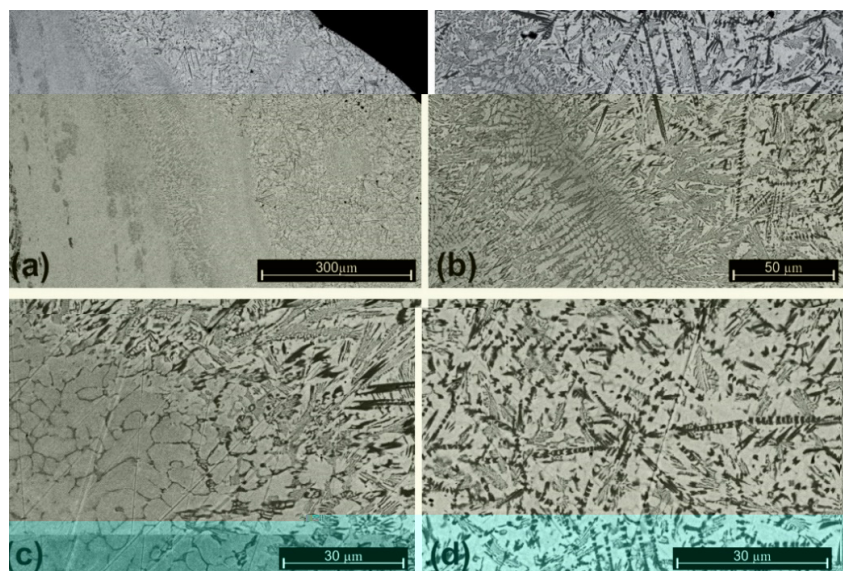
Fig. 4.6. SEM micrographs of the reconditioned ring edge R2 from Figure 4.3 [PSR19].

The SEM analyses of the ring edge R2 is presented in the Figure 4.6. The details show the diffusion zone characterised by the dendrite formation with pyramidal growth in the direction of the thermal gradient. The dendrite formations are smaller and uniform distributed in the Ni matrix on the upper part of the coating where the distance from the interface with the substrate increase.

The EDS micro chemical analysis indicates the presence of hard phases distributed in the nickel-iron matrix. The high amount of iron is resulted by the mixing and diffusion phenomena with the substrate. In the Figure 4.7, it can be seen several darker areas that indicates, according with the EDS results, the presence of phases rich in C and Cr, chromium carbides that are embedded in the Ni-Fe matrix. The presence of hard phases ensures the hardness and wear resistance of the coating.

EDS	Wt. %				
	C	Ni	Cr	Fe	Si
	38.41	10.85	37.14	10.61	2.99

EDS	Wt. %				
	C	Ni	Cr	Fe	Si
	63.11	11.75	12.12	9.90	3.13
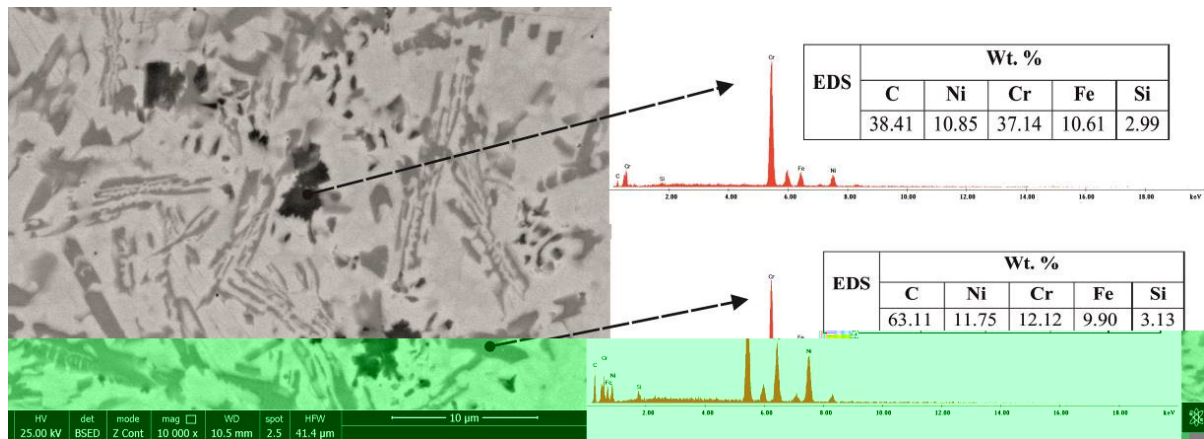
Fig. 4.7. EDS analyses of different phases identified on the clad cross-section (ring edge R2) [PSR19].

The hardens of the cladded layers is influenced by the microstructure, grain size and dilution with the substrate. Figure 4.8 show the microhardness values measured on the coating, heat affected zone and base material of the mould 4 (M4). The highest hardness (~ 600 HV02) was measured on the R1 ring mainly due to the low dilution with the material. The obtained hardness is in accordance with the technical specification of the Metco 15E alloy deposited by laser cladding. In the case of R2 and R3 cladded area, the microhardness is with almost 150 units lower mainly due to the diffused iron from the substrate.

The heat affected zone is hardened and have 620 HV02 compared with the base material characterises by a microhardness of 575-590 HV02 [PSR19].
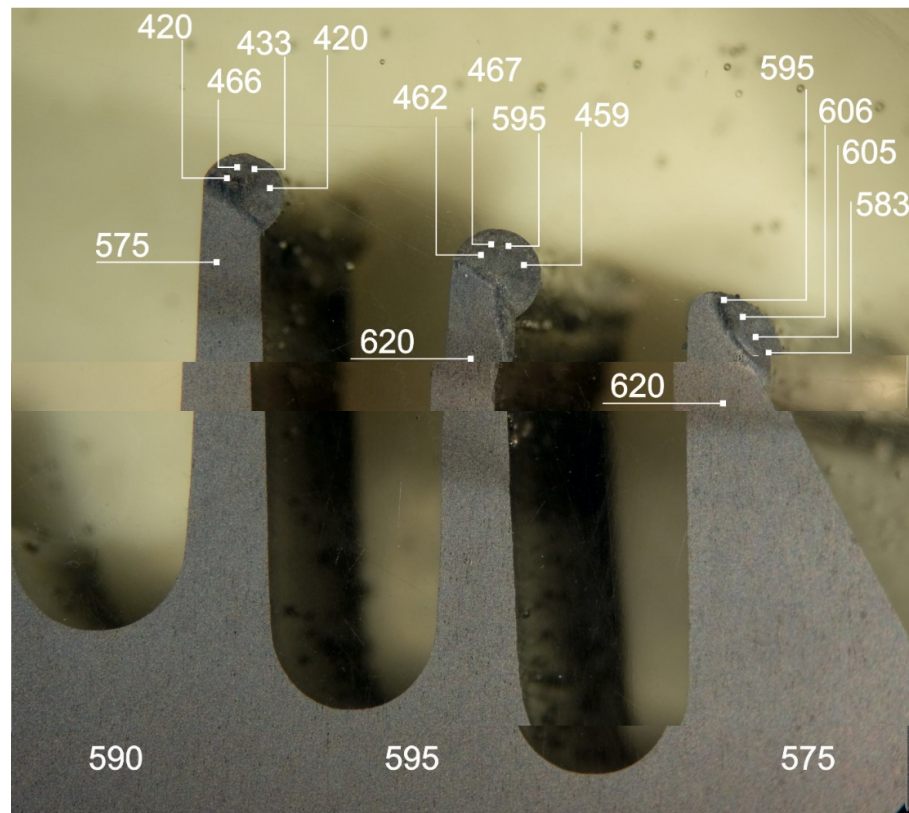
Figure 4.8. Results of the microhardness testing of the mould M4.

Indicated values are Vickers microhardness tests results at 200 g load: HV02 [PSR19].

Considering the above results [PSR19], laser cladding with coaxial powder injection is a suitable technology for the reconditioning of compression moulds/ dies. Dense and crack free cladded layers can be fabricated by this reconditioning technique and by parameter optimization and fine-tuning of the desired coating geometry can be obtained. Furthermore, the Metco 15 proves to be well suited to be used as filler material for reconditioning due to its corrosion and wear resistance capabilities. The analyses show good metallurgy between the Ni17Cr4Fe4Si3.5B1C coating and P20 + Ni steel without signs of segregation or microcracks at the materials interface

This case study, finalised with reconditioning of more than 100 compression moulds, proves the viability of the laser cladding technology in an industry covering a broad range of applications.

4.2. Reconditioning of compressor jet engine blades

The new trends in energy recovering necessitates new methods to save raw materials. In the automotive and aeronautics industry, the recycling of worn parts/components can be a solution for reducing costs, but the best way to reduce the environmental impact is to repair the worn components, reducing all the energy needed to refabricate the original component.

4.2.1 Concept

The second case studies presented in this habilitation thesis is the reconditioning of a titanium compressor jet engine blade [PMS19]. This experimental-based study intends to prove the versatility of the laser cladding technology to produce a crack free, dense coating, even when some difficult materials, such as titanium, are used. In addition to the material issues, in the case of the airplane industry, the quality requirements are also strictly controlled, and the reconditioning technology must provide the highest quality available.

Airplane jet engine blades are high value components and are the elements with the highest susceptibility to wear due to the extreme condition of exploitation, i.e., high speeds at different temperatures, high friction with the air and with various type of debris (sand, rain). All these factors reduce the normal exploitation lifetime of the jet blades and increase the possibility of premature damage with considerable safety issues and financial loses. A damaged or worn blade must be immediately replaced. The worn piece can be scrapped or repaired but the repair process must fulfil high-quality requirements.

Commonly, the jet engine compressor blades are fabricated from Ni-based superalloys (high pressure turbine) or from Ti alloys (low pressure compressor / compressor blade), titanium has gained usability in the last decade due to its exceptional characteristics. The role of the Ti compressor blades is to give velocity to the air in the compressor stator and they are fabricated from VT8, VT3-1 titanium alloys (TiAlMo) having a hardness up to 50 HRC. Reconditioning of titanium jet engine blades require special conditions, such as low heat input, localized and precise material additions and perfect bonding with the substrate. The laser technology can ensure that all the specific conditions imposed for the reconditioning of airplane components are met. A titanium compressor blade was chosen to exemplify the laser cladding capabilities in term of the reconditioning of components fabricated from sensitive materials or super-alloys [PMS19].

4.2.2 Methods, materials and results

The reconditioning of a jet engine compressor blade made of titanium WT3 is presented as case study. Usually, the wear signs appear on the blade tip and shorten the blade length with negative impact on the air flow. In this particular case [PMS19], the blade presents worn sings on the entire external contour as illustrated in the Figure 4.9 and the objective is to recondition the lateral side of the blade, by adding a high strength and temperature resistant coating by coaxial laser cladding and powder.

Fig. 4.9 Titanium jet engine blade (compressor blade); yellow arrows indicate the worn-out area [PRS19].

The jet engine blade is fabricated from VT3-1 alloy (Ti−6Al−1.5Cr−2.5Mo− 0.5Fe−0.3Si). It is a martensite type alloy that can be hardened by thermal treatments. VT3-1 has a high corrosion resistance and are commonly used in aircraft components (Russian) with an exploitation limit of 450 °C.

Metco 4110 powder was used as coating material. The Metco 4110 with an apparent density of 1.8 − 2.5 g/cm3 have high strength-to-weight ratio and is resistant to most corrosives [***OER]. Figure 4.10(c) shows the typical powder morphologies obtained from wrought raw material. Chemical composition of the powder is presented in Table 4.3.
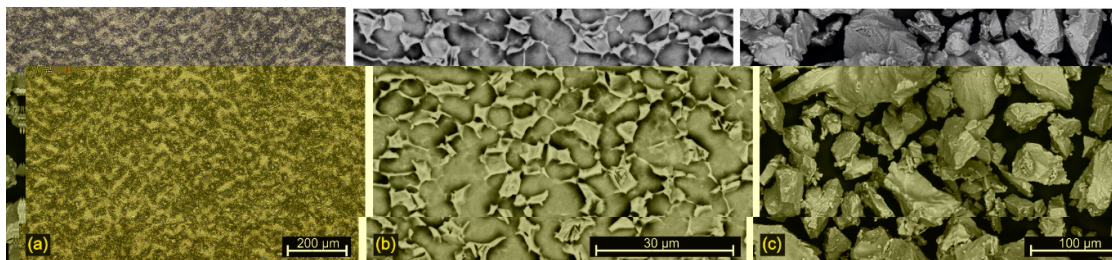
Fig. 4.10 (a) and (b) specific microstructure of VT3-1 titanium alloy, electron microscopy of Metco 4010 powder [PMS19].

Chemical composition of Ti based powder   Table 4.3

Power type	Chemical Element (wt. %) *					Powder average dimension
	Ti	Fe	O	N	H	
Metco 4010 A	Bal.	< 0.5	<0.4	<0.05	<0.015	−90 +22 μm Mesh -170 +575

*According Oerlikon Metco data sheet

The experimental reconditioning of the worn blade has been conducted using an TRUMPH TruPulse 556 laser and an optical cladding module PRECITEC YC50 manipulated by a robotic arm synchronized with a rotational Table. The powder was delivered to the optical module by a powder feeding device, namely Termatech AD2000. The same equipment preheats the powder at 70 °C. Pure Ar was employed for the powder delivery and shielding of the melted bath.
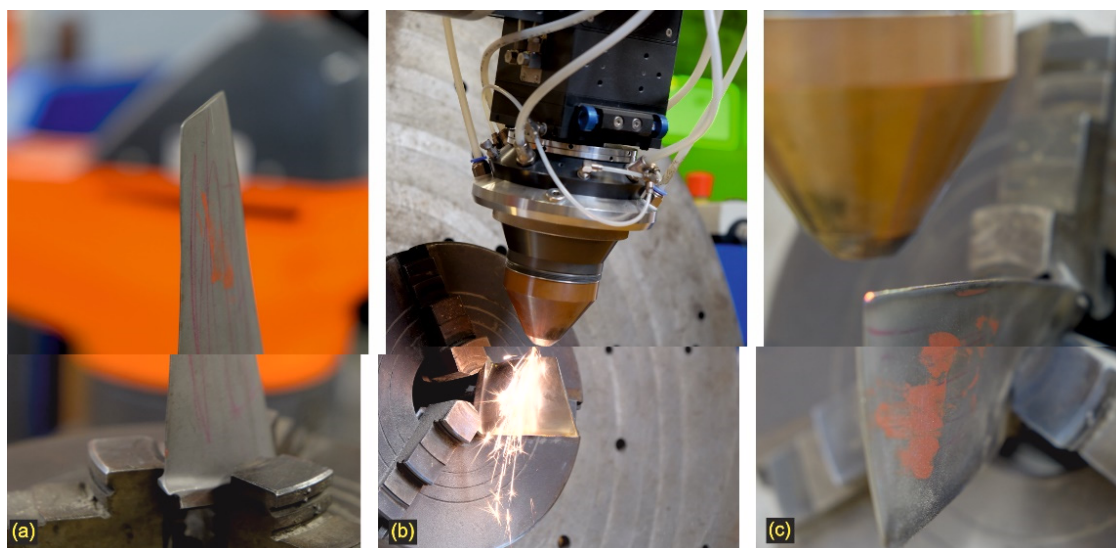
Fig. 4.11 Experimental repair of the jet blade, a) fastening and positioning of the VT3-1 titanium blade, b) laser cladding process, c) the blade after the reconditioning process [PMS19].

The parameters of the laser cladding process are summarized in Table 4.4. The parameters have been optimized after several preliminary tests. All tests were carried out at room temperature using a laser spot diameter of 1.6 mm and a stand-off distance of 10 mm.

Laser cladding parameters   Table 4.4.

Laser power [W]	Energy density [J]	Pulse duration [ms]	Frequency [Hz]	Cladding Speed [mm/s]	Powder feed rate [g/min]
2300	2.36	1	150	6	5

The jet engine blade was cut and prepared using standardized method for metallographically analyses. The cross-section of the coating was etched using Kroll reagent (100mL H_2O+ 4mL HNO_3+22mL HF).

As illustrated in Figure 4.12, a pore- and crack-free cladded layer has been fabricated on the contour of the worn blade. The clad is characterized by a good geometry profile without un-melted powder. The process speed was chosen to be as fast as possible to not overheat the substrate but to also obtain a proper bonding with the blade. Nevertheless, the substrate was heat affected and oxide, as revealed by the blue coloration under the coating. In the absence of a controlled atmosphere chamber the oxidation process is impossible to avoid, as the cladding head and the shield gas advances before the coating and substrate cools below 400 °C.
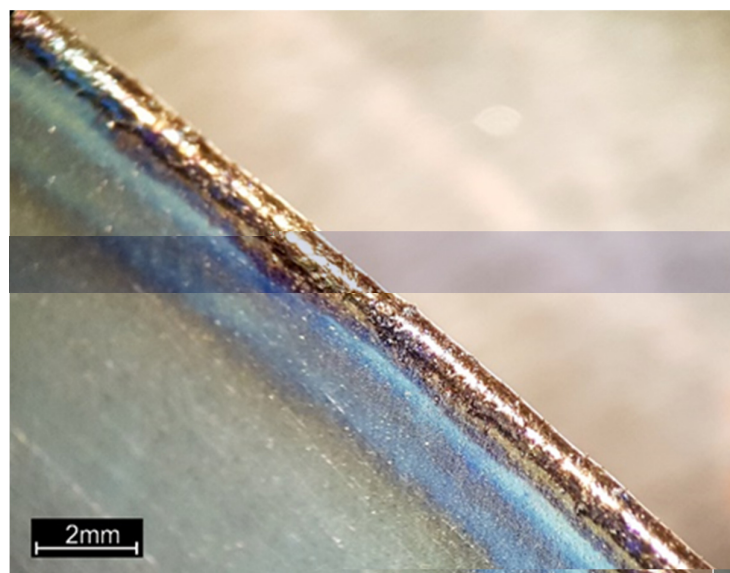
Fig. 4.12 Macro image of the cladded track on the blade contour [PMS19].

Figure 4.13 shows the main areas of the cladded track cross-section at different magnifications. The metallographic examination shows an uniform microstructure and a very good bonding, as no delimitation between the materials can be observed. The cladded layer is characterized by a martensitic structure with an incomplete Widmanstätten with a β phase formed due to the diffusion of Al, Fe from the substrate.
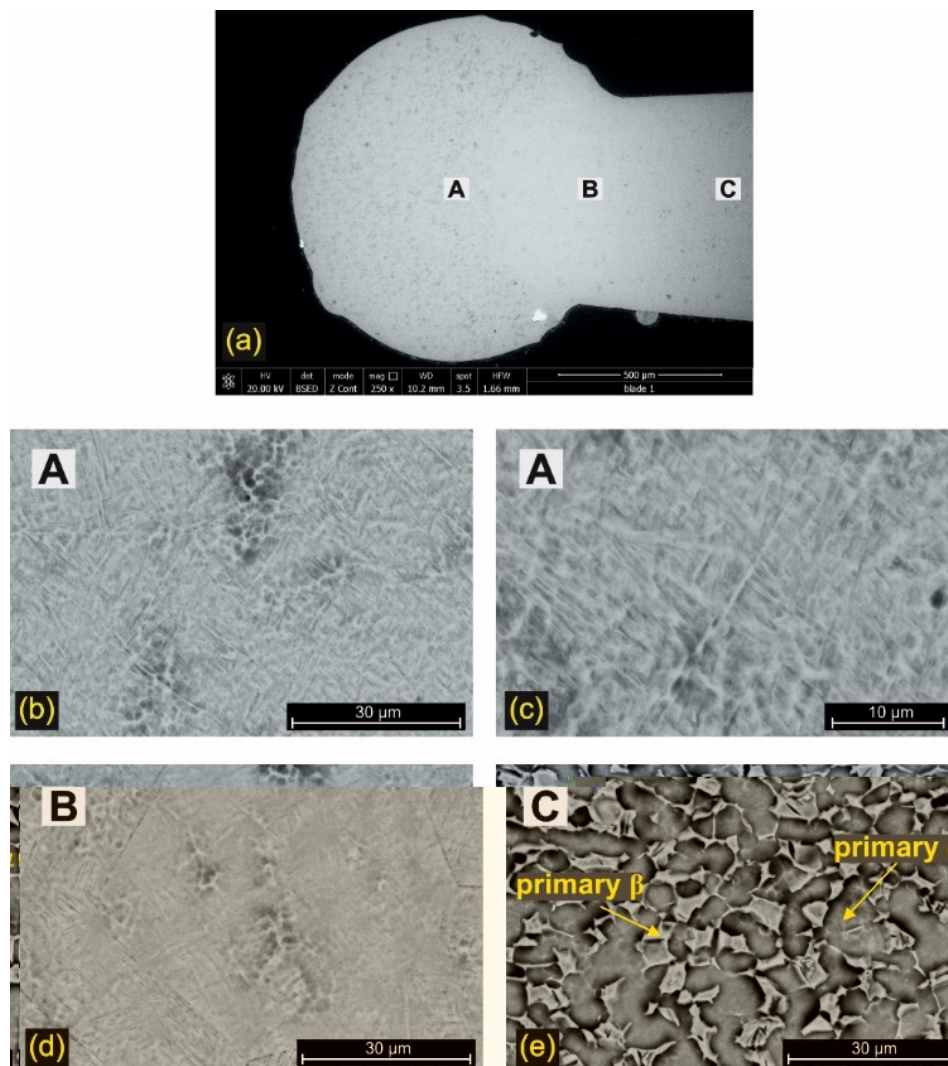
Fig. 4.13. Cross-section of the reconditioned blade, (a) overview of the cladded track on the blade contour, b) detail of zone A showing the microstructure of the coated layer; (d) microstructure of the interface zone (zone B), (e) specific microstructure of the base material (zone C) [PMS19].

The diffusion phenomena is more evident in the area B, where the grain boundaries are visible and the lamellar microstructure (α lamellae) is oriented as a *basket weave* form the Widmanstätten microstructure. The formation of the Widmanstätten microstructure is

promoted by the fast cooling of the β phase. The uneven distribution of the β phase stabilizer, diffused from the substrate, forms a different microstructure in the heat affected zone.

The microstructure of the substrate is presented in Figure 4.13(e). A typical platelet shaped microstructure is formed from the homogenous primary α and primary β phases [LDZ17].

The hardness behavior of the cladded layer has been determined using a Shimadzu HMV 2T microhardness tester with a set-up of 200 gf for a 10-second dwell time. The hardness of titanium alloys is influenced by the microstructure and grain size. The measurements results show a slightly decreasing of the microhardness of the cladded track and into the heat affected zone, namely 402 HV_{02} medium value of the coating compared with 463 HV_{02} microhardness registered on the blade material. The heat affected zone is alloyed by diffusion from the substrate and have a medium microhardness of 437 HV_{02}.
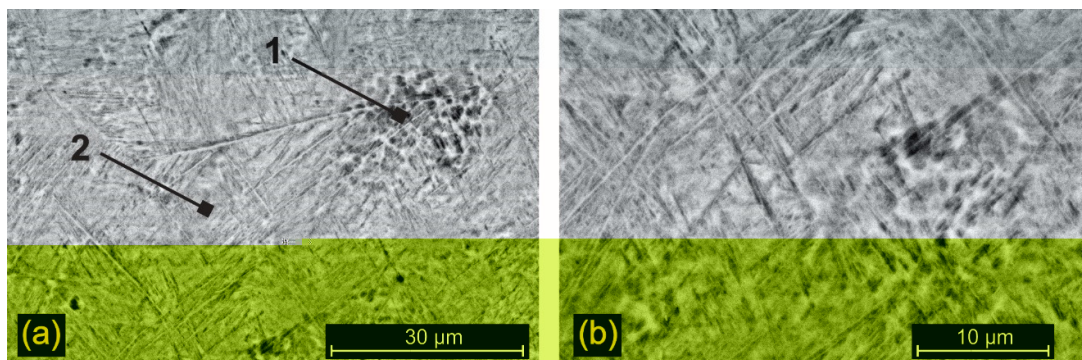
Fig. 4.14. Electron microscopy of the coated layer highlighting the Widmanstätten microstructure [PMS19].
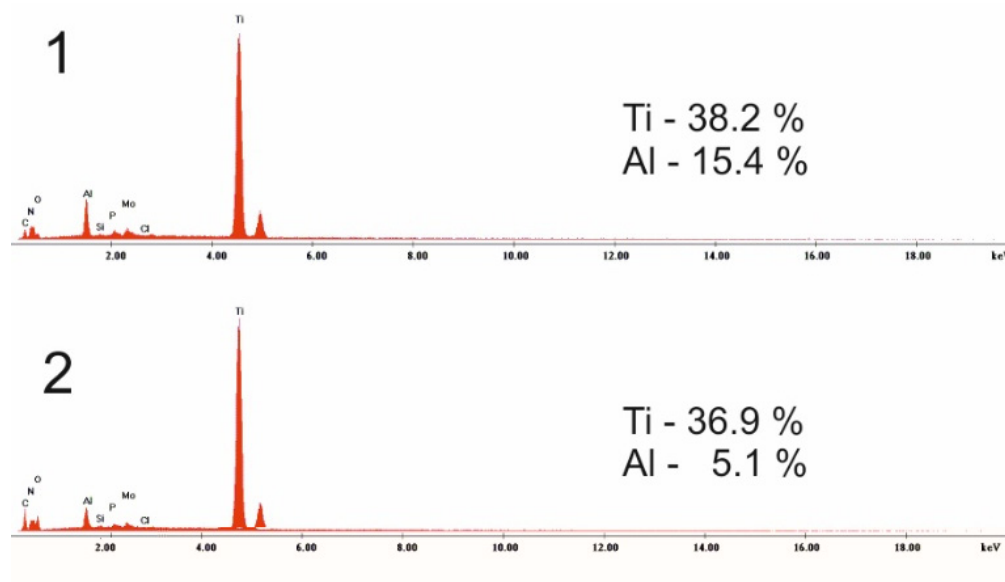
Fig. 4.15. EDS analyses of microzones 1 and 2 from Figure 4.14(a) [PMS19].

Figure 4.14 illustrate a microstructure defect represented by areas with higher concentration of Aluminum. As determined by EDS analyses the darker areas (areas that have been severely etched by the Kroll reagent) have higher Aluminum content being characterized by a higher harness (up to 569 HV_{02}). Islands with high concentration of Al are considered defects and must be avoided due to the increasing risk of cracks initiations from these areas.

Regarding the above ideas, laser cladding proves to be the best solution to recondition damaged airplane engine blades. Recently, the laser technology has spread into the industry and the cladding process, especially when the reconditioning with lasers and powders became a viable solution for industrial applications.

The presented study [PMS19] shows the advantages of using the pulsed laser cladding for the reconditioning of titanium jet engine blades. Due to its high ductility and high impact toughness compared with Ti6Al4V, the Metco 4010, grade 4 titanium powder proves to be a good material for reconditioning of VT3-1 blades. Thus, the pure titanium coating is softer than the substrate but has the advantage of very good post-processing machining. The results show a very good bonding with the substrate without a visible delimitation of materials. The cladded layer is dense, defect free and characterized by a uniform Widmanstätten microstructure.

CONCLUSIONS

The results and discussions presented in this habilitation thesis are based on my personal research activity in the fields of laser cladding with metallic powders. Through the presented data, I have demonstrated that laser cladding technology has advantages, such as high layer density, low porosity and very good bonding with the substrate, compared with the conventional technique of thermal spraying. During various research activities, I have been using the laser cladding technology to obtain pure, alloyed, composite and glassy coatings on metallic or non-metallic surfaces.

A novel approach was used for fabricating a glass/ceramic Al_2O_3-TiO_2 / hydroxyapatite composite cladding on an electrolytic copper substrate through a preplaced laser cladding technique. The results show the potential usage of the obtained material in a non-black solar collector design, as the solar absorptance coefficient is 0.816 and the transparency of the coating is optimal in the 500-800 nm domain.

Another promising result have been obtained by laser cladding and nickel-based powders. The coaxial laser cladding technique was employed to obtain crack and pore free Inconel 718 claddings with low dilution with the substrate. Thus, severe grain boundary segregation was observed as the Nb and Ti hard phases precipitated at the grain boundary of the cladded tracks. This segregation pattern was more pronounced near the interface with the substrate, where a high amount of iron was transferred from the base material. Applying a solar heat treatment to these coatings proved to have a positive influence on the microhardness and tribological behaviour of Inconel 718.

In addition, the Inconel 718 was used as intermediate layer between the substrate and a Metco 16C-NS hardfacing cladded layer. The Inconel layer was acting to (1) improve the metallurgical compatibility between materials with different thermal coefficients and (2) preserve the chemistry of the hardfacing by minimizing elemental dilution, resulting in an improvement of the corrosion and wear resistance in comparison with the reference material, obtained without an interlayer.

Further improvement of the Ni-based cladded layers was realized by the addition of single-walled carbon nanotubes. The addition of CNTs resulted in different crystallization patterns in the laser-cladded coatings, with a more uniform distribution of grain shape and dimensions, through the local disruption in the thermal gradient direction and growth hindrance. Improvement of the corrosion resistance of 40% and a microhardness of 25%, as well as the

enhancement of the wear resistance of 5.5% in comparation with the reference sample was realized without the addition of CNTs.

The laser cladding applicability to the industry was demonstrated by presenting two case studies consisting of the reconditioning of moulds/dies and titanium compressor blades. In the first case, a NiCrBFeSi thin layer was fabricated for restoring the original profile of the edges of worn moulds. The results show that laser cladding can be used as repair technology or as method to protect the component against corrosion or wear. The versatility of the laser cladding was also demonstrated by fabricating a pure titanium restoring layer on the contour of a compressor blade made of a VT3-1 alloy.

B3. Evolution and development plans for career development

The evolution plans of my academic career are based on my teaching and research activity within the Faculty of Materials Science and Engineering at Transilvania University of Brasov. Once the PhD supervisor title is awarded, my activity will be complemented by the tutoring and mentoring of young researchers, the creation of new research groups and attracting funds. An important pillar of my activity will be the implementation of higher educational standards and ethical principles in the research and academic activity through collaboration with prestigious research institutes and universities and by implementing of new research methods based on quality and robustness.

Teaching related plans

Teaching activity is the main reason for choosing the academic career and the teaching-learning process carried out inside and outside the classes is meant to form the future generation of engineers. It is a great responsibility and, therefore, lifelong learning is a personal commitment for improving my professional skills and teaching competence.

Several directions and activities regarding my teaching plans can be summarized as follows:

- Improving my presentation skills by attending training sessions for communications and large audience meetings;

- Updating and writing new courses and practical laboratories based on the feedback received from the students;

- Maintaining contact with the students after they graduate the licence or master programme is a good method to evaluate the education importance in their future career;

- Encouraging of practical activities by students during the technical laboratories;

- Participating in ERASMUS+ teaching and training programmes for improving my knowledge and teaching skills;

- Identifying and attracting students to follow the master's and PhD programmes at Transilvania University of Brasov;

- Developing new themes for licence and master's degree final projects in accordance with the requirements of the local industrial environment;

- Encouraging students to make Erasmus+ stages at our partner Universities;

- Involving of students in the ongoing research projects carried out at the Advance Welding Eco Technologies research centre.

Research related plans

The research in the field of industrial engineering is an ongoing activity that allows me to progress as a researcher and teacher. At the same time, research is the funding source of future projects but also for improving the infrastructure used for the teaching activities.

As coordinator of the Advance Welding Eco Technologies research centre, I want to further develop the research activity within the Materials Science and Welding department. Acquisition of a new generation pulsed LASER with high pulse-to-pulse stability and real-time power control is the short-term objective, aimed in the next year. The new generation of equipment's will provide a decisive advantage in the research of cutting, welding and cladding using the laser technology. Moreover, combing the laser processing with the spectroscopy technology will be the basis of several new projects in the field of industrial engineering.

My research activity is based on multidisciplinary domains; thus, all the long-term plans imply full collaborations with specialists in chemistry, materials science, tribology and solar energy.

The main objective and research-based activities can be summarized as follows:
- Attending to national and international research grants competitions;

- Continuously enlarging the research infrastructure;

- Engaging in new collaboration opportunities with high-ranked research institutes;

- Continuing the actual research and starting new projects. Dissemination of results in international journals, conferences and patent proposals will be continuously attended. At least two papers per year published in a minimum of Q2 ranked journals (according Web of Science Core Collection) is expected during my entire academic career.

In the light of above, three project plans can be briefly described as follows:

1. Designing of a novel laser cladding technique

The first project theme is based on the technology of laser cladding with metal powders. In the last decade, laser cladding technology has been tested and improved in the research laboratories worldwide. Furthermore, a growing transfer of laser cladding technology from research centres to different industries with direct practicability in worn surfaces improving or restoring is noted. Cladding of metal-matrix composite layers reinforced with hard particles is an actual topic worldwide, and research in this area focuses on finding new ways to clad and build up composite alloys. The experimental research is made using filler materials in the form of atomized powders containing all the alloying elements in each particle. The disadvantage of this method is the fact that the atomized powders are very expensive and commercial alloys products are few and often do not correspond to specific applications for improving or restoring by wear resistant cladded layers.

Through a novel project is aimed developing of a new laser cladding method that will allow two different filler materials to be simultaneously used. The research will be focused on the realization of ███████████ that will simultaneously inject two different types of powder, i.e., a powder meant to build the anti-wear layer core matrix and the second power meant to introduce hard particles in the working area. The novelty of the proposed method lies in the fact that ██ ██████████████████████████████████████ thereby avoiding the risk of separation of powders according to their density.

2. Innovative method of laser surface modification

In addition to laser welding and cutting, laser heat treatment is a surface modification process that can improve the component's mechanical proprieties. Laser heat treatment is the general term used for hardening, tempering and annealing. The process is characterized by a high accuracy and adaptability being a non-contact procedure that can locally heat the surface while preserving the metallurgical properties of the base material.

A close related process that use the laser for surface modification is the LSP, laser shock processing or laser shock peening. In LSP, a metallic surface is targeted with an intensive short pulse to produce a plastic deformation by the shock wave produced due to the interaction laser/plasma – material.

As stated before and in comparison with laser shock processing, laser heat treatment is a processing technique that allows the reaching of high heating and cooling rates of the processed surfaces. The conventional laser heat treatment (LHT) uses air (or argon) quenching of the treated area and can be realized with continuous or pulsed lasers.

The second theme aims to benefit from the advantages of both laser processing techniques, i.e., LSP and LHT. This double down in advanced laser processing is the basis of an ongoing research activity that aims to further improve the mechanical proprieties of metallic surfaces with no secondary machining.

3. Solar synthesis of carbonaceous materials

The third proposed research is based on the synthesis of carbon nanotubes using concentrated solar radiation. Carbonaceous nanomaterials, with emphasis on carbon nanotubes (CNTs) have gained widespread attention lately due to their exceptional optical, electrical and mechanical properties, shading new insights on the capabilities and performance-tuning of traditional materials such as metal alloys, polymers and ceramics. The technological boom of the nanoscience and nanomaterials field has determined an increase in the demand of CNTs with special proprieties and characteristics proper to different industrial applications. The results from previous authored work reveals that was were able to generate structures such as nanotubes with a single wall and other carbonaceous materials but with low efficiency and partly-entangled nanotube phase and also with the occurrence of nanoparticles. An already tested type of catalyst was used to promote the nucleation of carbon nanotubes. The ceramic/metallic hybrid catalyst fabricated by ███████ coating on pure copper is characterized by a mesoporous/mesopatterned surface which promote the NTs nucleation and growth in the nanopatterned porosity, with an average BET surface area of 374.5 m^2/g, a pore volume density of 0.28 cm^3/g.

A further project will improve the quality and the growth mechanism of the carbon nanotubes by adding ███████ into the solar reactor in order to promote the carbonaceous materials growth on the catalyst surface.

C. References

1. [***ARM]   http://www.wbdg.org/ccb/ARMYCOE/COEECB/ARCHIVES/ecb_2009
    _3.pdf

2. [***OER]   Material Product Data Sheet Pure Titanium and Titanium Alloy Powders,
    DSMTS-0089.5 – Pure and Alloyed Titanium Powders
    © 2017 Oerlikon Metco, http://www.oerlikon.com/metco

3. [BLA10]   Bakshi S.R., Lahiri D., Agarwal A., Carbon nanotube reinforced metal
    matrix composites - a review, Int. Mater. Rev. 55, 1, p. 41-64, (2010)
    doi:10.1179/095066009X12572530170543.

4. [BPF13]   Baldridge T., Poling G., Foroozmehr E., Kovacevic R., Metz T., Kadekar
    V., Gupta M.C., Laser cladding of Inconel 690 on Inconel 600 superalloy
    for corrosion protection in nuclear applications, Optics and Lasers in
    Engineering 51, p. 180-184, (2013).

5. [BRM04]   Biswas S., Reddy G. M., Mohandas T., Murthy V. S., Residual stresses in
    Inconel 718 electron beam welds, Journal of Material Science 39, p.
    6813-6815, (2004).

6. [BSB08]   Bakshi S.R., Singh V., Balani K., McCartney D.G., Seal S., Agarwal A.,
    Carbon nanotube reinforced aluminum composite coating via cold
    spraying. Surf. Coatings Technol. 202, p. 5162–5169, (2008)
    doi:10.1016/j.surfcoat.2008.05.042.

7. [CAV14]   Casati R., Vedani M., Metal Matrix Composites Reinforced by Nano-
    Particles—A Review. Metals 2014, p. 65-83, (2014)
    doi:10.3390/met4010065.

8. [CHH11]   Chien C.S., Hong T.F., Han T.J., Kuo T.Y., Liao T.Y., Effects of different
    binders on microstructure and phase composition of hydroxyapatite,
    Nd–YAG laser clad coatings, Applied Surface Science 257, p. 2387-
    2393, (2011).

9. [CJC13]   Chu K., Jia C. C, Improvement of interface and mechanical properties in
    carbon nanotube reinforced Cu-Cr matrix composites. Mater. Des. 45, p.
    407–411, (2013), doi:10.1016/j.matdes.2012.09.027

10. [CLS15]   Chen J.L., Li J., Song R., Bai L.L., Shao J.Z., Qu C.C., Effect of the scanning
    speed on microstructural evolution and wear behaviors of laser cladding
    NiCrBSi composite coatings, Optics & Laser Technology 72, p. 86-99,
    (2015).

11. [CRJ06]   Ci L., Ryu Z., Jin-Phillipp N.Y., Rühle M., Investigation of the interfacial reaction between multi-walled carbon nanotubes and aluminum. Acta Mater. 54(20), p. 5367-5375 (2006) doi:10.1016/j.actamat.2006.06.031.

12. [CTW03]   Chen W.X., Tu J.P., Wang L.Y., Gan H.Y., Xu Z.D., Zhang X.B., Tribological application of carbon nanotubes in a metal-based composite coating and composites. Carbon 41, p. 215–222, (2003) doi:10.1016/S0008-6223(02)00265-8.

13. [CWM13]   Chen Y., Wu D., Ma G., Lu W., Guo D., Coaxial laser cladding of Al_2O_3-13%TiO_2 powders on Ti-6Al-4 V alloy, Surface & Coatings Technology 228, p. 452 (2013).

14. [CZR14]   Cong D., Zhou H., Ren Z., Zhang H., Ren L., Meng C., Wang C., Thermal fatigue resistance of hot work die steel repaired by partial laser surface remelting and alloying process, Optics and Lasers in Engineering 54, p. 55–61, (2014).

15. [DFK18]   Devojno O.G., Feldshtein E., Kardapolava M.A., Lutsko N.I., On the formation features, microstructure and microhardness of single laser tracks formed by laser cladding of a NiCrBSi self-fluxing alloy, Optics and Lasers in Engineering 106, p. 32-38, (2018).

16. [DHS14]   Dhanda M., Haldar B., Saha P., Development and characterization of hard and wear resistant MMC coating on Ti-6Al-4V substrate by laser cladding, Procedia Mater. Sci. 6, p. 1226-1232, (2014) doi:10.1016/j.mspro.2014.07.196

17. [DIE11]   Dieringa, H., Properties of magnesium alloys reinforced with nanoparticles and carbon nanotubes: A review. J. Mater. Sci. 46, p. 289–306, (2011) doi:10.1007/s10853-010-5010-6

18. [DMA18]   Dilawary S. A. A., Motallebzadeh A., Atar E., Cimenoglu H., Influence of Mo on the high temperature wear performance of NiCrBSi hardfacings, Tribology International 127, p. 288-295, (2018).

19. [DPG15]   Deschuyteneer D., Petit F., Gonon M., Cambier F., Processing and characterization of laser clad NiCrBSi/WC composite coatings — Influence of microstructure on hardness and wear, Surface and Coatings Technology 283, p, 162-171, (2015).

20. [DPG17]   Deschuyteneer D., Petit F., Gonon M., Cambier F., Influence of large particle size – up to 1.2 mm – and morphology on wear resistance in

NiCrBSi/WC laser cladded composite coatings, Surface and Coatings Technology 311, p. 365-373, (2017).

21. [FCG05] Fernández E., Cadenas M., González R., Navas C., Fernández R., J. de Damborenea, Wear behaviour of laser clad NiCrBSi coating, Wear 259, 7–12, p. 870-875, (2005).

22. [FHC15] Fei W., Huijun Y, Chuanzhong C., Kai W., Influence of Nb and Y on hot corrosion behavior of Ni–Cr-based superalloys, Materials and Manufacturing Processes 30 (5), p. 677–684, (2015) doi: 10.1080/10426914.2014.994770

23. [GGF08] Gómez-del Río T., Garrido M.A., Fernández J.E., Cadenas M., Rodríguez J., Influence of the deposition techniques on the mechanical properties and microstructure of NiCrBSi coatings, Journal of Materials Processing Technology 204, 1–3, p. 304-312, (2008).

24. [GTL12] Gao X., Tian Z., Liu Z., Shen L., Interface characteristics of Al_2O_3-13%TiO_2 ceramic coatings prepared by laser cladding, Transactions of Nonferrous Metals Society of China 22, 10, p. 2498-2503, (2012).

25. [GVS19] Genta V., Voiculescu I., Stefanoiu R., Jianu A., Milosan I., Stanciu E.M., Pascu A., Vasile I.M., Titanium influence on the microstructure of FeCrAl alloys usedfor 4r generation nuclear power plants, REV.CHIM. 70, 2, , p. 549 – 554, (2019).

26. [HML19] Hao J., Meng Q., Li C., Li Z., Wu D., Effects of tilt angle between laser nozzle and substrate on bead morphology in multi-axis laser cladding, Journal of Manufacturing Processes 43, p. 311-322, (2019).

27. [HNS08] Hwang J.Y., Neira A., Scharf T.W., Tiley J., Banerjee R., Laser-deposited carbon nanotube reinforced nickel matrix composites. Scr. Mater. 59, p. 487-490, (2008) doi:10.1016/j.scriptamat.2008.04.032.

28. [HOH13] Hemmati, I., Ocelík, V., De Hosson, J. Th. M., Effects of the alloy composition on phase constitution and properties of laser deposited Ni-Cr-B-Si coatings. Physics Procedia 41, p. 302–311, (2013) doi:10.1016/j.phpro.2013.03.082.

29. [HRO13] Hemmati, I., Rao J. C., Ocelík V., De Hosson J. Th. M., Phase formation and properties of vanadium-modified Ni–Cr–B-Si–C laser-deposited coatings. Journal of Materials Science 48 (8), p. 3315-3326, (2013) doi: 10.1007/s10853-012-7117-4.

30.   [HTS11]   Hamedi M.J., Torkamany M.J., Sabbaghzadeh J., Effect of pulsed laser parameters on in-situ TiC synthesis in laser surface treatment, Opt. Lasers Eng. 49, p. 557-563, (2011)
doi:10.1016/j.optlaseng.2010.12.002

31.   [HXS18]   Huaming L ., Xunpeng Q., Song H., Zeqi H., Mao N., Geometry modeling of single track cladding deposited by high power diode laser with rectangular beam spot, Optics and Lasers in Engineering 100, p. 38-46, (2018)

32.   [ISK19]   Mahmoud Z. Ibrahim, Ahmed A.D. Sarhan, Kuo T.Y., Hamdi M., Farazila Y., Chien C.S., Chang C.P., Lee T.M., Advancement of the artificial amorphous-crystalline structure of laser cladded FeCrMoCB on nickel-free stainless-steel for bone-implants, Materials Chemistry and Physics 227, p. 358-367, (2019).

33.   [ISM10]   Iqbal M., Shaukat I., Mahmood A., Abbas K., Haq M.A., Surface modification of mild steel with Boron Carbide reinforcement by electron beam melting. Vacuum 85, p. 45-57, (2010)
doi:10.1016/j.vacuum.2010.03.009.

34.   [IWS19]   https://www.iws.fraunhofer.de/en/business_fields/surface_treatment/laser_cladding/system_technology/COAXwire.html

35.   [JAN15]   Janicki D., Laser cladding of Inconel 625-based composite coatings reinforced by porous chromium carbide particles, Optics & Laser Technology, Vol. 94, p. 6–14, (2017)

36.   [JLJ19]   Juan Y.F., Li J., Jiang Y.Q., Jia W.L., Lu Z.J., Modified criterions for phase prediction in the multi-component laser-clad coatings and investigations into microstructural evolution/wear resistance of FeCrCoNiAlMox laser-clad coatings, Applied Surface Science 465, 28, p. 700-714, (2019).

37.   [JOH05]   JOHN C. I., Laser processing of engineering materials, ISBN 0 7506 6079 1, Elsevier Butterworth-Heinemann, (2005).

38.   [JOW15]   Jonathan R., Lawrence D Waugh, Laser Surface Engineering: Processes and Applications, Woodhead Publishing, ISBN 978-1-78242-079-8, (2015).

39.   [KTG19]   Khamidullin B.A., Tsivilskiy I.V., Gorunov A.I., Gilmutdinov A.Kh., Modeling of the effect of powder parameters on laser cladding using coaxial nozzle, Surface and Coatings Technology Volume 364, p. 430-443, (2019).

40. [KTK13]   Kwon H., Takamichi M., Kawasaki A., Leparoux M., Investigation of the interfacial phases formed between carbon nanotubes and aluminum in a bulk material. Mater. Chem. Phys. 138, p. 787-793, (2013) doi:10.1016/j.matchemphys.2012.12.062.

41. [KUM14]   S.Kumar ,10.05 - Selective laser sintering/melting, Comprehensive Materials Processing Volume 10, p. 93-134, (2014).

42. [LDZ17]   Lei X., Dong L., Zhang Z., Liu Y., Hao Y., Yang R., Zhang L.-C., Microstructure, texture evolution and mechanical properties of VT3-1 titanium alloy processed by multi-pass drawing and subsequent isothermal annealing, Metals 7, p. 131, (2017).

43. [LGV15]   Lucchetta G., Giusti R., Vezzu S., Bariani P.F., Investigation and characterization of Stellite-based wear-resistant coatings applied to steel moulds by cold-spray, CIRP Annals - Manufacturing Technology 64 p. 535–538, (2015).

44. [LHW18]   Lu Y., Huang G., Wang Y., Li H., Qin Z., Lu X., Crack-free Fe-based amorphous coating synthesized by laser cladding, Materials Letters 210, p. 46-50, (2018).

45. [LIR14]   Lin D., Richard Liu C., Cheng G.J., Single-layer graphene oxide reinforced metal matrix composites by laser sintering: Microstructure and mechanical property enhancement. Acta Mater. 80, p. 183-193, (2014) doi:10.1016/j.actamat.2014.07.038

46. [LLG15]   Luo X., Li J., Li G.J., Effect of NiCrBSi content on microstructural evolution, cracking susceptibility and wear behaviors of laser cladding WC/Ni–NiCrBSi composite coatings, Journal of Alloys and Compounds 626, p.102-111, (2015).

47. [LLL15]   Luo X., Li J., Li G.J., Effect of NiCrBSi content on microstructural evolution, cracking susceptibility and wear behaviors of laser cladding WC/Ni–NiCrBSi composite coatings, Journal of Alloys and Compounds 626, p. 102–111, (2015).

48. [LRC14]   Lin D., Richard Liu C., Cheng G.J., Single-layer graphene oxide reinforced metal matrix composites by laser sintering: Microstructure and mechanical property enhancement. Acta Mater. 80, p. 183-193, (2014) doi:10.1016/j.actamat.2014.07.038

49. [LRI14]   Lin, D., Richard Liu C., Cheng, G.J., Laser sintering of separated and uniformly distributed multiwall carbon nanotubes integrated iron nanocomposites. J. Appl. Phys. 115, (2014) doi:10.1063/1.4869214

50. [LSZ14] Li Q.H., Savalani M.M., Zhang Q.M., Huo L., High temperature wear characteristics of TiC composite coatings formed by laser cladding with CNT additives. Surf. Coatings Technol. 239, p. 206–211,(2014) doi:10.1016/j.surfcoat.2013.11.043

51. [LSZ18] Lei J.o, Shi C., Zhou S, Gu Z, Zhang L-C, Enhanced corrosion and wear resistance properties of carbon fiber reinforced Ni-based composite coating by laser cladding, Surface & Coatings Technology 334, p. 274–285, (2018).

52. [MAZ17] Mazumder J., Laser-aided direct metal deposition of metals and alloys, Laser Additive Manufacturing, Woodhead Publishing Series in Electronic and Optical Materials, (2017).

53. [MBS04] Berni A., Mennig M., Schmidt H., Sol-Gel technologies for glass producers and users, Ed. Springer US, p. 88-89, (2004).

54. [MHH17] Mohammad E., Hassan A.-P., Hamidreza M.-S., Reza S.-R., An empirical-statistical model for laser cladding of WC-12Co powder on AISI 321 stainless steel, Optics and Laser Technology 97, p. 180–186, (2017).

55. [MKP18] Mohanty D., Kar S., Paul S., Bandyopadhyay P.P., Carbon nanotube reinforced HVOF sprayed WC-Co coating. Mater. Des. 156, p. 340-350, (2018) doi:10.1016/j.matdes.2018.06.054.

56. [MVG14] Mithilesh P., Varun D., Gopi Reddy A. R., Ramkumar K. D., Arivazhagan N., Narayanan S., Investigations on dissimilar weldments of Inconel 625 and AISI 304, Procedia engineering 75, p. 66-70, (2014).

57. [MWZ15] Ma M., Wang Z., Zeng X., Effect of energy input on microstructural evolution of direct laser fabricated IN718 alloy, Materials Characterization 106, p. 420–427, (2015).

58. [NHL17] Ning F., Hu Y., Liu Z., Cong W., Li Y., Wang X., Ultrasonic vibration-assisted laser engineered net shaping of Inconel 718 parts: A feasibility study, Procedia Manufacturing 10, p. 771-778, (2017).

59. [NIS18] Nagulin K.Yu., Iskhakov F.R., Shpilev A.I., Gilmutdinov A.Kh., Optical diagnostics and optimization of the gas-powder flow in the nozzles for laser cladding, Optics & Laser Technology 108, p. 310-320, (2018).

60. [NOP14] Nenadl O., Ocelík V., Palavra A., DeHosson J.Th.M., The prediction of coating geometry from main processing parameters in laser cladding, Physics Procedia 56, p. 220 – 227, (2014).

61.   [NRT17]   Niste V.B., Ratoi M., Tanaka H., Xu F., Zhu Y., Sugimura J., Self-lubricating Al-WS2 composites for efficient and greener tribological parts. Sci. Rep. 7, (2017) doi:10.1038/s41598-017-15297-6

62.   [OER19]   https://www.oerlikon.com/metco/en/products-services/coating-materials/

63.   [OGC17]   Ortiz A., García A., Cadenas M., Fernández M.R., Cuetosc J.M., WC particles distribution model in the cross-section of laser cladded NiCrBSi + WC coatings, for different wt% WC, Surface and Coatings Technology 324, p. 298-306, (2017).

64.   [OLO05]   Oliveira U., Oceli̇́k V., DeHosson J.Th.M., Analysis of coaxial laser cladding processing conditions, Surface & Coatings Technology 197, p. 127-136, (2005).

65.   [PBP16]   Puig J., Balat-Pichelin M., Production of metallic nanopowders (Mg, Al) by solar carbothermal reduction of their oxides at low pressure, Journal of Magnesium and Alloys 4, p.140–150, (2016).

66.   [PHT16]   Pascu A., Hulka I., Tierean M. H., Croitoru C., Stanciu E.M., Roata I.C., A comparison of flame coating and laser cladding using Ni based powders, Solid State Phenomena, Vol. 254, p. 77-82, (2016).

67.   [PII11]   Pascu A., Iovanas R., Iordachescu D., Cuesta A., Effects of the laser beam intensity on the cladded layer geometry and microstructure, Metalurgia International, 16 (5), p. 125-128, (2011).

68.   [PRC14]   Parimi L., Ravi G. A., Clark D., Moataz M, Microstructural and texture development in direct laser fabricated IN718, Materials Characterisation 89, p. 102-111, (2014).

69.   [PRC14]   Parimi L., Ravi G. A., Clark D., Moataz M., Microstructural and texture development in direct laser fabricated IN718, Materials Characterisation 89, p. 102-111, (2014).

70.   [PMS19]   Pascu A., Marza Rosca J., Stanciu E. M, Laser cladding: from experimental research to industrial applications, Materials Today: Proceedings 19, (3), p. 1059-1065, (2019).

71.   [PSC18]   Pascu A., Stanciu E. M., Croitoru C., I. Roata C., Tierean M. H., Pulsed laser cladding of Ni based powder, IOP Conf. Ser.: Mater. Sci. Eng. 209, 012058, (2018).

72.   [PSC19]   Pascu A., Stanciu E.M., Croitoru C., Roată I. C., Tierean M.H., Mirza Rosca J., Cimpoesu N., Bogatu C., Pulsed laser cladding of NiCrBSiFeC

hardcoatings using single-walled carbon nanotubes additives, Journal of Nanomaterials 2019, p. 1-12, (2019).

73. [PSR 16]   Pascu A., Stanciu E. M., Roata I., Croitoru C., Baltes L., Tierean M., Parameters and behaviour of NiCrFeSiB Laser cladding in overlapped geometry, Bulletin of the Transilvania University of Brașov 9 (58), p. 9-16, (2016).

74. [PSR15]   Pascu A., Stanciu E.M., Roată I. C., Laser cladding of Metco 68F-NS-1 cobalt based powder, RECENT 16, 2 (45), p. 115-118, (2015).

75. [PSR17]   Pascu A., Stanciu E.M., Roată I. C., Hulka I., Uțu D., Maior I., Influence of the laser cladding parameters and solar heat treatment on the properties of biocompatible Inconel 718 coatings, Romanian Journal of Materials 47 (2), p. 157 – 165, (2017).

76. [PSR18]   Pascu A., Stanciu E.M., Croitoru C., Roată I. C., Tierean M.H., Carbon nanoparticle-supported Pd obtained by solar physical vapor deposition, Advances in Materials Science and Engineering 2018, p. 1-7, (2018). doi.org/10.1155/2018/4730192

77. [PSR19]   Pascu A., Stanciu E. M., Roată I., Croitoru C., Tierean M., Hulka I., Mirza Rosca J., Reconditioning of compression moulds by laser cladding, Annals of Faculty of Engineering Hunedoara – International Journal of Engineering XVII (4), p. 41-44, (2019).

78. [PSS17]   Pascu A., Stanciu E.M., Savastru D., Geanta V., Croitoru C., Optical and microstructure characterisation of ceramic – hydroxyapatite coating fabricated by laser cladding, Journal of Optoelectronics and Advanced Materials 19, (1-2), p. 66-72, (2017).

79. [PWW11]   Pei X., Wang J., Wan Q., Kang L., Xiao M., Bao H., Functionally graded carbon nanotubes/hydroxyapatite composite coating by laser cladding, Surface & Coatings Technology 205, p. 4380-4387, (2011).

80. [QAR09]   Qi H., Azer M., Ritter A., Studies of standard heat treatment effects on microstructure and mechanical properties of laser net shape manufactured INCONEL 718, Metallurgical and Materials Transactions A, 40(10), p. 2410-2422, (2009).

81. [QID14]   Qingbo J., Dongdong G., Selective laser melting additive manufacturing of Inconel 718 superalloy parts: Densification, microstructure and properties, Journal of Alloys and Compounds 585, p. 713-721, (2014).

82. [QLX12]   Qu F., Liu X., Xing F., Zhang K., High temperature tensile properties of laser buttwelded plate of Inconel 718 superalloy with ultrafine grains, Trans. Nonferrous Met. Soc. China 22, p. 2379-2388, (2012).

83. [RCP19]   Roată I. C., Croitoru C., Pascu A., Stanciu E.M., Photocatalytic coatings via thermal spraying: a mini-review, AIMS Materials Science 6 (3), p. 335-353, (2019) 10.3934/matersci.2019.3.335.

84. [REA97]   Ready J.F., Industrial applications of lasers, 2nd edition, Academic Press, ISBN 0-12-583961-8, (1997).

85. [RIP13]   Roata I.C., Iovanas R., Pascu A., Influence of the metallizing distance variation and of the electric field voltage on the ohmic resistance of the layers deposited by thermal spraying, Metalurgia International XVII, Special Issue 6, p. 73-76, (2013).

86. [RKP16]   Raveendra R. S., Krupakara P. V., Prashanth P. A., Prashanth B., Enhanced mechanical properties of Al-6061 metal matrix composites reinforced with α --Al_2O_3 nanoceramics. J. Mater. Sci. Surf. Eng. 4, p. 483-487, (2016)

87. [RML13]   Riveiro A., Mejías A., Lusquiños F., J. del Val, Comesaña R., Pardo J., Pou J., Optimization of laser cladding for Al coating production, Physics Procedia 41, p. 327-334, (2013).

88. [RPS14]   Roată I. C., Pascu A., Stanciu E. M., Influence of the electric field voltage on the microhardness of the layers coated by thermal spraying, Solid State Phenomena 216, p. 316-321, (2014).

89. [RPS18]   Reddy L., Preston S.P., Shipway P.H., Davis C., Hussain T., Process parameter optimisation of laser clad iron-based alloy: Predictive models of deposition efficiency, porosity and dilution, Surface and Coatings Technology 349, p. 198-207, (2018).

90. [RRR05]   Ram G.D.J., Reddy A.V., Rao K.P., Reddy G.M, Sundar J.K.S., Microstructure and tensile properties of Inconel 718 pulsed Nd- YAG laser welds, J Mater Process Technol 167, p. 73, (2005).

91. [RRR16]   Riquelme A., Rodrigo P., Escalera-Rodríguez M. D., Rams J., Analysis and optimization of process parameters in Al–SiCp laser cladding, Optics and Lasers in Engineering 78, p. 165-173, (2016).

92. [SAN12]   Sanaty-Zadeh, A., Comparison between current models for the strength of particulate-reinforced metal matrix nanocomposites with emphasis

on consideration of Hall-Petch effect. Mater. Sci. Eng. A. 531, p. 112-118, (2012) doi:10.1016/j.msea.2011.10.043

93. [SCH98]   Schneider M.F., Laser cladding with powder, Ph.D. Thesis University of Twente, Enschede, The Netherlands, ISBN: 90 365 1098 8, (1998).

94. [SCM19]   Shang S., Jing C., Liang M., Wei F., Hua T., Fencheng L., Xin L., Microstructures and stress rupture properties of pulse laser repaired Inconel 718 superalloy after different heat treatments, Journal of Alloys and Compounds 770, p. 125-135, (2019).

95. [SHY08]   Song R., Hanaki S., Yamashita M., Uchida H., Reliability evaluation of a laser repaired die-casting die, Materials Science and Engineering A 483–484, p. 343–345, (2008).

96. [SII13]   Staicu A.R., Iovanas R, Iovanas D.M., Pascu A., Pop A., Laser cladding of Ni based CW composite powder, Metalurgia International 6, ISSN 1528-2214, p.147-150, (2013).

97. [SLF09]   Song J., Li Y., Fu J., Deng Q., Hu D.: Cracking behavior of laser cladding forming nickel based alloys, Technology and Innovation Conference 2009 (ITIC 2009), (2009).

98. [SLH03]   Shorowordi K.M., Laoui T., Haseeb A.S.M.A., Celis J.P., Froyen L., Microstructure and interface characteristics of B_4C, SiC and Al_2O_3 reinforced Al matrix composites: A comparative study. J. Mater. Process. Technol.142, p. 738-743, (2003) doi:10.1016/S0924-0136(03)00815-X

99. [SLX19]   Song X., Lei J., Xie J., Fang Y., Microstructure and electrochemical corrosion properties of nickel-plated carbon nanotubes composite Inconel718 alloy coatings by laser melting deposition, Optics & Laser Technology 119, 105593, (2019).

100. [SLZ18]   Shu F.Y., Liu S., Zhao H.Y., He W.X., Sui S.H., Zhang J., He P., Xu B.S., Structure and high-temperature property of amorphous composite coating synthesized by laser cladding FeCrCoNiSiB high-entropy alloy powder, Journal of Alloys and Compounds 731, p. 662-666, (2018).

101. [SLZ18]   Shi C., Lei J., Zhou S., Dai X., Zhang L.-C., Microstructure and mechanical properties of carbon fibers strengthened Ni-based coatings by laser cladding: The effect of carbon fiber contents, Journal of Alloys and Compounds 744, p. 146-155, (2018).

102. [SNL12]   Savalani M.M., Ng C.C., Li Q.H., Man H.C., In situ formation of titanium carbide using titanium and carbon-nanotube powders by laser cladding. Appl. Surf. Sci. 258, p. 3173-3177, (2012) doi:10.1016/j.apsusc.2011.11.058.

103. [SPG18]   Stanciu E. M., Pascu A., Gheorghiu I., CMT welding o f low carbon steel thin sheets, IOP Conf. Ser.: Mater. Sci. Eng. 209, 012051, (2018).

104. [SPR18]   Stanciu E.M., Pascu A., Roată I.C., Croitoru C., Tierean M., Rosca J. Mirza, Hulka I., Solar radiation synthesis of functional carbonaceous materials using Al_2O_3/TiO_2-Cu-HA doped catalyst, Applied Surface Science 438, p. 33–40, (2018).

105. [SPT16]   Stanciu E.M, Pascu A, Tierean M.H., Voiculescu I, Roata I.C., Croitoru C., Hulka I., Dual coating laser cladding of NiCrBSi and Inconel 718, Materials and Manufacturing Processes 31, 12, p. 1556-1564, (2016).

106. [SPT18]   Stanciu E.M., Pascu A., Tierean M.H., Roata I.C., Voiculescu I., Hulka I., Croitoru C., Dissimilar laser welding of AISI 321 and AISI 1010, Technical Gazette 25/No. 2, p. 344-349, (2018).

107. [SUH12]   Sun Y., Hao M., Statistical analysis and optimization of process parameters in Ti6Al4V laser cladding using Nd:YAG laser, Optics and Lasersin Engineering 50, p. 985–995, (2012).

108. [SWZ18]   Shu F.Y., Wu L., Zhao H.Y., Sui S.H., Zhou L., Zhang J., He W.X., He P., Xu B.S., Microstructure and high-temperature wear mechanism of laser cladded CoCrBFeNiSi high-entropy alloy amorphous coating, Materials Letters 211, p. 235-238, (2018).

109. [SYD18]   Shu F., Yang B., Dong S., Zhao H., Xu B., Xu F. , Liu B., He P., Feng J., Effects of Fe-to-Co ratio on microstructure and mechanical properties of laser cladded FeCoCrBNiSi high-entropy alloy coatings, Applied Surface Science Volume 450,p. 538-544, (2018).

110. [SYG00]   Sun R.L, Yang D.Z, Guo L.X, Dong S.L, Microstructure and wear resistance of NiCrBSi laser clad layer on titanium alloy substrate, Elsevier Surface and Coatings Technology 132, 2–3, p. 251-255, (2000).

111. [SZL19]   Shu F., Zhang B., Liu T., Sui S., Liu Y., He P., Liu B., Xu Bi., Effects of laser power on microstructure and properties of laser cladded CoCrBFeNiSi high-entropy alloy amorphous coatings, Surface and Coatings Technology 358, p. 667-675, (2019).

112. [TAA08]   Tobar M.J., Amado J.M., Álvarez C., García A., Varela A., Yáñez A., Characteristics of Tribaloy T-800 and T-900 coatings on steel

substrates by laser cladding, Surface and Coatings Technology 202, p. 2297-2301, (2008).

113. [TGM11]   Tsaprailis H., Garfias-Mesias L.F., Rapid evaluation of metallic coatings on large cylinders exposed to marine environments, Corrosion 67, p. 126002-1-126002-9, (2011) doi: ttp://dx.doi.org/10.5006/1.3666861

114. [TJO13]   Tjong S.C., Recent progress in the development and properties of novel metal matrix nanocomposites reinforced with carbon nanotubes and graphene nanosheets. Mater. Sci. Eng. R Reports. 74, p. 281-350, (2013) doi:10.1016/j.mser.2013.08.001

115. [TKC04]   Toyserkani E., Khajepour A., Corbin S., Laser cladding, CRC Press, ISBN 0-8493-2172-7, (2004).

116. [TLY18]   Tianbiao Y., Lin Y., Yu Z., Jiayu S., Baichun L., Experimental research and multi-response multi-parameter optimization of laser cladding Fe313, Optics and Laser Technology 108, p. 321–332, (2018).

117. [TOR13]   Torims T., The application of laser cladding to mechanical component repair, renovation and regeneration, DAAAM International Scientific Book 32, p. 587-608, (2013).

118. [TYW01]   Tu J.P., Yang Y.Z., Wang L.Y., Ma X.C., Zhang X.B., Tribological properties of carbon-nanotube-reinforced copper composites. Tribol. Lett. 10, p. 225–228, (2001) doi:10.1023/A:1016662114589.

119. [UKK15]   Uhlmann E., Kersting R., Klein T. B., Cruz M. F., Borille A. V., Additive manufacturing of titanium alloy for aircraft components, Procedia CIRP 35, p. 55–60, (2015).

120. [UMW10]   Uddin, S.M., Mahmud, T., Wolf, C., Glanz, C., Kolaric, I., Volkmer, C., Höller, H., Wienecke, U., Roth, S., Fecht, H.J., 2010. Effect of size and shape of metal particles to improve hardness and electrical properties of carbon nanotube reinforced copper and copper alloy composites. Compos. Sci. Technol. doi:10.1016/j.compscitech.2010.07.012

121. [WCM08]   Wang D.G., Chen C.Z., Ma J., Zhang G., In situ synthesis of hydroxyapatite coating by laser cladding, Colloids and Surfaces B: Biointerfaces 66, p. 155-162, (2008).

122. [WIE08]   Wielligh L. G., Characterizing the influence of process variables in laser cladding Al-20wt%Si onto an aluminium substrate, PhD thesis, Nelson Mandela Metropolitan University.

123. [WLC08]   Wang D., Liang E., Chao M, Yuan B. Investigation on the microstructure and cracking susceptibility of laser-clad V2O5 /NiCrBSiC alloy coatings. Surface and Coatings Technology 202 (8), p. 1371–1378, (2008) doi: 10.1016/j.surfcoat.2007.06.036.

124. [WMZ08]   Wang F., Mao H., Zhang D., Zhao X., Shen Y., Online study of cracks during laser cladding process based on acoustic emission technique and finite element analysis. In: Applied Surface Science 255, p.3267–3275, (2008).

125. [WZG17]   Wang S.L., Zhang Z.Y., Gong Y.B., Nie G.M., Microstructures and corrosion resistance of Fe-based amorphous/nanocrystalline coating fabricated by laser cladding, Journal of Alloys and Compounds 728, p. 116-1123, (2017).

126. [XLL13]   Xu F., Lv Y., Liu Y., Xu B., He P., Effect of heat treatment on microstructure and mechanical properties of Inconel 625 alloy fabricated by pulsed plasma arc deposition, Physics Procedia 50, p. 48-54, (2013).

127. [XZZ12]   Xue-song G., Zong-jun T., Zhi-dong L., Li-da S., Interface characteristics of Al_2O_3-13%TiO_2 ceramic coatings prepared by laser cladding, Trans. Nonferrous Met. Soc. China 22, p.2498–2503, (2012).

128. [YDD11]   Yu T., Deng Q., Dong G., Yang J., Effects of Ta on microstructure and microhardness of Ni based laser clad coating, Applied Surface Science 257, p. 5098-5103, (2011).

129. [YRW19]   Yanan L., Ronglu S., Wei N., Tiangang Z., Yiwen L., Effects of CeO_2 on microstructure and properties of TiC/Ti_2Ni reinforced Ti-based laser cladding composite coatings, Optics and Lasers in Engineering 120, p. 84-94, (2019).

130. [YSH11]   Yang Y., Serpersu K., He W., Paital S. R., Dahotre N. B., Osteoblast interaction with laser cladded HA and SiO_2-HA coatings on Ti–6Al–4V, Materials Science and Engineering: C Volume 31, p. 1643-1652, (2011).

131. [YYZ18]   Yu T., Yang L., Zhao Y., Sun J., Li B., Experimental research and multi-response multi-parameter optimization of laser cladding Fe313, Optics & Laser Technology 108, p. 321-332, (2018).

132. [ZBK16]   Zhou W., Bang S., Kurita H., Miyazaki T., Fan Y., Kawasaki A., Interface and interfacial reactions in multi-walled carbon nanotube-reinforced aluminum matrix composites. Carbon 96, p. 919-928, (2016) doi:10.1016/j.carbon.2015.10.016

133. [ZBZ19]   Zhai L.L., Ban C.Y., Zhang J.W., Microstructure, microhardness and corrosion resistance of NiCrBSi coatings under electromagnetic field auxiliary laser cladding, Surface and Coatings Technology 358, p. 531-538, (2019).

134. [ZLH12]   Zhu Y., Li Z., Huang J., Li M., Li R., Wu Y., Amorphous structure evolution of high power diode laser cladded Fe–Co–B–Si–Nb coatings, Applied Surface Science 261, p. 896-901, (2012).

135. [ZLN13]   Zhang Y., Li Z., Nie P., Wu Y., Carbide and nitride precipitation during laser cladding of Inconel 718 alloy coatings, Optics & Laser Technology 52, p. 30-36, (2013).